Avaliação da biocompatibilidade e do efeito no reparo ósseo de um *scaffold* manufaturado a partir de um material vítreo fibroso

Paulo Roberto Gabbai Armelin

São Carlos

2015

PAULO ROBERTO GABBAI ARMELIN

Avaliação da biocompatibilidade e do efeito no reparo ósseo de um *scaffold* manufaturado a partir de um material vítreo fibroso

Tese apresentada ao Programa de Pós-Graduação em Biotecnologia da Universidade Federal de São Carlos para obtenção do título de Doutor em Biotecnologia

Orientadores: Profa. Dra. Ana Cláudia Muniz Rennó
Prof. Dr. Oscar Peitl-Filho
Co-orientador: Prof. Dr. Paulo Sérgio Bossini

São Carlos
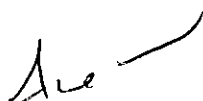2015

Paulo Roberto Gabbai Armelin
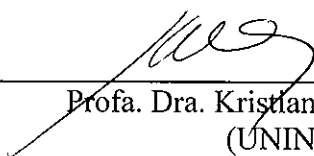
Tese de Doutorado submetida à Coordenação do Programa de Pós-Graduação em Biotecnologia, da Universidade Federal de São Carlos, como requisito parcial para a obtenção do título de Doutor em Biotecnologia

Aprovado em: 27/03/2015

BANCA EXAMINADORA
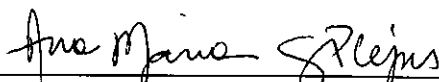
Profa. Dra. Ana Claudia Muniz Renno (Orientador)
(UNIFESP)

Profa. Dra. Kristianne P. S. Fernandes
(UNINOVE)

Prof. Dr. Clovis Wesley Oliveira de Souza (UFSCar)

Profa. Dra. Ana Maria de Guzzi Plepis (USP)

Profa. Dra. Karina Nogueira Zambone Pinto (UFSCar)

Dedico este trabalho e todos os esforços para cumpri-lo (pois, sim, o considero uma 'missão') aos meus amados pais Paulo e Vera, com todo meu amor e respeito. Conseguimos!
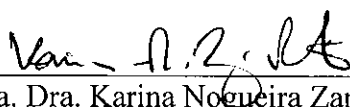
Agradecimentos especiais

Agradecimentos

Ao G.A.D.U. pela proteção, por ter iluminado meus caminhos e ideias e por ter me dado força para superar todos os obstáculos durante minha caminhada

A toda minha família, que sempre me apoiou, torceu por mim e vibrou com minhas conquistas. Deixo aqui também minha eterna gratidão aos meus avôs Alcides e Josefina & Benedito e América, pois eles foram a base e o início de tudo!

Ao Prof. Dr. Oscar Peitl-Filho pela orientação, principalmente no que se diz respeito à produção do biomaterial utilizado no trabalho.

Aos professores: Dra. Ana Maria de Guzzi Plepis, Dra. Kristianne Porta Santos Fernandes, Dr. Clovis Wesley Oliveira de Souza e Dra. Karina Nogueira Zambone Pinto Rossi, que se prontificaram a compor a banca examinadora, proporcionando valiosas contribuições científicas.

Ao meu grande amigo Dr. Hueliton Wilian Kido por toda ajuda, suporte e confiança. Também pelas horas que tomamos umas juntos, jogamos conversa fora e batemos aquele futi com o pessoal da pós. Que a nossa amizade seja para a vida toda!

Ao Prof. Dr. Nivaldo Antonio Parizotto por me acolher em seu laboratório e disponibilizar todos os recursos e espaço para realização de meus trabalhos, em especial, para os trabalhos de experimentação animal.

À Profa. Dra. Keico Okino Nonaka por disponibilizar o equipamento para análise biomecânica.

Às professoras Dra. Kristianne P. S. Fernandes e Dra. Raquel A. Mesquita-Ferrari por disponibilizar o laboratório e materiais para os testes com cultura de células.

Ao pessoal do Laboratório de Materiais Vítreos (LaMav) do Departamento de Engenharia de Materiais da UFSCar por produzir o biomaterial utilizado no trabalho.

À ONG Teto e a meus amigos que fazem parte dela por me mostrar os 'verdadeiros' problemas na vida e por me ajudar a olhar o mundo e as pessoas ao meu redor a partir de outra perspectiva.

E por final, para que eu não seja traído por minha memória... agradeço a todos que contribuíram direta ou indiretamente para a realização deste trabalho.

Muito obrigado!

"A ciência se compõe de erros que, por sua vez, são os passos até a verdade".

(Júlio Verne)

Resumo

GABBAI-ARMELIN, Paulo Roberto. **Avaliação da biocompatibilidade e do efeito no reparo ósseo de um *scaffold* manufaturado a partir de um material vítreo fibroso**. 2015. 119 f. Tese (Doutorado em Biotecnologia) – Programa de Pós-Graduação em Biotecnologia, Universidade Federal de São Carlos, São Paulo, 2015.

Milhões de fraturas ósseas ocorrem anualmente no mundo todo e o processo de reparo é complexo, envolvendo muitos eventos biológicos até que se atinja a restauração da integridade do tecido. Problemas nessa regeneração podem ocorrer, levando a não união óssea. Assim, faz-se necessária a busca por novas tecnologias que atuem na restauração da integridade do tecido ósseo e promovam a osteocondução e a osteoindução. Para tanto, uma alternativa promissora é a utilização de materiais bioativos para o reparo ósseo. Seguindo essa linha, foram realizados dois estudos (I e II) acerca de um novo *scaffold* vítreo fibroso, sendo estes estudos baseados em três linhas de investigação: (i) caracterização do novo *scaffold* vítreo fibroso; (ii) avaliação da biocompatibilidade desse material bioativo e (iii) análise do desempenho biológico desse novo *scaffold* no reparo ósseo. Mais especificamente, no estudo I foi feita a caracterização dos *scaffolds* em termos de porosidade, mineralização e características morfológicas. Adicionalmente, fibroblastos e osteoblastos foram cultivados em contato com extratos dos *scaffolds* para avaliação da proliferação celular e genotoxicidade após 24, 72 e 144 h. Finalmente, nesse mesmo estudo, os *scaffolds* foram implantados subcutaneamente em ratos por 15, 30 e 60 dias. No que se refere ao estudo II, foram feitas avaliações da estrutura morfológica dos *scaffolds* (via microscopia eletrônica de varredura) imersos em tampão fosfato salino (PBS) após 1, 7 e 14 dias, além de investigações do efeito no reparo ósseo do novo *scaffold* utilizando implantação do mesmo em defeitos ósseos tibiais em ratos. Análises histopatológicas, imunohistoquímicas e biomecânicas foram realizadas 15, 30 e 60 dias após a implantação. Os *scaffolds* apresentaram estruturas altamente porosas (porosidade de ~75%) e interconectadas, e o biovidro precursor mineralizou uma camada de hidroxicarbonatoapatita (HCA) em SBF (*simulated body fluid*) após o curto período de 12 h. A incubação em PBS indicou que as fibras do *scaffold* apresentaram sinais de degradação com o passar do tempo. Sobre os testes biológicos, o novo biomaterial levou a um aumento da proliferação de fibroblastos e osteoblastos, e nenhum dano ao DNA foi observado. Os experimentos de implantação do material no subcutâneo indicaram degradação do biomaterial acompanhada do crescimento interno de tecido mole e presença de células gigantes multinucleadas ao redor do implante. Após 60 dias, os *scaffolds* estavam quase completamente absorvidos e um tecido de granulação organizado preenchia a área de implantação. Adicionalmente, as análises histológicas dos *scaffolds* em defeitos ósseos revelaram uma degradação progressiva do biomaterial e substituição do mesmo por tecido de granulação e tecido ósseo neoformado. A histomorfometria mostrou uma maior quantidade de osso neoformado no grupo controle (CG) comparado ao grupo biomaterial (BG) 15 dias após a cirurgia. No entanto, depois de 30 e 60 dias, CG e BG apresentaram quantidades similares de osso neoformado. Além disso, o novo biomaterial aumentou a expressão de RUNX-2 e RANK-L, e também melhorou as propriedades mecânicas do calo tibial 15 dias após a cirurgia. Os resultados indicam que o novo *scaffold* vítreo fibroso é bioativo, não-citotóxico, biocompatível e promissor para utilização na engenharia do reparo ósseo.

Palavras-chave: caracterização, biocompatibilidade, biomaterial, vidro bioativo, *scaffold* fibroso, reparo ósseo, citotoxicidade.

Abstract

GABBAI-ARMELIN, Paulo Roberto. **Biocompatibilty of a scaffold obtained from a fibrous glassy material and its effect on bone repair**. 2015. 119 p. Thesis (PhD in Biotechnology) – Postgraduate Course in Biotechnology, Federal University of São Carlos, São Paulo, 2015.

Millions of bone fractures occur annually worldwide and the consequent bone repair process is complex, involving many biological events until it reaches the restoration of the tissue integrity. During that process some problems can occur due to delays in the bone healing, which does not allow the proper joining of the tissue. Thus, it is necessary to search for new technologies that work in restoring the integrity of the bone tissue and that promote the osteoconduction and the osteoinduction. In this sense, the use of bioactive materials in the bone repair process is a promising alternative. Following this, two studies (I and II) were developed in order to investigate a new fibrous glassy scaffold, and these studies were based in three lines of research: (i) the characterization of the new fibrous glassy scaffold; (ii) the biocompatibility evaluation of this bioactive material; (iii) the analysis of the biological performance of this new scaffold in the bone repair. More specifically, in the study I the developed scaffolds were characterized in terms of porosity, mineralization and morphological features. Additionally, fibroblast and osteoblast cells were seeded in contact with extracts of the scaffolds to assess cell proliferation and genotoxicity after 24, 72 and 144 h. Finally, scaffolds were placed subcutaneously in rats for 15, 30 and 60 days. In regards to study II, the morphological structure of the scaffolds upon incubation in phosphate buffered saline (PBS) (via scanning electron microscope) was assessed after 1, 7 and 14 days and, also, the *in vivo* tissue response to the new biomaterial was evaluated using implantation in rat tibial defects. The histopathological, immunohistochemistry and biomechanical analyzes after 15, 30 and 60 days of implantation were performed to investigate the effects of the material on bone repair. The scaffolds presented interconnected porous structures (porosity of ~75%), and the precursor bioglass could mineralize a hydroxycarbonate apatite (HCA) layer in SBF after only 12 h. The PBS incubation indicated that the fibers of the glassy scaffold degraded over time. With regards to the biological investigations, the biomaterial elicited increased fibroblast and osteoblast cell proliferation, and no DNA damage was observed. The *in vivo* experiment showed degradation of the biomaterial over time, with soft tissue ingrowth into the degraded area and the presence of multi-nucleated giant cells around the implant. At day 60, the scaffolds were almost completely degraded, and an organized granulation tissue filled the area. Additionally, the histological analysis of the implants in the bone defects revealed a progressive degradation of the material with increasing implantation time and also its substitution by granulation tissue and woven bone. Histomorphometry showed a higher amount of newly formed bone area in the control group (CG) compared to the biomaterial group (BG) 15 days post-surgery. After 30 and 60 days, CG and BG showed a similar amount of newly formed bone. The novel biomaterial enhanced the expression of RUNX-2 and RANK-L, and also improved the mechanical properties of the tibial callus at day 15 after surgery. These results indicate that the new fibrous glassy scaffold is bioactive, non-cytotoxic, biocompatible and promising for using in bone tissue engineering.

Keywords: characterization, biocompatibility, biomaterial, bioactive glass, fibrous scaffold, bone repair, cytotoxicity.

Lista de abreviaturas e símbolos

ANOVA	Análise de Variância
a.u.	*Arbitrary Unit*
B	*Bone Formation*
BG	Grupo Biomaterial
BGs	*Bioactive Glasses*
BMP	*Bone Morphogenetic Proteins*
CAPES	Coordenação de Aperfeiçoamento de Pessoal de Nível Superior
CaP	*Calcium Phosphate*
CeRTEV	*Center for Research Technology, and Education in Vitreous Materials*
CG	Grupo Controle
CNPq	Conselho Nacional de Desenvolvimento Científico e Tecnológico
COL-1	Colágeno tipo 1
CSD	*Critical-size Bone Defects*
D	*Defect Line*
DEMa	Departamento de Engenharia de Materiais
DMEM	Meio de Eagle Modificado por Dulbecco
ECM	*Extracellular Matrix*
EDTA	Ácido Etilenodiaminotetraacético
F	*Fibrous Capsule*
FAPESP	Fundação de Amparo à Pesquisa do Estado de São Paulo
G	*Granulation tissue*
HCA	Hidroxicarbonatoapatita
HE	Hematoxilina e Eosina
IgG	Imunoglobulina G
IN	*Inflammatory Cells*
IUPAC	*International Union of Pure and Applied Chemistry*
PvPi	Iodo Povidine
kN	Quilonewton
LaMaV	Laboratório de Materiais Vítreos
LLLT	*Low Level Laser Therapy*
MEV / SEM	Microscópio Eletrônico de Varredura / *Scanning Electron Microscopy*
mM	Milimolar

mA	Miliampere
M	*Medullar Tissue*
MTT	Brometo de 3-[4,5-dimetil-tiazol-2-il]-2,5-difeniltetrazólio
μL	Microlitro
μm	Micrômetro
nm	Nanômetro
Ob	*Osteoblasts*
Oc	*Osteocytes*
PBS	*Phosphate-Buffered Saline*
PPGBiotec	Programa de Pós-graduação em Biotecnologia
RANK-L	*Receptor Activator of Nuclear Factor Kappa-B Ligand*
ROI	Região de Interesse
RUNX-2	*Runt-related Transcription Factor 2*
S	*Fibers of the bioactive glassy scaffold*
SBF	*Simulated Body Fluid*
SE	*Standard Error*
SFB	Soro Fetal Bovino
SCGE	*Single Cell Gel Electrophoresis Assay*
Si	Silício
TM	*Trade Mark*
Tris	2-Amino-2-hidroximetil-propano-1,3-diol
UFSCar	Universidade Federal de São Carlos
UNIFESP	Universidade Federal de São Paulo
V	Volt
W	Watt

Lista de figuras

Lista de tabelas

Apresentação da Tese

A presente tese foi estruturada na forma de artigos e redigida de acordo com as normas metodológicas da Associação Brasileira de Normas Técnicas (ABNT). Esta tese é constituída basicamente dos seguintes itens: (1) contextualização; (2) objetivos; (3) materiais e métodos; (4) estudo I; (5) estudo II; (6) considerações finais e perspectivas futuras e (7) referências bibliográficas e anexos. Os estudos I e II compreendem dois artigos científicos que têm como fundamentação os itens (1), (2) e (3). O estudo I aborda a caracterização e biocompatibilidade de um novo *scaffold* vítreo fibroso e é denominado: "*Characterization and biocompatibility of a fibrous glassy scaffold*", publicado no periódico *Journal of Tissue Engineering and Regenerative Medicine* em fevereiro de 2015. O estudo II aborda os aspectos relacionados ao efeito do novo biomaterial no reparo ósseo em defeitos induzidos em tíbias de ratos e é intitulado: "*Effect of a new bioactive fibrous glassy scaffold on bone repair*", aceito para publicação no periódico *Journal of Materials Science: Materials in Medicine* em março de 2015. Os manuscritos científicos aqui apresentados seguem as normas dos referidos periódicos.

Sumário

1   Contextualização

O reparo ósseo é um processo regenerativo complexo, que inclui a interação de uma série de eventos biológicos, como a síntese ativa de genes e a ação de um grande número de células e proteínas, que determinarão a restauração da integridade do tecido (CLAES e WILLIE, 2007; TSIRIDIS, UPADHYAY e GIANNOUDIS, 2007; SCHINDELER *et al.*, 2008). No entanto, no decorrer desse processo, podem ocorrer alterações que culminarão na deficiência da regeneração e, consequentemente, no atraso da consolidação, e mesmo, na não união óssea. Estima-se que nos Estados Unidos (EUA), das 6,2 milhões de fraturas que ocorrem anualmente, cerca de 10% evoluem para a não consolidação e para a pseudoartrose (SENA *et al.*, 2005; CALORI *et al.*, 2007). Além disso, cerca de 25 mil dólares são gastos por tratamento de cada caso de não união óssea (WIESE e PAPE, 2010). As ocorrências destes casos refletem diretamente nas perdas da produtividade e da independência do indivíduo (AARON, CIOMBOR e SIMON, 2004). Estatísticas no Brasil também indicam um alto índice de traumas e fraturas, gerando custos consideráveis para o sistema de saúde público (PORTAL DA SAÚDE, 2011). Diante do exposto, nota-se a necessidade do desenvolvimento de substitutos ósseos eficazes e de custo reduzido para serem utilizados no processo de enxertia (AXELRAD, KAKAR e EINHORN, 2007).

Nesse contexto, diferentes recursos terapêuticos têm sido investigados na tentativa de prevenir e/ou minimizar o surgimento de complicações advindas do processo de consolidação anormal (HADJIARGYROU *et al.*, 1998). Algumas intervenções vêm apresentando resultados positivos na aceleração da consolidação de fraturas. Dentre estas, podem ser citadas: (i) a aplicação de ultrassom terapêutico de baixa intensidade (RUTTEN *et al.*, 2007; COORDS *et al.*, 2011); (ii) campos eletromagnéticos (PICKERING e SCAMMELL, 2002; JING *et al.*, 2011); (iii) aplicação de proteínas ósseas morfogenéticas (*Bone Morphogenetic*

Proteins, BMP) (YAOITA *et al.*, 2000; SHYNG *et al.*, 2010)e (iv) laser terapêutico de baixa intensidade (*Low Level Laser Therapy*, LLLT) (NICOLA *et al.*, 2003; RENNO *et al.*, 2007; FERNANDES *et al.*, 2013; PATROCINIO-SILVA *et al.*, 2014; TIM *et al.*, 2014). Recentemente vêm se destacando as propriedades osteogênicas dos biomateriais, tais como, metais, cerâmicas e polímeros (HADJIARGYROU *et al.*, 1998; HENCH e POLAK, 2002; MOURA *et al.*, 2007; GABBAI-ARMELIN *et al.*, 2014).

O biomaterial ou material bioativo pode ser definido como um material capaz de produzir uma resposta biológica específica em uma interface material/tecido - formando uma forte ligação entre esses − sem induzir toxicidade ou resposta inflamatória acentuada (HENCH e POLAK, 2002; HENCH, 2013).

Dentre os biomateriais mais comumente utilizados, estão os vidros bioativos (*Bioactive Glasses*, BGs), que integram uma classe de compostos vítreos de silicato. Esses vidros apresentam alta bioatividade, formando forte ligação com o tecido ósseo por meio do desenvolvimento de uma camada de hidroxicarbonatoapatita (HCA) na interface osso-material. Tal camada é um ambiente ideal para atração, diferenciação e proliferação de osteoblastos (HUBBELL, 1998; HENCH e POLAK, 2002; HENCH, 2006; HENCH e THOMPSON, 2010). As reações para a formação dessa camada de HCA são dividas por Hench em 5 etapas (HENCH, 2013). Na etapa I, íons alcalinos e alcalino-terrosos são liberados pelo biovidro no fluído e substituídos por íons H^+ ou H_3O^+ na estrutura vítrea. Esta reação faz com que ocorra o aumento do pH local, levando a quebra das ligações Si-O-Si. Na etapa II, o silício é liberado no fluído na forma de grupos silanóis ($Si(OH)_4$). Na etapa III, os silanóis condensam formando uma camada polimerizada de sílica gel na superfície do vidro. Posteriormente, na etapa IV, íons de cálcio e fosfato, que difundiram do vidro ou fluído, formam uma camada de fosfato de cálcio amorfa sobre a camada de sílica gel. Seguindo essas

reações, na etapa V, a camada de fosfato de cálcio amorfa incorpora carbonatos, formando a camada de HCA (HENCH, 2013). Adicionalmente, foi reportado que os produtos de dissolução de BGs modulam a expressão de 7 famílias de genes nos osteoblastos (HENCH, 2003).

O Bioglass® 45S5 é o mais conhecido dos vidros bioativos e considerado padrão-ouro por apresentar o maior índice de bioatividade do mercado (HENCH, 2003; 2006; HENCH e THOMPSON, 2010). Este biomaterial, desenvolvido por Hench e colaboradores, é um vidro produzido por fusão composto por quatro componentes (46,1% SiO_2, 24,4% Na_2O, 26,9% CaO and 2,6% P_2O_5, em mol). Diversos estudos demonstraram que o Bioglass® 45S5 estimula a osteogênese *in vitro*, induzindo a proliferação de osteoblastos humanos, e acelera a consolidação óssea em modelos experimentais em animais (XYNOS *et al.*, 2000; XIE *et al.*, 2009; GRANITO *et al.*, 2011). Adicionalmente, o potencial angiogênico do Bioglass® 45S5 também já foi demonstrado (DAY *et al.*, 2005; GORUSTOVICH, ROETHER e BOCCACCINI, 2010). Assim, o Bioglass® 45S5 tem sido usado em vários procedimentos clínicos, incluindo o reparo de defeitos periodontais, reconstrução de defeitos maxilofaciais, cirurgias espinhais e de substituição óssea (HENCH, 2003; 2006).

Em geral, apesar dos efeitos benéficos dos vidros bioativos para a formação óssea, sua utilização ainda é restrita devido à limitação de formas (JAMES, 1995; OREFICE *et al.*, 2010). Os BGs estão disponíveis principalmente na forma de pó e monolitos. Uma das principais desvantagens do uso destas formas reside no fato de que o preenchimento de defeitos ósseos irregulares e complexos torna-se extremamente difícil. Além disso, a falta de poros interconectados nestes implantes acaba por limitar o crescimento celular no interior dessas estruturas (BOCCACCINI e MAQUET, 2003; DAY *et al.*, 2005; MASTROGIACOMO *et al.*, 2006; SPECTOR, 2006; VALLET-REGI, 2006; WU *et al.*,

2010). Com o intuito de superar essas limitações, o interesse em produtos alternativos, tais como implantes porosos maleáveis/fibrosos e *scaffolds* produzidos a partir de BGs, tem aumentado (CHEN, THOMPSON e BOCCACCINI, 2006; RAHAMAN *et al.*, 2011; JONES, 2013; LACROIX, JALLOT e LAO, 2014). Estes produtos são particularmente interessantes pelo fato de serem mais adequados para o preenchimento de defeitos ósseos com diferentes formas e tamanhos, além de apresentar estruturas porosas interconectadas (MOIMAS *et al.*, 2006; BROWN *et al.*, 2008). Vale ressaltar que os espaços entre fibras pode promover maior vascularização e transporte de nutrientes por todo o *scaffold* (POOLOGASUNDARAMPILLAI *et al.*, 2014). Ainda, substratos vítreo-fibrosos podem favorecer a adesão, proliferação e diferenciação celular na região do defeito, permitindo que as células secretem matriz extracelular (*extracellular matrix*, ECM) para mineralização e formação óssea (PASCU, STOKES e MCGUINNESS, 2013).

Lin *et al*. (2014) investigaram os efeitos angiogênicos de fibras produzidas a partir de biovidro de borato implantadas subcutaneamente em ratos e mostraram que o biovidro de borato promoveu maior angiogênese comparado ao 45S5 e ao grupo controle. A biocompatibilidade das fibras também foi avaliada por meio de histologia e nenhuma evidência de anormalidades hispatológicas foram encontradas, indicando que o uso das fibras de biovidro pode ser seguro e efetivo na regeneração tecidual (LIN *et al.*, 2014). Em outro estudo, Poologasundarampillai *et al*. (2014) produziram *scaffolds* com fibras flexíveis de sílica (SiO_2-CaO) a partir do método sol-gel, buscando materiais que tivessem um melhor ajuste a defeitos ósseos complexos. Tal estudo indicou a formação de camada de HCA sobre as fibras no período de 12 h após imersão em SBF (*simulated body fluid*), além de nenhum efeito citotóxico das fibras em cultura com MC3T3, inclusive favorecendo a adesão e proliferação celular (POOLOGASUNDARAMPILLAI *et al.*, 2014). Estudos *in vivo*

conduzidos por Gu *et al*. (2013) investigaram os efeitos de *scaffolds* fibrosos compostos por silicato e borato na regeneração óssea de defeitos em calvária de ratos. Gu *et al*. (2013) observaram que estes *scaffolds* fibrosos apresentaram uma arquitetura porosa e interconectada que favoreceu a indução e condução do reparo ósseo, além de uma taxa de degradação controlada, características que podem beneficiar a regeneração óssea (GU *et al*., 2013).

Seguindo essa linha, com a intenção de buscar novas formas de apresentação de biovidros e aumentar seu espectro de utilização clínica, os pesquisadores Souza, Zanotto e Peitl-Filho do Laboratório de Materiais Vítreos (LaMaV) do Departamento de Engenharia de Materiais (DEMa) da Universidade Federal de São Carlos (UFSCar) desenvolveram um novo *scaffold* vítreo fibroso, pertencente ao sistema $SiO_2-Na_2O-K_2O-MgO-CaO-P_2O_5$ (Patent Application BR 10 2013 020961 9; Fundação Universidade Federal de São Carlos, 2013) (SOUZA, 2013). A hipótese levantada foi a de que este novo biomaterial poderia levar a uma melhoria no desempenho biológicos dos BGs, ao integrar alta porosidade e alta bioatividade, apresentando morfologia mais adequada para facilitar a migração celular e vascularização. Isto proporcionaria um enxerto ósseo com vantagens adicionais para o uso clínico, expandindo-se as possíveis aplicações do biomaterial. Na medicina, tais fibras que compõem o *scaffold* podem vir ser utilizadas em cirurgias ortopédicas, no tratamento de fraturas e de deformidades craniofaciais (SOUZA, 2011; 2013). Além disso, as fibras poderiam substituir malhas de titânio utilizadas tanto na odontologia como na medicina. Tal substituição diminuiria os riscos de infecção, as perdas de enxerto e o próprio desconforto do paciente em cirurgias de fraturas, pois não haveria a necessidade de remoção da malha após a integração do enxerto ósseo com o tecido local (CORTEZ, RABELO e MAZZONETTO, 2004). Outra aplicação das fibras bioativas é sua utilização em feridas e ulcerações cutâneas que demoram

a cicatrizar ou não conseguem se regenerar sem o auxílio de uma intervenção terapêutica (MELICAN, 2008; LIN *et al.*, 2014).

Cumpre ressaltar que, apesar das atuais pesquisas com vidros bioativos, pouco se sabe sobre os possíveis efeitos adversos induzidos pelo material, bem como seus efeitos no tecido ósseo. Por meio disto, nota-se a necessidade de estudos que possam: (i) investigar as características morfológicas de novas composições e formas de biomateriais; (ii) comprovar sua viabilidade biológica, através de testes que verifiquem sua biocompatibilidade, bem como seu potencial osteogênico.

Diante do exposto e tomando por base o fato de não existirem na literatura estudos que investiguem a biocompatibilidade e o potencial osteogênico desse novo *scaffold* vítreo fibroso, este trabalho visa contribuir de forma significativa com informações importantes para a viabilização desse biomaterial.

Nesse sentido, foram feitos testes essenciais para avaliar a possível existência de reações indesejadas com a aplicação do material, levando em consideração a sua compatibilidade com o tecido biológico adjacente e sua possível toxicidade celular e genética. Essa avaliação biológica dos *scaffolds* é indispensável, pois se pode verificar se este material possui um potencial tóxico que perturbe o sistema celular, levando a inibição do crescimento e/ou morte das células, ou criando danos ao material genético, podendo desencadear diversos problemas ao organismo onde será implantado. Além disso, os testes de *performance* do material durante o processo de reparo ósseo são de grande importância para a verificação da biocompatibilidade com o tecido em questão e para a busca e desenvolvimento de novas abordagens clínico-terapêuticas no reparo ósseo.

2 Objetivos

Os objetivos deste estudo podem ser sistematizados em três pontos principais:

(i) avaliar a bioatividade do vidro bioativo precursor (por meio de solução de SBF-K9; *Simulated Body Fluid*) e caracterizar o novo *scaffold* vítreo fibroso em termos de estrutura morfológica, medidas de pH e perda de massa;

(ii) avaliar a biocompatibilidade desse novo biomaterial, por meio da avaliação das respostas biológicas induzidas pelo mesmo. Mais especificamente, foram utilizados testes *in vitro*, com a introdução dos *scaffolds* em cultura de células e testes *in vivo*, com a implantação subcutânea desse biomaterial no dorso de ratos;

(iii) verificar os efeitos desse novo *scaffold* vítreo fibroso na consolidação de defeitos ósseos induzidos em tíbias de ratos.

3 Materiais e métodos

3.1 Preparo dos *scaffolds* vítreo-fibrosos

Os *scaffolds* vítreo-fibrosos foram obtidos a partir de uma nova composição vítrea bioativa desenvolvida por pesquisadores do LaMaV. O vidro bioativo pertence ao sistema SiO_2-Na_2O-K_2O-MgO-CaO-P_2O_5 (SOUZA, 2013) e foi preparado e homogeneizado em um cadinho de platina, misturando-se cuidadosamente e fundindo os reagentes químicos a 1200 ºC (triturando-se e refundindo a mistura a 1200 ºC por 5 vezes adicionais). Após a produção do vidro, fibras bioativas foram puxadas em uma torre de fibras produzida também no LaMav. Posteriormente, *scaffolds* circulares altamente porosos foram obtidos utilizando-se fibras com 3 mm de comprimento a temperatura ambiente. As fibras foram pesadas e, aleatoriamente, colocadas em um molde cilíndrico de politetrafluoroetileno para a obtenção de amostras na forma de discos. *Scaffolds* de 10 mm x 2 mm (diâmetro x espessura) foram utilizados para os testes de biocompatibilidade e para os estudos de caracterização do material. Adicionalmente, *scaffolds* de 3 mm x 1 mm (diâmetro x espessura) foram utilizados para os estudos do efeito desse novo biomaterial no reparo ósseo.

3.2 Caracterização dos *scaffolds* vítreo-fibrosos

3.2.1 Morfologia via microscopia eletrônica de varredura (MEV)

A estrutura dos *scaffolds* foi analisada através de um microscópio eletrônico de varredura (LEO 440, LEO Electron Microscopy, Ltd.). Adicionalmente, a morfologia dos *scaffolds* – após 1, 7 e 14 dias de imersão em tampão fosfato salino (phosphate-buffered saline, PBS, 10 mM, pH 7,4) – também foi avaliada via MEV para visualização, em diferentes aumentos, da degradação do biomaterial.

3.2.2 Porosidade

Para análise da porosidade, os *scaffolds* foram imersos em resina epóxi sob vácuo e, após endurecimento, eles foram polidos com lixas (200 a 1200 grit), recobertos com ouro e examinados via MEV (Phenom™, FEI, Company) (KARAGEORGIOU e KAPLAN, 2005; GHASEMI-MOBARAKEH, SEMNANI e MORSHED, 2007; NARAYAN, 2009; MIRHADI, 2014). A razão de área vidro/epóxi foi medida usando o programa Image J (1,46r), utilizando-se 15 imagens fotográficas representativas para determinação da porosidade média dos *scaffolds*.

3.2.3 Avaliação da mineralização

Testes *in vitro* utilizando solução de SBF-K9 foram conduzidos seguindo a metodologia de Kokubo (KOKUBO *et al.*, 1990) com a intenção de se comprovar a bioatividade da nova composição vítrea e avaliar a taxa de degradação e formação da camada de HCA. Para tal, amostras do vidro foram cortadas em cilindros de aproximadamente 2 mm de altura x 12 mm de diâmetro, e então, polidas com lixas de carbeto de silício (400 grit). Todas as amostras foram lavadas e limpas com solução de álcool isopropilíco em um limpador ultrassônico por 20 minutos (min). Posteriormente, as amostras foram imersas em SBF-K9 e colocadas em recipientes de polietileno com razão da área de superfície do vidro/volume de 0,1 cm^{-1}. A formação da camada de HCA foi analisada usando Espectroscopia de Infravermelho por Transformada de Fourier (FTIR) (Perkin Elmer, Spectrum GX, DE) depois de 4, 8, 12 e 16 horas (h).

3.2.4   Medidas de pH e perda de massa

Para as avaliações de pH e perda de massa, os *scaffolds* foram colocados em 3 mL de PBS e incubados a 37 ºC em banho-maria sobre mesa agitadora (70 rpm) durante 1, 7, e 14 dias. Os ensaios foram realizados em triplicata (n=3). Após cada período experimental, os *scaffolds* foram retirados da solução e submetidos às análises.

3.2.4.1   pH

Diretamente após a retirada dos *scaffolds* do banho-maria, o pH da solução de PBS foi medido (Meterlab PHM210, calibrado com tampões IUPAC, S11M002, S11M004, S11M007 da Radiometer Analytical, Villeurbanne, França).

3.2.4.2   Perda de massa

A cada período experimental, os *scaffolds* foram retirados da solução e secos a vácuo durante a noite antes de se medir a massa. A perda de massa de cada amostra foi calculada utilizando a seguinte fórmula:

$$\% \text{ perda de massa} = [(M_f - M_i)/M_i] \times 100\%,$$

Onde M_i é massa da amostra antes da imersão em PBS e M_f é a massa da amostra depois da imersão em PBS.

3.3   **Estudo *in vitro***

Para a avaliação biológica *in vitro*, foram realizados os testes de citotoxicidade e genotoxicidade em cultura de células. Estes testes foram desenvolvidos no Laboratório de

Cultivo Celular da Universidade Nove de Julho e no Laboratório Multidisciplinar do Departamento de Biociências da UNIFESP/BS respectivamente.

3.3.1 Cultura de células

As linhagens de células L929 (fibroblastos) e OSTEO-1 (osteoblastos) murinos foram utilizadas nos experimentos *in vitro* de citotoxicidade e genotoxicidade do biomaterial. Tais tipos celulares foram cultivados em garrafas de cultura, utilizando meio de Eagle Modificado por Dulbecco (DMEM, Vitrocell, Campinas, SP, Brazil) suplementado com 10% de Soro Fetal Bovino (SFB) e 1% de solução antibiótica-antimicótica (Vitrocell, Campinas, SP, Brazil) a 37 ºC em atmosfera úmida de 5% de CO_2. As células foram mantidas em densidades subconfluentes e passadas a cada 2-3 dias até a sua utilização.

3.3.2 Ensaio de citotoxicidade

Com a análise de citotoxicidade foram avaliados os efeitos dos produtos de lixiviação dos *scaffolds* vítreo-fibrosos na proliferação celular das linhagens OSTEO-1 e L929. A citotoxicidade foi avaliada pelo ensaio MTT. Nesse ensaio colorimétrico quantitativo, as células viáveis metabolizam o MTT (brometo de 3-[4,5-dimetil-tiazol-2-il]-2,5-difeniltetrazólio), produzindo cristais de formazan de cor violeta. Estes cristais podem ser observados ao microscópio ou extraídos e dissolvidos com solventes orgânicos, permitindo quantificação por espectrofotometria (MOSMANN, 1983). Assim, é possível verificar a viabilidade celular.

Para isso, cada linhagem celular foi dividida em dois grupos, controle (CG) e biomaterial (BG), analisados em períodos distintos de cultivo de 24, 72 e 144 h. No CG as células foram cultivadas apenas com o meio DMEM suplementado com SFB. No BG as

células foram cultivadas com meio DMEM suplementado com SFB, contendo produtos da lixiviação dos *scaffolds* (extratos). Para a obtenção dos extratos, o biomaterial foi introduzido em tubos Falcon e imerso em DMEM seguindo a relação de 1:5 (g/mL). O meio com o material foi incubado a 37 ºC e após 7 dias de incubação, o extrato foi obtido e testado, em diferentes concentrações, com as culturas de células (ISO IOFS, 2009; FERNANDES *et al.*, 2010). O meio DMEM em contato com o biomaterial por 7 dias será considerado meio concentrado 100%. A partir desse serão realizadas diluições de 50, 25 e 12,5% (LIU *et al.*, 2009) para avaliar a influência dessas diferentes concentrações na proliferação celular das linhagens testadas.

Para a realização da análise de MTT, uma concentração de 1×10^3 células foi semeada diretamente em cada poço de uma placa de cultura de 96 poços e depois da confluência, o meio será substituído pelo extrato (200 µL/poço). Posteriormente, foi adicionada 50 µL da solução de MTT (0,5 mg/mL) (Sigma–Aldrich, St. Louis, MO) em cada poço. Subsequentemente, as células foram incubadas em 5% de CO_2 a 37 ºC por 3 h. Por final, o MTT foi descartado e adicionado isopropanol a todos os poços. A absorbância foi medida a 620 nm utilizando um espectrofotômetro Anthos 2020 (Anthos Labtec Instruments, Wals, Austria). Foram realizados 3 experimentos independentes sempre em quadruplicata.

3.3.3 Ensaio de genotoxicidade

O ensaio de genotoxicidade foi feito através do teste Cometa ou SCGE (*Single Cell Gel Electrophoresis Assay*) (TICE *et al.*, 2000) capaz de detectar danos no DNA das células OSTEO-1 e L929 cultivadas com o extrato dos *scaffolds*. Com esta finalidade, as células das culturas subconfluentes foram contadas e distribuídas em placas de cultura de 12 poços. Foram utilizadas 2×10^4 células em 2 mL de meio DMEM com 10% de SFB em cada poço da

placa de cultura. Cada linhagem celular foi dividida em dois grupos (CG e BG), avaliados em períodos distintos de 24, 72 e 144 h. Como CG as células foram cultivadas em meio DMEM suplementado com SFB. Por sua vez, o BG foi cultivado em contato com os *scaffolds* (1 *scaffold* por poço), previamente condicionados por um período de 7 dias em meio DMEM (1 *scaffold*/2 mL de meio DMEM), durante todos os períodos experimentais. Os experimentos foram realizados em triplicata.

Subsequentemente a cada período experimental, os poços das placas de cultura foram lavados com PBS, tripsinizados e as células adicionadas em tubos de 50 mL. Os tubos foram centrifugados a 1200 rpm por 5 min. O meio DMEM foi descartado e as células ressuspendidas com 1 mL de um novo meio DMEM. Depois de realizada esta etapa, um volume de 100 µL de meio DMEM foi adicionado a 120 µL de agarose de baixo ponto de fusão à 37 ^{o}C e depositado sobre lâminas histológicas recobertas com 0,5% agarose de ponto de fusão normal (Invitrogen Corporation, Nova York) a 37 ºC. Após, as lâminas foram recobertas com lamínulas para a homogeneização adequada do material e em seguida colocadas em solução de lise (2,5 M NaCl, 100 mM EDTA, Merck, St. Louis; 10 mM tampão Tris–HCl pH10, Sigma–Aldrich, St. Louis; 1% sarcosinato de sódio, Sigma–Aldrich, St. Louis; com 1% Triton X-100, Sigma–Aldrich, St. Louis; e 10% dimetilsulfóxido, Merck, St. Louis) por aproximadamente 1 h. Posteriormente, as mesmas foram lavadas com PBS durante 5 min e colocadas em uma cuba de eletroforese contendo solução tampão alcalina, pH>13 (0,3 mM NaOH, Merck, St. Louis; e 1 mM EDTA, Merck, St. Louis), até o líquido as cobrirem totalmente. Antes da eletroforese, as lâminas permaneceram por um período de descanso de 20 minutos, seguida por um período de eletroforese de 20 min a 25 V (0,86 V/cm) e 300 mA. Findada esta etapa, as lâminas foram lavadas com solução de neutralização

(0,4 M Tris, pH 7,5) e fixadas com etanol 100% (Merck, Darmstadt, Alemanha). Após a fixação, as lâminas foram coradas com 100 µL de brometo de etídio (50 mg/mL).

A análise de 50 cometas por tratamento e por período foi realizada em um aumento de 400x. Esta avaliação foi feita utilizando uma câmera montada em um microscópio de fluorescência (Olympus, Orangeburg) e conectada a um programa de análise de imagens (Comet Assay II, Perceptive Instruments, Sufolk, Haverhill, RU). Para quantificar o dano ao DNA, foi utilizado o momento da cauda. O momento da cauda foi calculado como o produto do comprimento da cauda pela fração de DNA contida nesta área. O momento da cauda do cometa é positivamente correlacionado com o nível de quebras no DNA em uma célula. O valor médio do momento da cauda em uma determinada amostra foi adotado como o índice de danos no seu DNA.

3.4   Estudos *in vivo*

Os experimentos foram realizados no laboratório de Eletrotermofototerapia do Departamento de Fisioterapia da UFSCar, sob responsabilidade e supervisão da Profa. Dra. Ana Cláudia Muniz Rennó e do Prof. Dr. Paulo Sérgio Bossini. Os estudos foram conduzidos conforme o Guia de Cuidados e Uso de Animais de Laboratório e com a aprovação da Comissão de Ética em Experimentação Animal da UFSCar (ANEXO A – Parecer da Comissão de Ética n° 043/2012).

3.4.1 Animais utilizados nos experimentos

Para a realização dos experimentos foram utilizados 60 ratos (*Rattus norvegicus: varalbinus, Rodentia, Mammalia*), da linhagem *Wistar*, machos, com três meses de idade e cerca de 300g de massa corporal média. Os animais permaneceram em biotério apropriado,

em gaiolas de polipropileno padrão e foram mantidos em ambiente higienizado. A iluminação foi ciclo claro/escuro de 12 h e os animais receberam água e ração balanceada à vontade.

3.4.2 Grupos experimentais

Os animais foram distribuídos aleatoriamente nos seguintes grupos:

(A) Grupo Controle (CG): os ratos deste grupo foram submetidos à cirurgia no dorso e nas tíbias[1] sem a implantação dos *scaffolds*. O GC foi composto por 30 animais, sendo 10 animais por período experimental, com sacrifícios no 15º, 30º e 60º dia pós-cirúrgico.

(B) Grupo Biomaterial (BG): os ratos deste grupo foram submetidos às cirurgias[2] com a implantação de *scaffolds* tanto no tecido subcutâneo dorsal, como nos defeitos ósseos induzidos de ambas as tíbias. Tal grupo foi composto por 30 animais, sendo 10 animais por período experimental, com sacrifícios no 15º, 30º e 60º dia pós-cirúrgico.

3.4.3 Cirurgias

Todos os ratos utilizados na pesquisa passaram por pesagem e de acordo com a proporção da massa corporal, foram anestesiados com uma associação de Ketamina/Xilazina (80/10 mg/kg). Os anestésicos foram injetados via intraperitoneal com uma seringa do mesmo tipo da utilizada na aplicação de insulina. Além disso, buprenorfina foi administrada também intraperitonealmente (0,02 mg/kg) logo após a cirurgia e subcutaneamente no 1º e 2º dias pós-cirúrgicos.

---

[1] Os detalhes das cirurgias estão na seção 3.4.3.
[2] Idem.

3.4.3.1 Implantação dos *scaffolds* no tecido subcutâneo dos animais para os testes de biocompatibilidade

Após anestesia, a região dorsal foi tricotomizada digitalmente, expondo a pele e, em seguida, foi feita assepsia do local com gaze embebida no Iodo Povidine (PvPi). Utilizando-se de um bisturi, foi realizada uma incisão reta, paralela à linha sagital mediana, expondo o tecido subcutâneo dorsal. Em seguida, foi realizado um divulsionamento do espaço subcutâneo para a confecção de uma bolsa, no interior da qual foram implantados os *scaffolds* vítreo-fibrosos. O grupo controle foi submetido á cirurgia sem a implantação dos *scaffolds*. Terminado o procedimento cirúrgico, foram realizadas suturas com fio cirúrgico Vicryl® 5-0 (Johnson&Johnson, St.Stevens-Woluwe, Bélgica) e os animais foram acondicionados no biotério, em caixas com livre acesso à ração e água até o momento da eutanásia.

3.4.3.2 Defeito ósseo e tratamento com o biomaterial

O defeito ósseo foi realizado em ambas as tíbias de todos os animais. As lesões foram feitas com a utilização de uma mini-furadeira (450 rpm) acionada por um minidril com uma broca trefina de 2 mm de diâmetro interno, irrigada constantemente com soro fisiológico para evitar queimaduras do tecido ósseo. Com essa broca trefina foi possível a confecção de defeitos ósseos de 3 mm de diâmetro que foram preenchidos pelo *scaffold* (3 mm de diâmetro x 1 mm de espessura). Todo o procedimento foi realizado sob anestesia de Ketamina/Xilazina.

Após anestesia, tricotomia e assepsia do local a ser operado, os defeitos ósseos foram feitos 10 mm abaixo da articulação do joelho, por meio de uma incisão no terço proximal da tíbia. A lesão foi realizada com a broca mantida na posição vertical e perpendicular em relação ao eixo longitudinal do osso, de modo a penetrar a cortical medial, mas sem atingir a face contralateral. Logo após a realização do defeito ósseo, os *scaffolds* foram aplicados, por

meio de uma pinça, para o preenchimento do defeito. Em seguida, a musculatura e a pele foram suturadas com fio cirúrgico Vicryl® 5-0 (Johnson&Johnson, St.Stevens-Woluwe, Bélgica). Em relação ao grupo controle, os ratos foram submetidos a todo o procedimento cirúrgico acima descrito, mas sem a implantação dos *scaffolds*. Por fim, os animais foram mantidos em caixas individuais com livre acesso á água e ração até o momento da eutanásia.

3.4.4 Eutanásia

Os animais foram sacrificados após 15, 30 e 60 dias dos procedimentos cirúrgicos por asfixia com CO_2. Após tal procedimento, foi realizada a retirada cirúrgica das tíbias esquerda e direita, assim como do material implantado no subcutâneo dorsal de cada animal. Todo material coletado foi devidamente armazenado para processamento e utilização em análises posteriores.

3.4.5 Procedimentos histológicos

Após a coleta das amostras (implantes subcutâneos e tíbias direitas), tais materiais foram fixados com formalina tamponada a 10% (Merck, Darmstadt, Alemanha) por 24 h. Em seguida, as tíbias passaram por descalcificação com solução de EDTA 10%. Ambas as amostras passaram por processamento histológico com inclusão em parafina para posterior obtenção de cortes histológicos. Foram preparadas seções de aproximadamente 5 μm perpendiculares ao eixo médio-lateral dos implantes utilizando um micrótomo (Leica Microsystems SP 1600, Nussloch, Alemanha). A análise das lâminas, coradas com Hematoxilina e Eosina (H.E.Stain, Merck), foi realizada com o auxílio de microscópio óptico (Olympus, Optical Co. Ltd, Tokyo, Japão).

3.4.5.1 Análise histopatológica semiquantitativa dos implantes subcutâneos dorsais

A avaliação semiquantitativa dos implantes com o tecido adjacente foi feita em quatro campos pré-determinados com o auxílio de uma escala de classificação histológica (Tabela 1). Os dados foram representados como a média desses quatro campos de análise (LINK *et al.*, 2008). Tal análise foi feita através de avaliação cega por pares.

Tabela 1. Escala de classificação histológica para os implantes subcutâneos (Adaptada de LINK *et al.*, 2008)

Avaliação	Resposta	*Score*
Quantitativa de fibroblastos	1-4	4
	5-9	3
	10-30	2
	>30	1
	Não aplicável	0
Qualitativa da cápsula	A cápsula é fibrosa, madura e não densa	4
	A cápsula é fibrosa, mas imatura, apresentando fibroblastos e pouco colágeno	3
	A cápsula é granulosa e densa. Presença de fibroblastos e muitas células inflamatórias	2
	A cápsula é composta por grande quantidade de células inflamatórias com pouca ou nenhuma organização do tecido conjuntivo	1
	Não pode ser avaliada por causa da infecção ou outros fatores não necessariamente relacionados ao material	0
Qualitativa da interface	Fibroblastos em contato com a superfície do implante. Ausência de macrófagos ou leucócitos	4
	Presença de focos espalhados de macrófagos e leucócitos	3
	Presença de uma camada de macrófagos e leucócitos	2
	Presença de múltiplas camadas de macrófagos e leucócitos	1
	Não pode ser avaliada por causa da infecção ou outros fatores não necessariamente relacionados ao material	0

3.4.5.2 Análise histopatológica dos implantes tibiais

Com o auxilio de um microscópio óptico (Olympus, Optical Co. Ltd, Tokyo, Japão) foi possível observar com esta análise as seguintes características no local da lesão: infiltrado inflamatório, tecido de granulação, tecido ósseo neoformado, organização tecidual óssea, biomaterial e necrose tecidual. Estes achados foram classificados em leve, moderado e intenso de acordo com os aspectos histológicos presentes. Esta análise foi realizada através de avaliação cega por pares.

3.4.6 Análise morfométrica

Para a análise morfométrica, cortes histológicos das tíbias foram quantitativamente avaliados utilizando técnicas de análise de imagens computacionais (Axioplan 2, Carl Zeiss, Jena, Alemanha). Imagens digitalizadas dos defeitos (20x) foram obtidas e a quantidade de osso neoformada foi determinada em 3 regiões de interesse: ROI1 (margem esquerda superior), ROI2 (margem esquerda inferior) e ROI3 (região central da margem direita) (OLIVEIRA *et al.*, 2010; BOSSINI *et al.*, 2011). A quantidade total de osso neoformada foi representada com ROI1+ROI2+ROI3 (em micrômetros quadrados; μm^2). A presente análise foi feita por meio de avaliação cega por pares.

3.4.7 Análise imunohistoquímica dos implantes tibiais

Para a análise imunohistoquímica, xileno foi utilizado para remoção da parafina dos cortes seriados de 5 μm. Depois desta etapa, os cortes foram reidratados em etanol e pré-tratados em um micro-ondas (Electrolux, São Paulo, Brasil) com 0,01 M de tampão de ácido cítrico (pH 6) por três ciclos de 5 min cada a 850 W para recuperação antigênica. O material

resultante foi pré-incubado com solução de 0,3% de peróxido de hidrogênio em PBS por 5 min para inativação da peroxidase endógena. Posteriormente, as amostras foram bloqueadas com 5% de soro de cabra em PBS por 10 min. As amostras foram incubadas com anticorpos primário policlonal: anti-RUNX-2 (código: sc-8566, Santa Cruz Biotechnology, EUA), anti-RANK-L (código: sc-7627, Santa Cruz Biotechnology, EUA) e anti-COL-1 (código sc-8784, Santa Cruz Biotechnology, EUA), todos nas concentrações de 1:200. A incubação foi feita durante a noite a 4 ºC em refrigerador. Esta etapa foi seguida de duas lavagens em PBS por 10 min. Os cortes foram então incubados com biotina conjugada ao anticorpo secundário anti-IgG de coelho (Vector Laboratories, Burlingame, CA, EUA) a uma concentração de 1:200 em PSB por 1 h. Os cortes foram lavados duas vezes com PBS, seguido da aplicação do complexo avidina-biotina-peroxidase (Vector Laboratories) por 45 min. Para a visualização dos complexos, foi aplicada diaminobenzidina e contracoloração com Hematoxilina de Harris. Como controle dos anticorpos, houve o tratamento dos cortes histológicos com anticorpo IgG (Vector Laboratories) em uma concentração de 1:200.

A imunoexpressão de RUNX-2, RANK-L e COL-1 foram avaliadas qualitativamente e quantitativamente. A análise qualitativa foi realizada para se avaliar a presença (ou ausência) e região de ocorrência dos imunomarcadores. No que se refere à investigação quantitativa, esta análise foi feita para se avaliar a intensidade da imunomarcação de cada imunomarcador, em 4 campos pré-determinados no interior do defeito, de acordo com uma escala de *scores* de 1 a 4 (1=ausente, 2=fraco, 3=moderado e 4=intenso) (PEDROSA *et al.*, 2009; MATSUMOTO *et al.*, 2012). A análise foi realizada por meio de avaliação cega por pares, utilizando-se um microscópio óptico (Leica Microsystems AG, Wetzlar, Alemanha).

3.4.8 Análise biomecânica

A análise biomecânica foi realizada por meio do teste de flexão de três pontos na tíbia esquerda dos animais de todos os grupos. Para tanto, foi utilizada uma máquina de ensaio universal Instron, modelo 4444.

Na realização dos testes foi utilizada uma célula de carga com capacidade máxima de 1 kN, pré-carga de 5 N e velocidade constante de 0,5 cm/min. Ambas as extremidades das tíbias foram apoiadas em dois suporte metálicos. As tíbias foram posicionadas com a região do defeito voltado para baixo e a força foi aplicada perpendicularmente ao eixo longitudinal do osso por uma haste cilíndrica até o momento da fratura. A força aplicada e o deslocamento do endentador foram monitorados e registrados por meio de um *software* do próprio equipamento. A partir da curva de carga/deformação foram obtidos os valores de carga máxima (N) (RENNO *et al.*, 2006).

3.5 Análise estatística

Os dados dos estudos de caracterização e biológicos (*in vitro* e *in vivo*) foram analisados na forma de médias, desvios-padrão e erro padrão da média. O teste de normalidade de Shapiro-Wilk's foi utilizado para todas as variáveis. Nos casos de distribuição normal da amostra, as comparações foram feitas pela análise de variância (ANOVA), complementada pelo teste *post-hoc* de Tukey. As análises foram realizadas no software STATISTICA 7.0 (data analysis software system - StatSoft Inc.). Para as conclusões das análises estatísticas foi utilizado o nível de significância de 5% ($p \leq 0,05$).

4 Estudo I – Publicado no periódico "*Journal of Tissue Engineering and Regenerative Medicine*" (ANEXO B)

Characterization and biocompatibility of a fibrous glassy scaffold

Gabbai-Armelin PR, Ms[1,4]; Souza MT, Ms[2]; Kido HW, Ms[1,4]; Tim CR, Ms[1,4]; Bossini PS, PhD[3]; Fernandes KR, Ms[3]; Magri AMP, Ms[3];Parizotto NA, PhD[4]; Fernandes KPS, PhD[5]; Mesquista-Ferrari RA, PhD[5]; Ribeiro DA, PhD[3]; Zanotto, ED, PhD[2]; Peitl-Filho O, PhD[2],Renno ACM, PhD[3,*].

[1]*Post-Graduate Program of Biotechnology, Federal University of São Carlos (UFSCar), São Carlos, SP, Brazil*

[2]*Vitreous Materials Laboratory (LaMaV), Department of Materials Engineering, Federal University of São Carlos (UFSCar), São Carlos, SP, Brazil*

[3] *Department of Biosciences, Federal University of São Paulo (UNIFESP), Santos, SP, Brazil*

[4]*Department of Physiotherapy, Federal University of São Carlos (UFSCar), São Carlos, SP, Brazil*

[5] *Department of Rehabilitation Sciences and Biophotonics Applied to Health Sciences, Nove de Julho University (UNINOVE), São Paulo, SP, Brazil*

* Corresponding author:

Ana Claudia Muniz Renno, PhD

Dept. of Biosciences

Federal University of São Paulo (UNIFESP)

Avenida Ana Costa 95, Santos, SP

Zip code: 11050-240

Brazil

Phone: +55-13-32218303

Fax: +55-13-32218305

E-mail: a.renno@unifesp.br

Abstract. Bioactive glasses (BGs) are known for their ability to bond to living bone and cartilage. In general, they are readily available in powder and monolithic forms, which are not ideal for the optimal filling of bone defects with irregular shapes. In this context, the development of BG-based scaffolds containing flexible fibers is a relevant approach to improve the performance of BGs. This study is aimed at characterizing a new highly porous fibrous glassy scaffold and evaluating its *in vitro* and *in vivo* biocompatibility. The developed scaffolds were characterized in terms of porosity, mineralization and morphological features. Additionally, fibroblast and osteoblast cells were seeded in contact with extracts of the scaffolds to assess cell proliferation and genotoxicity after 24, 72 and 144 h. Finally, scaffolds were placed subcutaneously in rats for 15, 30 and 60 days. The scaffolds presented interconnected porous structures, and the precursor bioglass could mineralize a hydroxycarbonate apatite (HCA) layer in SBF after only 12 h. The biomaterial elicited increased fibroblast and osteoblast cell proliferation, and no DNA damage was observed. The *in vivo* experiment showed degradation of the biomaterial over time, with soft tissue ingrowth into the degraded area and the presence of multi-nucleated giant cells around the implant. At day 60, the scaffolds were almost completely degraded, and an organized granulation tissue filled the area. The results highlight the potential of this fibrous glassy material for bone regeneration due to its bioactive properties, non-cytotoxicity and biocompatibility. Future investigations should focus on translating these findings to orthotopic applications.

Keywords: Biocompatibility, biomaterial, bioactive glass, fibrous scaffold, bone repair, cytotoxicity

4.1 Introduction

Bone fractures occur daily worldwide, with 6.2 million cases being reported per year in the United States alone (CLAES e WILLIE, 2007). Among these, 5-10% showed delayed healing, with some persisting for more than nine months or even resulting in non-union fractures. Multiple factors can impair fracture consolidation, including significant bone loss caused by diseases, trauma or tumor resection (GAUTIER e SOMMER, 2003). To ensure the proper repair of the skeleton and decrease the chances of complications from abnormal bone repair, the development of strategies based on the mechanisms of the fracture healing process is required (GAUTIER e SOMMER, 2003).

Biomaterials that can induce bone biomineralization have been in high demand for clinical regenerative medicine and tissue engineering (HENCH, 2006). They combine a number of materials of natural or synthetic origins that have the capacity to chemically adhere to bone tissue (HUBBELL, 1998; HENCH e POLAK, 2002).

Bioactive glasses (BGs) have been widely used to improve bone healing and accelerate bone metabolism (HENCH, 2006). The most known bioactive glass is Bioglass[®] 45S5, which presents the highest bioactivity index so far reported. It is a silica-based melt or gel-derived glass characterized by a SiO_2 content of less than 60%, high Na_2O and CaO contents, and a high $CaO:P_2O_5$ ratio. Many studies have shown that Bioglass[®] 45S5 stimulates *in vitro* osteogenesis, inducing the proliferation of human osteoblasts, and accelerates bone consolidation in animal experimental models (XYNOS *et al.*, 2000; XIE *et al.*, 2009; GRANITO *et al.*, 2011). Additionally, the angiogenic potential of Bioglass[®] 45S5 has been demonstrated (DAY *et al.*, 2005; GORUSTOVICH, ROETHER e BOCCACCINI, 2010).

In general, bioactive glasses are primarily available as powders and monoliths. One of the main disadvantages of those forms is that an optimal filling of irregularly shaped bone defects is extremely difficult (DAY *et al.*, 2005; VALLET-REGI, 2006). Additionally, the lack of interconnected pores in the implants limits inner cell ingrowth. To overcome these limitations, the interest in alternative products, such as malleable/fibrous porous implants and BG-based scaffolds, has increased (CHEN, THOMPSON e BOCCACCINI, 2006; RAHAMAN *et al.*, 2011; JONES, 2013; LACROIX, JALLOT e LAO, 2014). These products are particularly interesting because they are a more suitable filler for different size or forms of bone defects and present an interconnected porous structure (MOIMAS *et al.*, 2006; BROWN *et al.*, 2008).

In view of the growing interest in the development of more efficient materials to be used as bone grafts, it is hypothesized that the development of a brand new porous fibrous glassy scaffold, belonging to the SiO_2-Na_2O-K_2O-MgO-CaO-P_2O_5 system, might offer a novel way of improving the biological performance of BGs.

The new fibrous biomaterial aims to integrate high porosity with high bioactivity, which is typical of BGs, to increase the application range of the material. Despite these possible advantages, before this biomaterial can be used clinically, it is necessary to investigate its physico-chemical characteristics and subsequent biological responses. Consequently, the aim of the current study was to investigate the morphological features and the *in vitro* and *in* vivo biocompatibilities of the new fibrous glassy scaffolds. To this end, the precursor bioactive glass was evaluated by *in vitro* studies with SBF-K9 solution, and the manufactured scaffolds were analyzed by scanning electron microscopy (SEM), pH measurements and mass loss quantification. In addition, the biocompatibility was evaluated by *in vitro* (i.e., indirect cell proliferation and evaluation of DNA damage) and *in vivo* (i.e., subcutaneous implantation)

studies. For this purpose, MTT and comet assays were performed in fibroblast and osteoblast cells, which were seeded in contact with biomaterial extracts after 24, 72 and 144 h. Also, scaffolds were implanted subcutaneously in rats for histocompatibility evaluation after 15, 30 and 60 days of implantation.

4.2 Materials and methods

4.2.1 Material preparation

The fibrous glassy scaffolds were manufactured using fibers obtained from a new bioactive glass composition of the SiO_2-Na_2O-K_2O-MgO-CaO-P_2O_5 system (SOUZA, 2013). The bioactive glass was prepared and homogenized in a platinum crucible by thoroughly mixing and melting the chemical reagents at 1200°C (crushing and remelting at 1200°C 5 additional times). After the production of the glass, bioactive fibers were drawn in a homemade fiber tower. This new composition was developed with the specific aim of producing fibers because the traditional 45S5 glass is not able to be drawn into fibers.

After this procedure, highly porous circular scaffolds (10 mm x 2 mm) were obtained using chopped fibers (3 mm length) at room temperature. The fiber fragments were weighed and randomly placed in a cylindrical poly tetrafluoroethylene mold to obtain a disc-shaped sample using moderate compression stress.

The morphology of the scaffolds was analyzed by a scanning electron microscope (LEO 440, LEO Electron Microscopy, Ltd.).

4.2.2 Characterization of the fibrous glassy scaffold

4.2.2.1 Porosity measurements

To measure their porosity, the scaffolds were immersed in epoxy resin under vacuum and, after hardening, they were polished from 200 to 1200 grit, sputter coated with gold and examined by SEM (Phenom™, FEI, Company) (KARAGEORGIOU e KAPLAN, 2005; GHASEMI-MOBARAKEH, SEMNANI e MORSHED, 2007; NARAYAN, 2009; MIRHADI, 2014). The glass/epoxy area ratio was measured using the ImageJ (1,46r) software, using 15 representative photographic images to determine the mean porosity of the scaffolds.

4.2.2.2 Mineralization Evaluation

In vitro tests using simulated body fluid K9 (SBF-K9) solution were conducted using Kokubo's methodology (KOKUBO *et al.*, 1990) to verify the bioactivity of this new glass composition and evaluate the degradation rate and formation of HCA layer. Briefly, glass samples were cut into cylinders of approximately 2 mm height and 12 mm diameter and then polished with 400-grit silicon carbide paper. All samples were rinsed and cleaned with isopropyl alcohol solution in an ultrasonic cleaner for 20 minutes. Then, the samples were immersed in SBF-K9 solution and placed into a sealed polyethylene bottle with a glass surface area to volume ratio of 0.1 cm^{-1}. The HCA layer formation was analyzed by Fourier transform infrared spectroscopy (FTIR) (Perkin Elmer, Spectrum GX, DE) after periods of 4, 8, 12 and 16 h.

4.2.2.3 pH measurements and mass loss quantification

For the pH and mass loss evaluations, the scaffolds were placed in 3 ml of phosphate buffered saline (PBS, 10 mM, pH 7.4) and incubated at 37°C in a water bath on a shaker table (70 rpm) for 1, 7 and 14 days. The assays were performed in triplicate (n=3). After the experimental periods, scaffolds were removed from the solution and subjected to analysis.

4.2.2.3.1 pH measurements

Directly after the removal of the scaffolds from the water bath, the pH of the PBS medium was measured (Meterlab PHM210, calibrated with IUPAC buffers, S11M002, S11M004, S11M007 from Radiometer Analytical, Villeurbanne, France).

4.2.2.3.2 Mass loss quantification

At each time point, the scaffolds were removed from the solution and vacuum-dried overnight before measuring the mass. The mass loss of a sample was calculated using the following formula:

$$\text{Mass loss \%} = [(W_t - W_0)/W_0] \times 100\%,$$

where W_0 is the weight of the sample before immersion in PBS and W_t is the weight of the sample after immersion in PBS.

4.2.3 *In vitro* study

4.2.3.1 *Cell culture*

In the *in vitro* study, L929 (murine fibroblasts) and OSTEO-1 (neonatal murine calvarial osteoblastic) cells were used for cytotoxicity and genotoxicity studies. These cell lineages were selected because of their close contact to the fibrous scaffold in ectopic and orthotopic applications of the biomaterial. Additionally, L929 lineages are widely used for biocompatibility tests (SERRANO *et al.*, 2008; NATH, KALMODIA e BASU, 2010; LIU e CHANG, 2012; KIDO *et al.*, 2013).

Both cell types were cultured in Dulbecco's Modified Eagle Medium (DMEM, Vitrocell, Campinas, SP, Brazil) supplemented with 10% fetal bovine serum (Vitrocell, Campinas, SP, Brazil) and 1% antibiotic–antimycotic solution (Vitrocell, Campinas, SP, Brazil) at 37°C in a humidified atmosphere of 5% CO_2. Cells were maintained at subconfluent densities and subcultured every 2–3 days until use.

4.2.3.2 Cytotoxicity analysis

In the cytotoxicity analysis, an indirect assay (MTT) was used to measure the effects on cell viability of the products leached from the fibrous glassy scaffolds (MOSMANN, 1983), according to Kido *et al*. (2013). L929 and OSTEO-1 cells were divided into a control group (CG) and a biomaterial group (BG). In the CG, only DMEM was used to culture the cells, whereas in the BG, the cells were grown with fibrous glassy scaffold extracts. These extracts were obtained by immersing and incubating the scaffolds in supplemented DMEM at 37°C for 7 days. This DMEM was considered to be 100% concentrated with the extracts. From this primer solution, different dilutions were obtained (50%, 25%, and 12.5%) (LIU *et*

al., 2009). This procedure was used to evaluate the influence on the cell proliferation of different ions concentrations leached from the biomaterial. CG and BG cells were cultured at 1×10^3 cells per well (96-well plates) for periods of 24, 72, and 144 h.

After finishing each time point, the culture plates wells were washed using PBS, and 50 µL of MTT solution (0.5 mg/mL) (Sigma–Aldrich, St. Louis, MO) was added to each well. Then, the cells were incubated in 5% CO_2 at 37°C for 3 h. Subsequently, each well received 100 µL of isopropanol to dissolve the formazan crystals. A microplate (Anthos 2020, Anthos Labtec Instruments, Wals, Austria) was used to measure the absorbance reader at 620 nm. Three independent measurements were taken in quadruplicate.

4.2.3.3 Genotoxicity analysis

The potential damage to the DNA of fibroblastic and osteoblastic cells, which were grown with the extract of the fibrous glassy scaffold, was evaluated through an electrophoresis test in a single cell gel (i.e., a comet assay) (TICE *et al.*, 2000). This test was necessary to guarantee the safety of this new biomaterial for using as bone graft in further investigations. It is worth mentioning that genotoxicity studies are also part of (ISO)-10993-3 (ISO IOFS, 2003) and have achieved general acceptance as serious and useful indicators of carcinogenicity (NAGHAVI *et al.*, 2014). For this purpose, 2×10^4 cells were added to each well of a 12-well plate. The cells were immersed in 2 mL of supplemented DMEM. Fibroblastic and osteoblastic cell lines were distributed in two groups (CG and BG) and were assessed at 24, 72, and 144 h. The CG cells were cultured in supplemented DMEM without any treatment, whereas the BG cells were cultured with fibrous glassy scaffold (one scaffold per well), which was previously incubated in DMEM for 7 days (1 scaffold per 2 mL of medium). This assay was performed in triplicate. As the experimental periods were reached,

the culture plate wells were washed with PBS, trypsinized, and the cells were placed into a 50-mL flask. The flasks were centrifuged for 5 min at 1200 rpm. Subsequently, the DMEM was removed, and the cells received 1 mL fresh DMEM. After this procedure, 100 μL of DMEM was added to 120 μL of 0.5% low-melting point agarose (Invitrogen Corporation, New York) at 37ºC. The material was gently placed onto a 1.5% agarose pre-coated slide and covered with a coverslip. After agarose solidification inside the refrigerator, the coverslip was removed and the slides were immersed for approximately 1 h in lysis solution (2.5 M NaCl, 100 mM EDTA, Merck, St. Louis; 10 mM Tris–HCl buffer pH10, Sigma–Aldrich, St. Louis; 1% sodium sarcosinate, Sigma–Aldrich, St. Louis; with 1% Triton X-100, Sigma–Aldrich, St. Louis; and 10% dimethyl sulfoxide, Merck, St. Louis). Prior to the electrophoresis, the slides were soaked in alkaline buffer for 20 min (0.3 mM NaOH, Merck, St. Louis; and 1 mM EDTA, Merck, St. Louis; pH >13). The electrophoresis was performed at 25 V (0.86 V/cm) and 300 mA for 20 min. After this procedure, the slides were neutralized in 0.4 M Tris–HCl (pH7.5), fixed in 100% ethanol (Merck, Darmstadt, Germany) and stained with 100 μL ethidium bromide (50 mg/mL). Ultraviolet radiation and reduced room lights were used in every step to reduce external DNA damage. The examination of 50 comets per treatment per period was performed at a magnification of 400x. This examination was captured with a black and white camera mounted on a fluorescence microscope (Olympus, Orangeburg) and connected to an image analysis software (Comet Assay II, Perceptive Instruments, Sufolk, Haverhill, UK). To measure the DNA damage, the tail moment was calculated. The comet tail moment is given by the product of the tail length and the fraction of DNA in the comet tail and is positively associated with the level of DNA damage in the cell. The tail moment mean value in a specific sample was assumed to be the index of DNA damage.

4.2.4 *In vivo* study

4.2.4.1 Experimental design and surgical procedure

In the *in vivo* investigation, 30[3] healthy young adult male Wistar rats (12 weeks old, weight 295 ± 29 g) were used. This study was approved by the Animal Care Committee guidelines of the Federal University of São Carlos (protocol 043/2012) and the Guiding Principles for the Care and Use of Laboratory Animals were observed. All animals received one implant placed subcutaneously into the dorsal area to evaluate the histopathological characteristics of this fibrous glassy scaffold.

Anesthesia was induced by intra-peritoneal injection of Ketamine/ Xylazine (80/10 mg/Kg). Buprenorfine (Temgesic; Reckitt Benckiser Health Care Limited, Schering-Plough, Hoddesdon, UK) was administered intraperitoneally (0.02mg/kg) directly after the operation and subcutaneously for 2 days after surgery, to minimize post-operative discomfort.

To insert the subcutaneous implants, the rats were immobilized on their dorsal region, and their skin was shaved and disinfected with iodine. A 2-cm incision was made in the median sagittal line 8 cm from the skull, and a subcutaneous pocket was created by blunt dissection. The implants were randomly placed (n = 1 per animal) and the skin was sutured with resorbable Vicryl® 5-0 (Johnson&Johnson, St.Stevens-Woluwe, Belgium).

The animals were housed in pairs and maintained at 24 ± 2°C, with light-dark periods of 12 h and free access to water and food. In the initial postoperative period, the intake of water and food was monitored. Furthermore, the animals were observed for signs of pain,

---

[3] Na seção 3.4.1 consta que 60 animais foram utilizados nos experimentos. No entanto, no presente manuscrito (Estudo I) são listados apenas 30 ratos. Isso se deve pelo fato dos outros 30 animais utilizados como controle (apenas cirurgia sem implantação do *scaffold*) não apresentarem nenhuma anormalidade, indicando que a cirurgia não causou nenhuma complicação aos animais. Assim, os animais utilizados como controle não são citados ou descritos no manuscrito para publicação.

infection and activity. After 15, 30 and 60 days post-surgery, the animals were sacrificed by CO_2 asphyxiation, and the biomaterials and the surrounding tissue were harvested for histopathological analyses.

4.2.4.2   Histological procedures

After the subcutaneous implants were harvested, all samples were fixated in 10% buffered formalin (Merck, Darmstadt, Germany) for 24h. Then, the samples were dehydrated in a graded series of ethanol and embedded in paraffin. After polymerization, the specimens were submitted to histological analysis. Thin sections (6µm) perpendicular to the longitudinal axis of the implants were prepared using a microtome (Leica Microsystems SP 1600, Nussloch, Germany). At least two sections of each specimen were stained with hematoxylin and eosin (H.E.Stain, Merck).

4.2.4.3   Histological evaluation

The qualitative and quantitative histological evaluations were performed under an optical microscope (Olympus, Optical Co., Ltd, Tokyo, Japan). In the qualitative analysis, the tissue response to each subcutaneous implant was assessed by evaluating the following aspects: inflammation, granulation tissue and the presence of the biomaterial. Concerning the quantitative analysis, a histological grading scale – established by Jansen *et al*. (1994) and posteriorly used by Link *et al*. (2008), and Renno *et al*. (2013) – was used to evaluate the capsule thickness, the tissue response of the capsule surrounding the subcutaneous implant and also the tissue directly adjacent to the implant surface. These evaluations were performed in 4 pre-determined fields of at least two sections of each specimen (JANSEN *et al.*, 1994;

LINK *et al.*, 2008; RENNO *et al.*, 2013). Two experienced observers (PA and HK) performed the scoring (table 1a) in a blinded manner.

Table 1a. Histological grading scale for soft tissues

Evaluation	Response	Score
Capsule thickness	1–4 cell layers	4
	5–9 cell layers	3
	10–30 cell layers	2
	>30 cell layers	1
	Not applicable	0
Tissue response of the capsule surrounding the implants	Fibrous, mature, not dense, resembling connective or fat tissue in the non-injured regions.	4
	Fibrous, but immature, showing fibroblasts and little collagen.	3
	Granulous and dense, containing both fibroblasts and many inflammatory cells.	2
	Consists of masses of inflammatory cells with little or no signs of connective tissue organization.	1
	Cannot be evaluated because of infection or factors not necessarily related to the material.	0
Tissue response directly adjacent to the implant surface (interface)	Fibroblasts contact the implant surface without the presence of macrophages or foreign body giant cells.	4
	Scattered foci of macrophages and foreign body cells are present.	3
	One layer of macrophages and foreign body cells is present.	2
	Multiple layers of macrophages and foreign body cells are present.	1
	Cannot be evaluated because of infection or other factors not necessarily related to the material.	0

4.2.5 Statistical analysis

Statistical data were expressed as the mean and the standard error (SE) of the mean values for each sample. The software utilized for this purpose was STATISTICA7.0. The statistical comparisons were performed using one-way analysis of variance (ANOVA) with a Tukey multiple comparison post-test. Differences were considered significant at $p \leq 0.05$.

4.3 Results

4.3.1 Characterization of the fibrous glassy scaffold

Figure 1(a) presents an overview of the fibrous glassy scaffold, which reveals that the fibers were displayed in a random way. Moreover, the SEM images at higher magnifications (i.e., 500x and 1000x, figures 1(b) and 1(c), respectively) demonstrated that the fibrous glassy scaffold was formed by interconnected porous structures.

4.3.1.1 Porosity measurements

The evaluation of porosity (via SEM) demonstrated a total porosity of $75 \pm 0.7\%$, with pores sizes up to 2 mm. In addition, the bioactive fibers presented diameters of approximately 45 µm (figure 1).

4.3.1.2 Mineralization evaluation

The infrared spectra of a newly formed bioactive glass surface, between 0 and 16 h, are presented in figure 2. After 12 h, peaks between 540 cm^{-1} and 415 cm^{-1} (Si–O–Si) were no longer detected, indicating that the silica-rich layer polymerized. The presence of two peaks at

approximately 610 and 560 cm^{-1} indicated that the HCA layer was formed and crystallized after only 12 h of soaking in SBF-K9 solution. These peaks became sharper and more intense over the immersion time, demonstrating the growth of crystalline apatite *in vitro*. For the morphological analysis of the HCA layer, SEM images were obtained after 16 h of immersion (figure 3). This SEM micrograph clearly shows the formation of the HCA layer on the glass surface. It is possible to observe the globular shape pattern that is commonly found after the precipitation and crystallization of HCA.
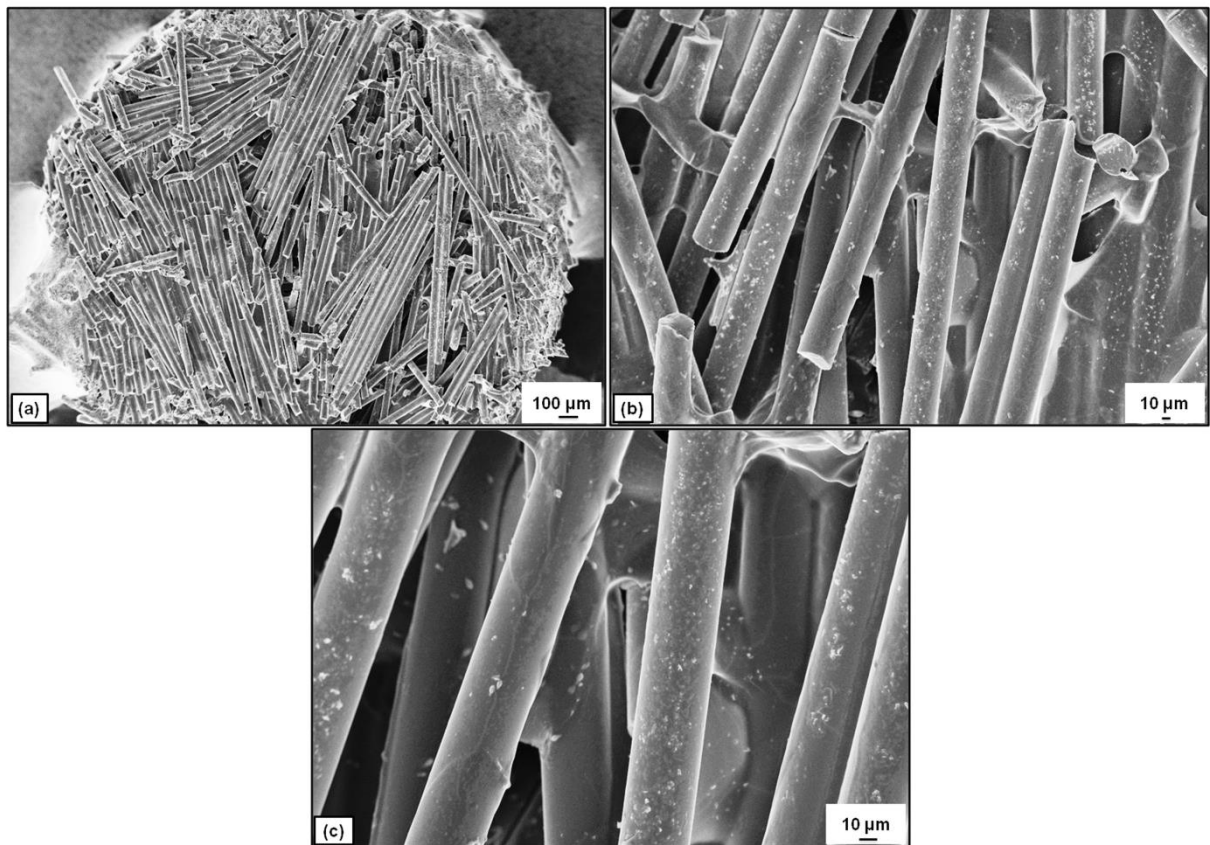
Figure 1. SEM images of the fibrous glassy scaffold: (a) overview, 100x; (b) and (c) higher magnifications of 500x and 1000x, respectively.
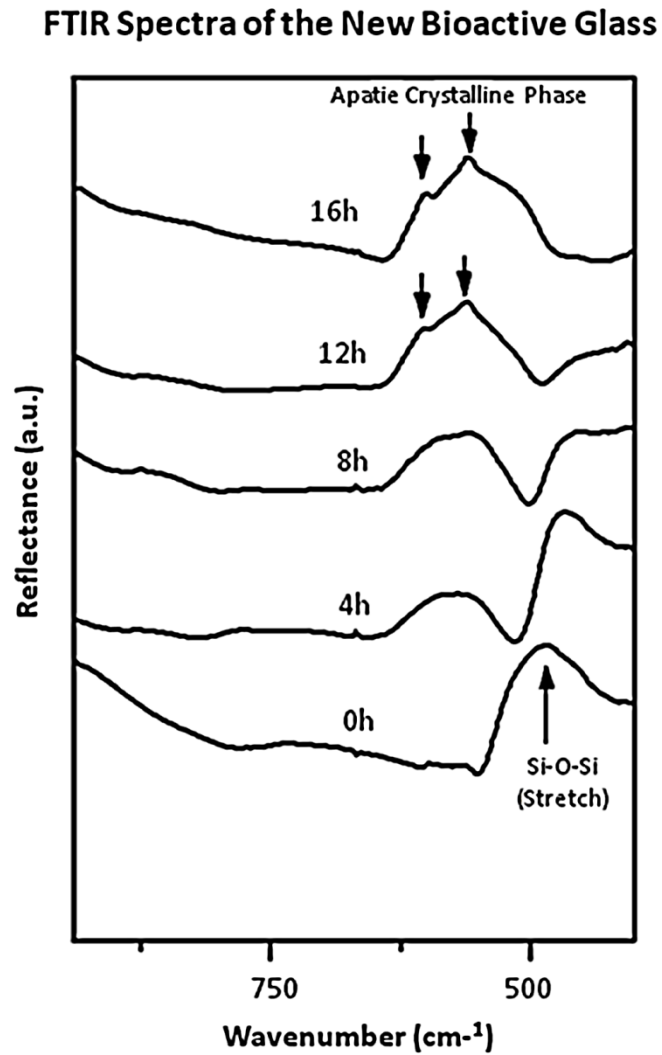
Figure 2. FTIR spectra of the new bioactive glass composition (samples in bulk form).

4.3.1.3 pH measurements

The results of the pH measurements during degradation are presented in figure 4. The medium of the pre-set samples showed a substantial pH increase reaching approximately 10 and 11 on days 1 and 7 of incubation, respectively. Furthermore, the pH significantly increased to 12 on day 14 of immersion ($p < 0.05$).
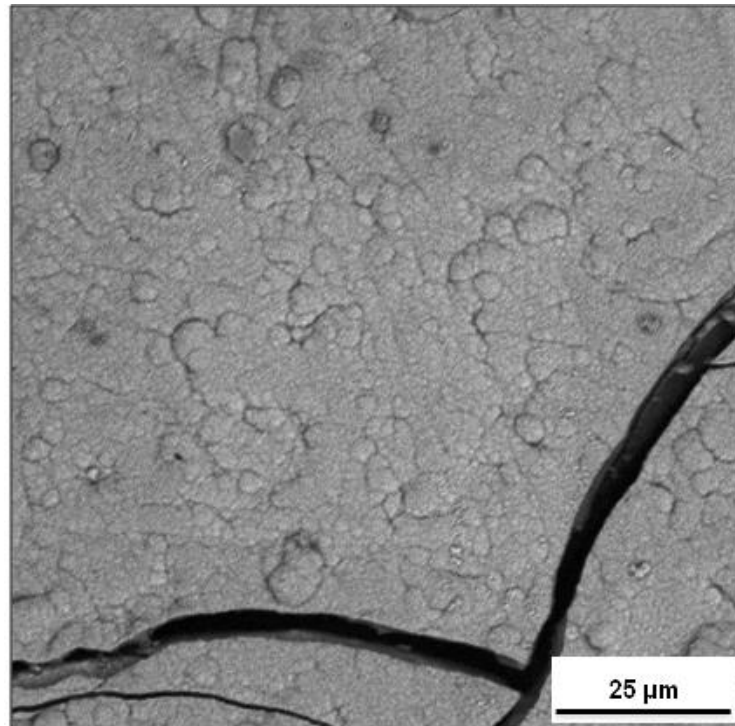
Figure 3. SEM micrograph of HCA layer on the glass surface after 16 h of immersion in SBF. Note the globular shape of the precipitated HCA. 2300x magnification.
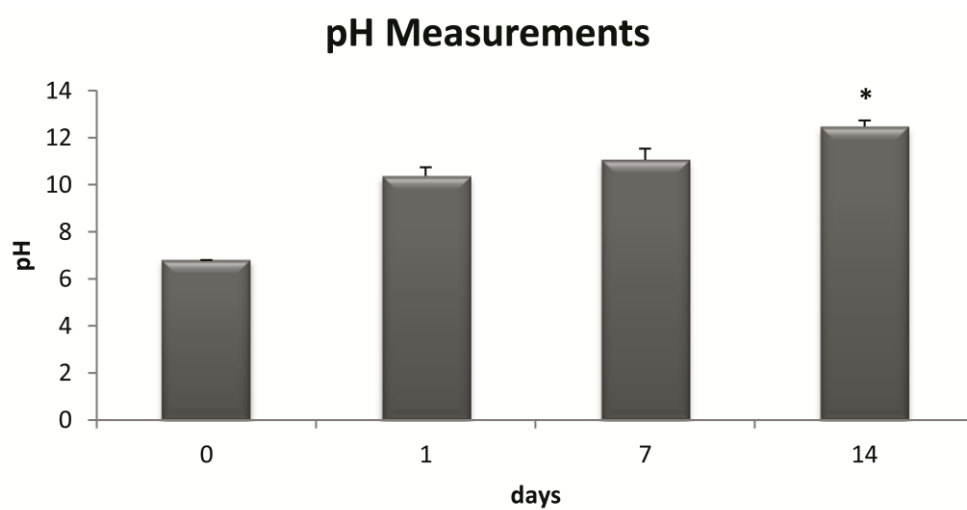
Figure 4. pH measurements of PBS after contact with fibrous glassy scaffold. (*)$p \leq 0.05$ versus 0, 1 and 7 days.

4.3.1.4   Mass loss quantification

The mass loss evaluation showed similar results when comparing the baseline measurements with the values found after 1 and 7 days of incubation ($p > 0.05$). On day 14, the mass loss significantly decreased compared with the other periods ($p < 0.05$) (figure 5).
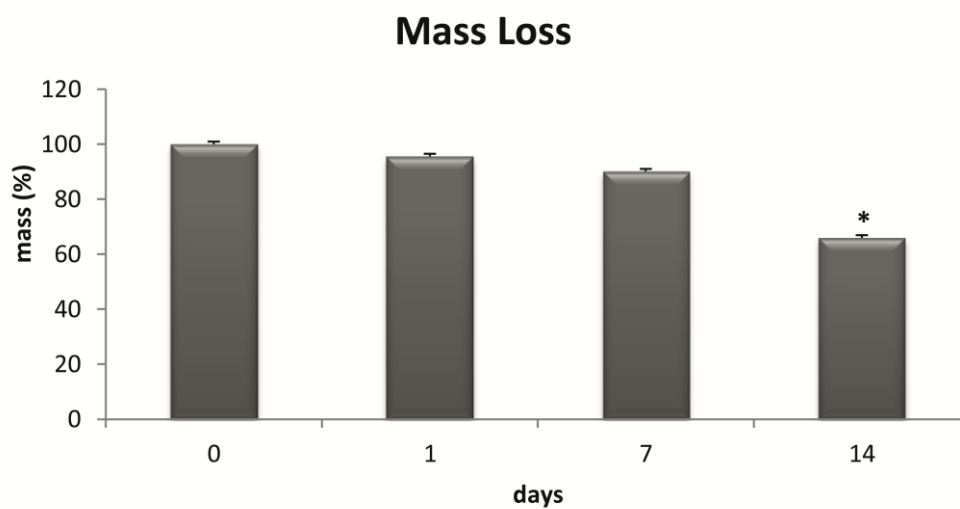
Figure 5. Mass loss of the fibrous glassy scaffold immersed in PBS up to 14 days. (*)$p \leq 0.05$ versus 0, 1 and 7 days.

4.3.2   *In vitro* results

4.3.2.1   Cytotoxicity analysis

In the fibroblast cytotoxicity assay, after 24 h, the CG cultures showed lower cell proliferation values compared with those of the groups cultured with 50% and 100% of biomaterial extract concentrations. Moreover, the group with a 100% concentration of the extract presented significantly higher fibroblast proliferation values compared with the groups

with 50%, 25% and 12.5% concentrations of the extract. After 72 h and 144 h, no significant differences were found among all groups (figure 6).
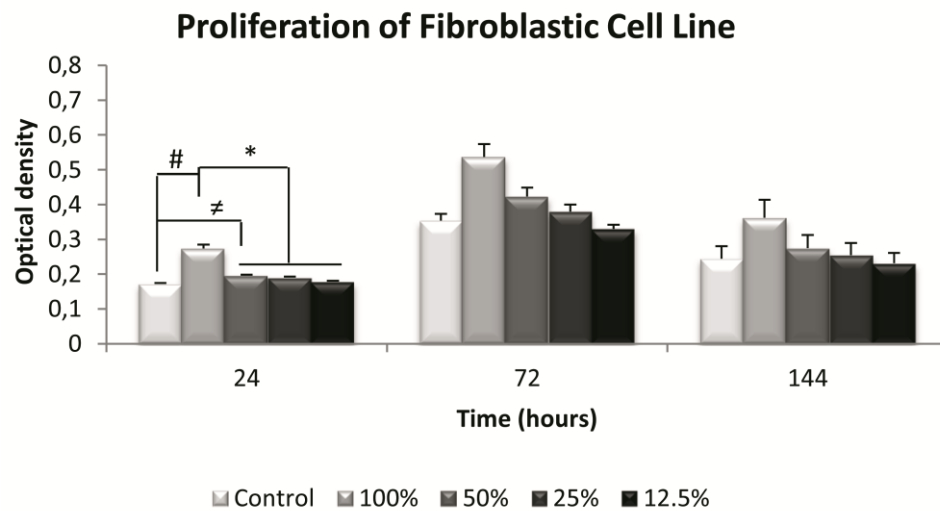
Figure 6. Proliferation of fibroblast cell line in solutions containing different concentrations of fibrous glassy scaffold extracts (100%, 50%, 25% and 12.5%) at different culture times (24, 72, and 144 h). (#)p ≤ 0.05 versus CG, (≠)p ≤ 0.05 versus CG, and (*)p ≤ 0.05 versus 50%, 25%, and 12.5%.

The osteoblast proliferation assay presented significant differences with the 3 different experimental periods. Twenty-four hours after seeding, the group with a 100% concentration of extract showed a significantly higher value of osteoblast cell proliferation than did the CG and the 12.5% group. After 72 h, a higher value of osteoblast proliferation in the 100% group was observed relative to the CG and 25% and 12.5% groups. Finally, 144 h after seeding, the 100% group showed a higher value of osteoblast proliferation compared with all other biomaterial extract concentrations groups. For this same period, a higher value of osteoblast proliferation in the 50% group was observed relative to the 25% and 12.5% groups (figure 7).

Proliferation of Osteoblastic Cell Line
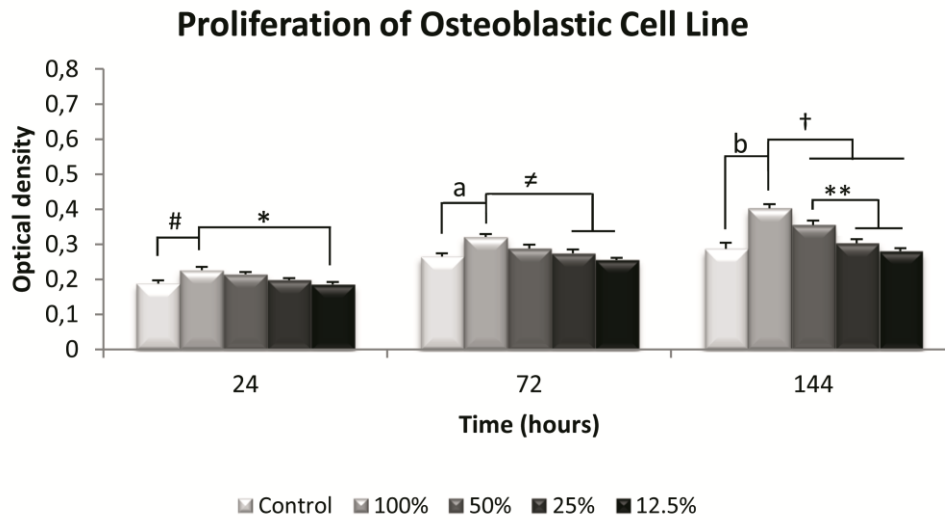
Figure 7. Proliferation of osteoblast cell line in solutions containing different concentrations of fibrous glassy scaffold extracts (100%, 50%, 25% and 12.5%) at different culture times (24, 72, and 144 h). (#)$p \leq 0.05$ versus CG, (*)$p \leq 0.05$ versus 12.5%, (a)$p \leq 0.05$ versus CG, ($\neq$)$p \leq 0.05$ versus 25% and 12.5%, (b)$p \leq 0.05$ versus CG, (†)$p \leq 0.05$ versus 50%, 25% and 12.5%, and (**)$p \leq 0.05$ versus 25% and 12.5%.

4.3.2.2 Genotoxicity analysis

The single cell gel (comet) assay was performed to measure DNA damage in fibroblastic and osteoblastic cell lines. There were no significant differences ($p > 0.05$) between the control and treated groups, indicating that the fibrous glassy scaffold did not induce DNA strand breaks in fibroblasts and osteoblasts for any evaluated period (table 2).

Table 2. Means and SE of the tail moment (DNA damage) in fibroblast and osteoblast cells

Time (h)	Experimental groups			
	Control[a]		Fibrous Glassy Scaffold	
	Fibroblast	Osteoblast	Fibroblast	Osteoblast
24	0.8+0.4	0.7+0.3	1.0+0.4	0.6+0.2
72	0.5+0.2	1.1+0.5	0.7+0.2	1.3+0.5
144	0.4+0.3	0.8+0.2	0.5+0.4	0.8+0.4

[a] DMEM, $p>0.05$.

4.3.3 *In vivo* results

4.3.3.1 General observation of the experimental animals

The animals showed no postoperative complications. They quickly returned to their normal diet and showed no loss of body mass. Furthermore, no animals died during the experiment, and no infections in the injured areas were detected.

4.3.3.2 Histopathological analysis of subcutaneous implants

15 days

Fifteen days after implantation, clear signs of material degradation were observed (figure 8(a)), with the presence of foreign body giant cells primarily around the fibers of the fibrous glassy scaffold. Granulation tissue was also noticed with moderate inflammation in the degraded area of the implant. Moreover, a granulous capsule was observed around the implant (figure 8(b)). In the biomaterial/tissue interface a moderate number of inflammatory cells were observed.
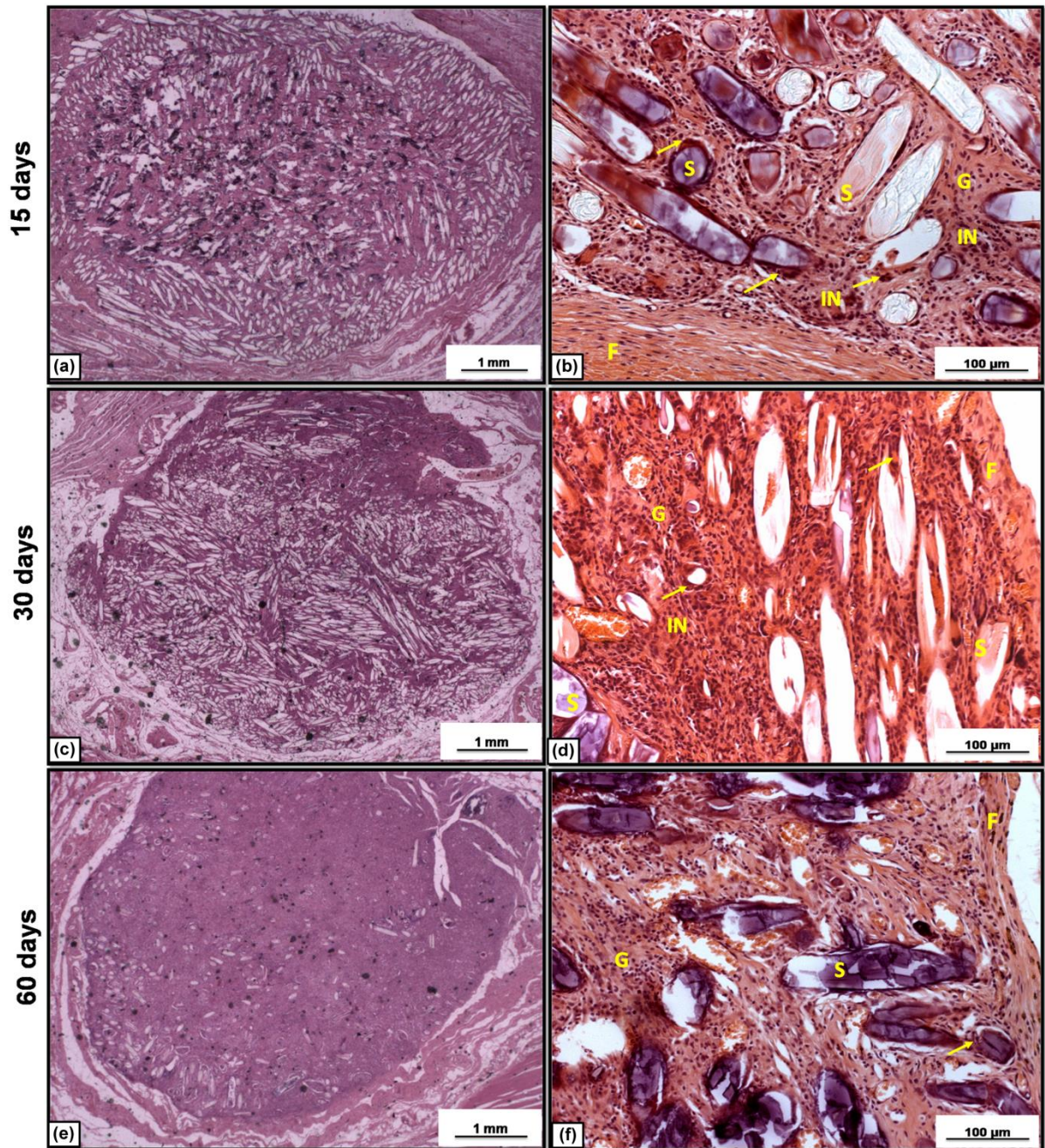
Figure 8. Representative histological subcutaneous implants of the three experimental periods; 15 days (ab), 30 days (c-d), and 60 days (e-f). Magnification of 12,5x: bar represents 1 mm. Magnification of 200x: Inflammatory cells (IN), Granulation tissue (G), Fibers of the bioactive glassy scaffold (S), Fibrous capsule (F), and multi-nucleated giant cells (arrows) are indicated in the sections. Bar represents 100 μm. Hematoxylin-Eosin staining.

30 days

After 30 days of implantation, the biomaterial degradation continued (figure 8(c)). Many foreign body giant cells, mainly around the fibers of the scaffold, were observed. Histological analyses revealed a greater amount of granulation tissue throughout the scaffold fibers compared with the previous period. Additionally, tissue ingrowth and inflammatory cells were noted in the voided spaces in the degraded biomaterial. Furthermore, a thinner mature fibrous capsule was observed, presenting fibroblasts and inflammatory cells (figure 8(d)). Directly adjacent to the surface of the implants (i.e., the interface), a moderate number of inflammatory cells were observed.

60 days

Implant degradation continued sixty days post-surgery to a larger extent compared with the other experimental periods (figure 8(e)). Tissue ingrowth was observed in the degraded areas, with an organized granulation tissue, resembling the connective tissue of the non-injured areas inside the implant. Some multi-nucleated giant cells were present around the fibers, though in some of the analyzed samples, no capsules were observed around the implants. The capsules, when present, had a thinner organized structure compared with the other periods (figure 8(f)). At the biomaterial/tissue interface, the fibroblasts contacted the implant surface without the presence of macrophages or other inflammatory cells.

4.3.3.3   Quantitative histological evaluation of subcutaneous implants

The results from the histological quantitative analysis of the subcutaneous implants are shown in figure 9. The capsules observed in the animals sacrificed on day 15 post-surgery were significantly thicker than those of the other groups (figure 9(a); $p < 0.05$). The quality of

the capsule and the quality of the interface were also significantly different between the samples at 60 days and at the other two analyzed periods (figures 9(b) and 9(c); $p < 0.05$).
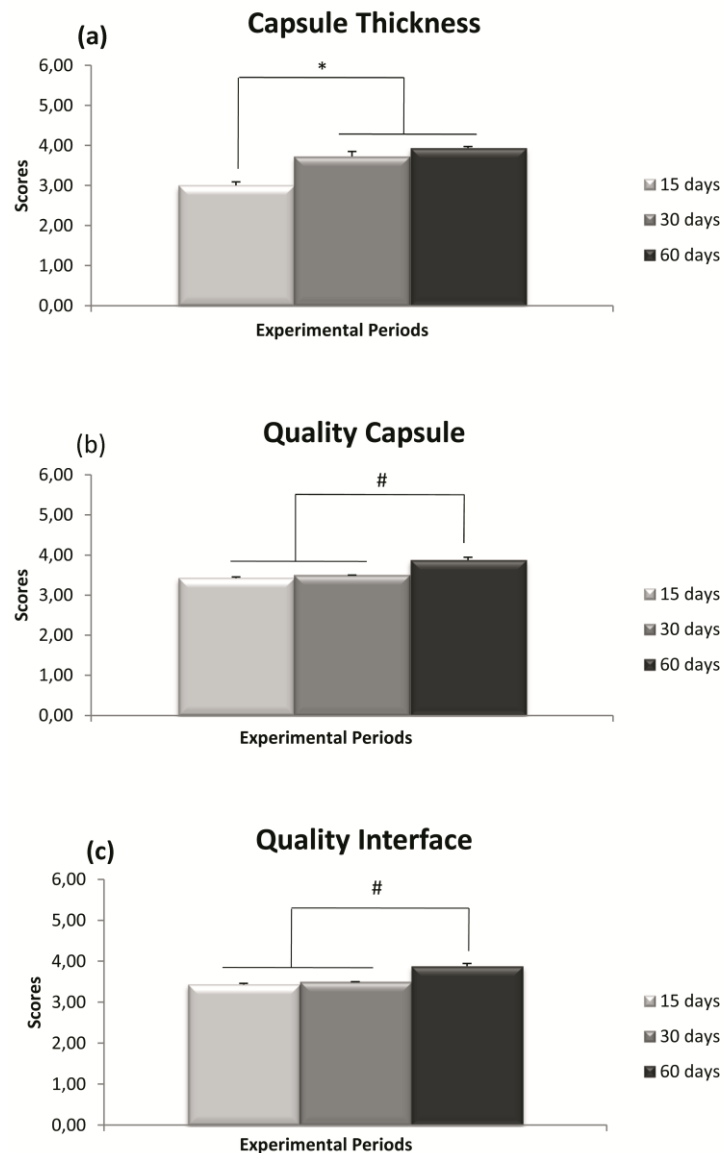
Figure 9. Histological evaluation of capsule thickness (a), the quality of the capsule (b) and the quality of the interface (c) of the subcutaneous implants after 15, 30 and 60 days of implantation using the histological grading scale. Error bars represent means ± standard error of the mean. (*)p < 0.05 compared with15 days, (#)p < 0.05 compared to with15 and 30 days.

4.4 Discussion

The present study evaluated the mineralization, physico-chemical properties, degradation behavior and biocompatibility of a fibrous glassy scaffold. The analysis demonstrated that the immersion of the scaffolds in SBF lead to the formation of a crystallized HCA layer on the material surface in a short period of only 12 h. Moreover, an increased pH and an accelerated mass loss were also observed in the samples upon immersion in PBS. The *in vitro* study demonstrated increased fibroblast and osteoblast cell proliferations and no cell DNA damage after cell seeding. The subcutaneous implantation showed that the biomaterial had indeed a favorable effect on soft tissue responses in terms of capsule thickness, capsule quality and interface quality.

Bioactivity is one of the most desirable characteristics for a material to be used for bone tissue engineering (HENCH, XYNOS e POLAK, 2004). The formation of the HCA layer observed in the FTIR evaluation indicates that this biomaterial possesses a very high *in vitro* bioactivity. Hence, it is possible to infer that for this new glass composition, the rate of *in vitro* formation of the HCA layer, as assessed using the SBF test, is similar to that for Bioglass 45S5, which takes approximately 8 h for an HCA layer formation (PEITL, DUTRA ZANOTTO e HENCH, 2001; HENCH, 2006; 2013). The SEM image for the 16-h sample clearly shows the presence of the HCA layer due to the easily detectable globular pattern of this crystalline phase. These data demonstrate that the porous fibrous glass composition is highly bioactive and reactive, and is suitable for the fabrication of scaffolds and tissue regeneration applications.

The pH measurements confirmed an alkalization of the immersion medium in the presence of the scaffold. The reactions at the sample interface were likely responsible for these observations. A release of ions (i.e., Si, Na, Ca and P) occurred immediately after the

BG scaffolds contacted the fluids, resulting in an increased pH (HENCH, XYNOS e POLAK, 2004; DAY *et al.*, 2005). Moreover, the mass loss evaluation showed a significant decrease in mass 14 days after immersion, but the samples did not collapse. This behavior may also be associated to the rapid ion release which is initiated immediately after the contact of BG with fluids, starting the degradation of the material (KOKUBO *et al.*, 1990; JONES, 2013). Accordingly, Misra *et al*. (2010) and Bretcanu *et al*. (2014)   also observed accelerated mass losses in a BG/poly(3-hydroxybutyrate) composite (approximately 15%) and in a resorbable phosphate glass scaffold (approximately 20%) after 14 days of immersion.

These leaching reactions (leading to ions release) are very common and well established for bioactive glasses and are defined by Hench as 5-stage reactions (HENCH, 2013). Briefly, in stage I, alkali and alkali earth ions are released from the glass into the fluid and are replaced by H^+ or H_3O^+ ions in the glass structure. This reaction increases the local pH, resulting in the rupture of Si-O-Si bonds. Then, in stage II, silicon is released into the fluid in the form of silanol groups ($Si(OH)_4$). In stage III, the silanols condensate forming a polymerized silica gel layer on the surface of the glass. Subsequently, in stage IV, calcium and phosphate ions, which had diffused from the glass or from the fluid, form an amorphous calcium phosphate layer over the silica gel. Following these reactions, in stage V, the amorphous calcium phosphate layer incorporates the carbonate species and crystallizes into HCA (HENCH, 2013).

The indirect cytotoxicity assay showed that the biomaterial at 100% concentration of extract produced a significant increase in fibroblast proliferation 24 h after seeding. For the osteoblast cells, increased proliferation rates were observed for all analyzed set points, especially for the 100% group. The differences between the behaviors of the cell lines may be explained by their morphological shapes. Fibroblasts are flattened cells; it has been reported

that this type of cell shows a higher proliferation rate than do round, spherical cells (FOLKMAN e MOSCONA, 1978; ARCHER, ROONEY e WOLPERT, 1982; WANG, 2003). Therefore, fibroblasts presented an earlier increased proliferation rate and earlier confluence compared with osteoblasts. The biomaterial degradation may have created a microenvironment that improved cellular activity and function. The cytotoxicity results demonstrated that the fibrous glassy scaffold did not present toxic potential. *In vitro* studies have demonstrated that different bioactive ceramics were also non-cytotoxic and were able to support significantly larger areas of *in vitro* calcified matrix in osteoblast cell cultures (MOURA *et al.*, 2007), to support the attachment of human bone-derived cells (RADETZKI *et al.*, 2011) and to stimulate the differentiation and proliferation of human osteoblastic-like cells (WU, RAMASWAMY e ZREIQAT, 2010).

The single cell gel (comet) assay detected no DNA damage for both tested cell lines, demonstrating that the fibrous glassy scaffold presented no genotoxic potential. From these results, it can be concluded that the dissolution products from the fibrous glassy scaffold did not affect the DNA cells. Such data are in agreement with the results of a previous study conducted by Kido *et al.* (2013), who observed no DNA strand breaks in fibroblasts and osteoblasts cultured on Biosilicate[®] scaffolds after 24, 72 and 96 h. Likewise, Pelaez *et al.* (2005) indicated no genotoxicity for ceramic coatings applied on stainless steel.

It is well known that biomaterial chemical features can affect tissue response and, consequently, modulate the foreign body reaction. Biomaterials may cause intense inflammatory responses and tissue irritation, which can culminate in delayed tissue healing (ANDERSON e MCNALLY, 2011). In contrast, the histopathological analysis showed that the implantation of the fibrous glassy scaffold produced a discrete foreign body reaction as evidenced by the presence of multinucleated giant cells around some fibers of the biomaterial

in all experimental periods. The granulation tissue was also observed to gradually occupy the spaces left by the degraded biomaterial. In addition, at day 60, an organized granulation tissue (resembling the connective tissue of non-injured regions) in larger degraded areas and a thinner-organized capsule with a better interface were observed compared with the other periods. Furthermore, the tissue organization in the implantation area improved over time. It was likely that the degradation products of the material did not cause a severe tissue irritation; instead, the degraded material was bioabsorped (AKAZAWA *et al.*, 2006; MURATA *et al.*, 2007), and consequently, the injured tissue gradually reorganized overtime.

Finally, the presence of interconnected pores is a key factor for tissue repair because it allows for the migration and proliferation of cells and promotes vascularization. Successful neovascularization results in higher oxygen supply and, consequently, in a readily available supply of nutrients for tissue repair (TABOAS *et al.*, 2003; KARAGEORGIOU e KAPLAN, 2005; REZWAN *et al.*, 2006; HOPPE, GULDAL e BOCCACCINI, 2011; BAINO e VITALE-BROVARONE, 2014; FRANCA *et al.*, 2014; YANG *et al.*, 2014). The high porosity and interconnected porous structures of the fibrous glassy scaffold, as assessed in this study, may be relevant to the success of the biological performance of the fibrous glassy material.

Based on the *in vitro* and *in vivo* results of the tested fibrous glassy scaffolds, this investigation shows that the present biomaterial may be used as a bone graft for accelerating tissue repair. Further histomorphometric and immunohistochemical studies on this new biomaterial, regarding bone defect models, are necessary to evaluate its *in vivo* efficacy.

4.5 Conclusions

Highly porous, fibrous glassy scaffolds (using a new bioactive glass composition, F18) were developed, showing high bioactivity and mineralization in SBF-K9 solution in approximately 12 h. These new fibrous glassy scaffolds were biocompatible. Preliminary cytotoxicity data justifies further biological studies to check how cells interact direct with the scaffolds. Taken together, these encouraging outcomes indicate the fibrous glassy scaffolds as promising materials for developing new types of therapeutic approaches related to health care and bone tissue engineering. However, additional long-term studies are required to fully investigate the behavior of this new biomaterial for potential ortothopic *in vivo* applications.

4.6 Acknowledgments

4.7 Justification for including each author

Concept and design: PR Gabbai-Armelin, MT Souza, PS Bossini, O Peitl-Filho, ACM Renno.

Acquisition of data: PR Gabbai-Armelin, HW Kido, CR Tim, KR Fernandes, AMP Magri, DA Ribeiro.

Analysis and interpretation: PR Gabbai-Armelin, HW Kido, CR Tim, PS Bossini, KR Fernandes, DA Ribeiro, ACM Renno.

Drafting of manuscript: PR Gabbai-Armelin, CR Tim, MT Souza, ED Zanotto, ACM Renno.

Critical revision of manuscript for important intellectual content: ED Zanotto, ACM Renno.

Statistical analyses: PR Gabbai-Armelin, AMP Magri, ACM Renno.

Funding: PR Gabbai-Armelin, MT Souza, NA Parizotto, KPS Fernandes, RA Mesquista-Ferrari, ED Zanotto, ACM Renno.

Technical support: PR Gabbai-Armelin, HW Kido, CR Tim, PS Bossini, KR Fernandes, AMP Magri, KPS Fernandes, RA Mesquista-Ferrari

Study supervision: O Peitl-Filho, ACM Renno.

4.8   Conflict of interest

There are no conflicts of interest.

5 Estudo II – Aceito para publicação no periódico "*Journal of Materials Science: Materials in Medicine*" (ANEXO C)

Effect of a new bioactive fibrous glassy scaffold on bone repair

Gabbai-Armelin PR, Ms[1,5,*]; Souza MT, Ms[2]; Kido HW, Ms[1,5]; Tim CR, Ms[1,5]; Bossini PS, PhD[3]; Magri AMP, Ms[3]; Fernandes KR, Ms[3]; Pastor FAC, PhD[4]; Zanotto ED, PhD[2]; Parizotto NA, PhD[5]; Peitl-Filho O, PhD[2]; Renno ACM, PhD[3].

[1] *Post-Graduate Program of Biotechnology, Federal University of São Carlos (UFSCar), Rodovia Washington Luís (SP-310), km 235, São Carlos, SP, Brazil*

[2] *Vitreous Materials Laboratory (LaMaV), Department of Materials Engineering, Federal University of São Carlos (UFSCar), Rodovia Washington Luís (SP-310), km 235, São Carlos, SP, Brazil*

[3] *Department of Biosciences, Federal University of São Paulo (UNIFESP), Avenida Ana Costa 95, Santos, SP, Brazil*

[4] *Department of Physiological Sciences, Federal University of São Carlos (UFSCar), Rodovia Washington Luís (SP-310), km 235, São Carlos, SP, Brazil*

[5] *Department of Physiotherapy, Federal University of São Carlos (UFSCar), Rodovia Washington Luís (SP-310), km 235, São Carlos, São Paulo, Brazil*

* Corresponding author:

Paulo Roberto Gabbai Armelin, Ms

Dept. of Physiotherapy

Federal University of São Carlos (UFSCar)

Rodovia Washington Luís (SP-310), km 235, São Carlos, SP

Brazil

Phone: +55-16-33518985

Fax: +55-16-33518980

E-mail: paulogabbai@gmail.com

Abstract

Researchers have investigated several therapeutic approaches to treat non-union fractures. Among these, bioactive glasses and glass ceramics have been widely used as grafts. This class of biomaterial has the ability to integrate with living bone. Nevertheless, bioglass and bioactive materials have been used mainly as powder and blocks, compromising the filling of irregular bone defects. Considering this matter, our research group has developed a new bioactive glass composition that can originate malleable fibers, which can offer a more suitable material to be used as bone graft substitutes. Thus, the aim of this study was to assess the morphological structure (via scanning electron microscope, SEM) of these fibers upon incubation in phosphate buffered saline (PBS) after 1, 7 and 14 days and, also, evaluate the *in vivo* tissue response to the new biomaterial using implantation in rat tibial defects. The histopathological, immunohistochemistry and biomechanical analyzes after 15, 30 and 60 days of implantation were performed to investigate the effects of the material on bone repair. The PBS incubation indicated that the fibers of the glassy scaffold degraded over time. The histological analysis revealed a progressive degradation of the material with increasing implantation time and also its substitution by granulation tissue and woven bone. Histomorphometry showed a higher amount of newly formed bone area in the control group (CG) compared to the biomaterial group (BG) 15 days post-surgery. After 30 and 60 days, CG and BG showed a similar amount of newly formed bone. The novel biomaterial enhanced the expression of RUNX-2 and RANK-L, and also improved the mechanical properties of the tibial callus at day 15 after surgery. These results indicated a promising use of the new biomaterial for bone engineering. However, further long-term studies should be carried out to provide additional information concerning the material degradation in the later stages and the bone regeneration induced by the fibrous material.

Keywords: Biomaterial, bioactive glasses, fibrous glassy scaffold, bone repair, tissue engineering

5.1   Introduction

Bone is one of the most replaced tissues of the body, with more than 500.000 bone graft procedures performed per year only in the USA (AXELRAD, KAKAR e EINHORN, 2007; VIRK *et al.*, 2013). In this context, researchers have investigated different solutions to treat non-union fractures and a series of bone replacement graft materials has been extensively used with varying degrees of success, such as autografts, allografts and synthetic bone substitutes (VALIMAKI *et al.*, 2005; DROSSE *et al.*, 2008).

The use of autologous bone grafts as bone substitutes is considered the gold standard, but their use involves several problems, such as donor site morbidity, the need of additional surgeries, and the relative small amounts of available bone (GIANNOUDIS, DINOPOULOS e TSIRIDIS, 2005). An alternative is the use of allogenic bone grafts, but their utilization is limited by the risks of rejection and transmission of diseases (DIAS *et al.*, 2006). Widespread interest has, therefore, focused on the development of synthetic bone substitutes, including mainly hydroxyapatite (HA), calcium phosphate (CaP) ceramics (DOROZHKIN e AJAAL, 2009) and polymer-based materials (HUTMACHER *et al.*, 2007).

Also, bioactive glasses (BGs) have been widely used as bone substitutes and grafts (HENCH *et al.*, 2002). It is a class of biomaterials that undergoes a series of surface reaction when in contact with fluids, forming a biologically active bone-like apatite layer on their surfaces (HENCH e POLAK, 2002). BGs are absorbable and their dissolution products (soluble silicon and calcium) have been found to up-regulate seven families of genes in osteoblasts (HENCH, 2003). The original bioactive glass developed by Hench and named Bioglass[®] 45S5 is a melt-derived glass with four components (46.1% SiO_2, 24.4% Na_2O, 26.9% CaO and 2.6% P_2O_5, in mol). Bioglass[®] 45S5 has been known for many years as the most bioactive composition among numerous bone-bonding glasses. It has been used in many

clinical procedures, including the repair of periodontal bone defects, maxillofacial defects reconstruction, spinal surgery and bone replacement (HENCH, 2003; 2006).

Bioglass and bioactive materials have been used mainly in powders and blocks (MASTROGIACOMO *et al.*, 2006; SPECTOR, 2006). Although, in most cases these materials permit and support cell migration and angiogenesis, they do not have the ability of acting as fillers for bone defects with irregular shapes (WU *et al.*, 2010). In this context, moldability, such as the one found in fibrous materials, is a desirable characteristic required for grafts, allowing to fit irregular bone defects (BOCCACCINI e MAQUET, 2003). Functional fibrous substrates will support cell attachment, proliferation and differentiation at the region of the defect, which permit cells to secrete extracellular matrix (ECM) for mineralization in order to form bone (PASCU, STOKES e MCGUINNESS, 2013). Thus, the obtainment of malleable fibers from bioactive glasses seems to be a promising therapeutic approach to be used for bone repair.

Toward this goal, fibrous glassy scaffolds, belonging to the SiO_2-Na_2O-K_2O-MgO-CaO-P_2O_5 system, have been recently developed (Patent Application BR 10 2013 020961 9; Fundação Universidade Federal de São Carlos, 2013) (SOUZA, 2013). The new fibrous material combines malleability with the high bioactivity of BGs, expanding the potential applications of the biomaterial.

Since there is a growing interest in the development of materials with improved osteogenic properties, it was hypothesized that this fibrous glassy scaffold would have improved *in vivo* bioactive properties and more adequate morphology to facilitate cell migration and vascularization, providing a bone graft with additional advantages for clinical use. Consequently, the present study aimed to assess the morphological structure of these fibrous glassy scaffolds and evaluate the temporal *in vivo* response of this novel biomaterial in

a tibial bone defect model in rats. To this end, scaffolds were analyzed via SEM and, also, implanted into created non-critical bone defects in rats. Histopathological, immunohistochemistry and biomechanical analyzes were evaluated after 15, 30 and 60 days of implantation.

5.2 Methodology

5.2.1 Fibrous Glassy Scaffolds

The fibrous scaffolds were obtained from a brand new highly bioactive glass developed by researchers of the Vitreous Materials Laboratory (LaMaV), Department of Materials Engineering, Federal University of São Carlos, São Carlos, São Paulo, Brazil. The bioactive glass belongs to the SiO_2-Na_2O-K_2O-MgO-CaO-P_2O_5 system and was prepared by melting the chemical reagents at $1200°C$ in a platinum crucible, crushed and remelted at $1200°C$ to provide homogenization. After the glass was produced, bioactive fibers were manufactured in a homemade fiber tower. After this procedure, highly porous circular scaffolds (3mm x 1mm) were obtained using chopped fibers. These fibers were weighed and put in a cylindrical polytetrafluoroethylene mold to obtain disc shaped samples. The structure of the scaffolds was evaluated using SEM (Phenom™, FEI, Company).

5.2.2 Morphology after incubation in phosphate buffered saline (PBS)

The morphology of the fibrous glassy scaffold - after 1, 7 and 14 days of immersion in PBS - was determined using SEM (LEO 440, LEO Electron Microscopy Ltd). The degradation behavior of the scaffolds was visualized at various magnifications.

5.2.3 Experimental design

In this study, sixty male Wistar rats (aged 12 weeks and weighing 250-300 g) were used. They were maintained under controlled temperature ($24 \pm 2^{o}C$), light-dark periods of 12 hours, with unrestricted access to water and commercial diet. Each animal handling and surgical procedures were strictly conducted according the Guiding Principles for the Use of Laboratory Animals. This study was approved by the Animal Care Committee guidelines of the Federal University of São Carlos (Protocol 043/2012).

Animals were divided into 2 groups: bone defect control group (CG), in which the bone defects received no filler, and the biomaterial group (BG), in which the bone defects were filled with fibrous scaffolds. Each group was divided into three different sub-groups (N=10) sacrificed in different periods (15, 30 and 60 days after surgery). As described below, a non-critical size bone defect was performed on both tibias.

5.2.4 Surgical procedures

All surgical procedures were performed under sterile conditions and general anesthesia was induced by intra-peritoneal injection of Ketamine/ Xylazine (80/10 mg/Kg). Buprenorfine (Temgesic; Reckitt Benckiser Health Care Limited, Schering-Plough, Hoddesdon, UK) was administered intraperitoneally (0.02mg/kg) directly after the operation and subcutaneously for 2 days after surgery, to minimize post-operative discomfort.

To insert implants into the tibial defects, the animals were immobilized and both hind limbs were shaved, washed and disinfected with povidone-iodine. The medial compartment of the tibia was exposed through a longitudinal incision on the shaved skin. After exposure, a 1.0 mm pilot hole was drilled. The hole was gradually widened with drills of increasing size until

a final defect size of 3 mm in width was reached. Low rotational drill speeds (max. 450 rpm) and constant physiologic saline irrigation were used. Surgery was performed bilaterally and one defect was created in each tibia. Immediately, a sterilized 3.0 mm diameter fibrous scaffold was implanted in the bone cavities, with the exception of control animals. After implantation, the cutaneous flap was replaced and sutured with absorbable Vicryl® 5-0 (Johnson&Johnson, St.Stevens-Woluwe, Belgium), and the skin was disinfected with povidone iodin. The health status of all animals was monitored daily.

On days 15, 30 and 60 post-surgery, rats were euthanized individually by carbon dioxide asphyxia. The tibias were defleshed and removed for analysis.

5.2.5 Histopathological analysis

In the histopathological and imunohistochemistry analysis, the right tibiae were removed and fixed in 10% buffer formalin (Merck, Darmstadt, Germany) for 24 hours. They were decalcified in 10% EDTA (Merck) and embedded in paraffin blocks. Five-micrometer slices were obtained perpendicular to the medial-lateral drilling axis of the implant using a microtome (Leica Microsystems SP 1600, Nussloch, Germany). At least, three sections of each specimen were stained with hematoxylin and eosin (H.E stain, Merck). Histopathological evaluation was performed under an optical microscope (Olympus, Optical Co. Ltd, Tokyo, Japan). The area of the bone defect was qualitatively evaluated considering the inflammatory process, granulation tissue and newly formed bone. At least three sections of each specimen were examined using light microscopy (Leica Microsystems AG, Wetzlar, Germany).

Additionally, morphometry analysis was performed and, in order to do that, histological sections were quantitatively evaluated via computer-based image analysis

techniques (Axioplan 2, Carl Zeiss, Jena, Germany). Digitalized images of the defect ($\times$20) were obtained and the amount of newly formed bone was determined within three regions of interest: ROI1 (upper left border), ROI2 (lower left border), and ROI3 (central region of the right border) (OLIVEIRA *et al.*, 2010; BOSSINI *et al.*, 2011). The total amount of newly formed bone was represented as ROI1+ROI2+ROI3 (in square micrometer). Two experienced observers (PRGA and ACMR) performed the analysis in a blinded manner.

5.2.6 Immunohistochemistry

For the immunohistochemistry analysis, xylene was used to remove the paraffin from the serial sections of 5 μm. After this procedure, the sections were rehydrated in graded ethanol and pretreated in a microwave (Electrolux, São Paulo, Brazil) with 0.01 M citric acid buffer (pH 6) for three cycles of 5 min each at 850 W for antigen retrieval. The resulting material was pre-incubated with 0.3% hydrogen peroxide in PBS solution for 5 min in order to inactivate the endogenous peroxidase. Then, the samples were blocked with 5% normal goat serum in PBS for 10 min. The specimens were incubated with anti-RUNX-2 polyclonal primary antibody (code: sc-8566, Santa Cruz Biotechnology, USA) at a concentration of 1:200, anti-RANK-L polyclonal primary antibody (code: sc-7627, Santa Cruz Biotechnology, USA) at a concentration of 1:200, and anti-COL-1 polyclonal primary antibody (code: sc-8784, Santa Cruz Biotechnology, USA) also at a concentration of 1:200. Incubation was carried out overnight at 4 °C into a refrigerator. This step was followed by two washes in PBS for 10 min. The sections were then incubated with biotin conjugated secondary antibody anti-rabbit IgG (Vector Laboratories, Burlingame, CA, USA) at a concentration of 1:200 in PBS for 1 h. The sections were washed twice with PBS followed by the application of preformed avidin biotin complex conjugated to peroxidase (Vector Laboratories) for 45 min. The bound complexes

were visualized by the application of a 0.05% solution of 3-3′-diaminobenzidine solution and counterstained with Harris hematoxylin (Sigma-Aldrich). For control studies of the antibodies, the serial sections were treated with rabbit IgG (Vector Laboratories) at a concentration of 1:200 in place of the primary antibody. Additionally, internal positive controls were performed with each staining bath.

RUNX-2, RANK-L and COL-1 immunoexpressions were evaluated qualitatively and quantitatively. The qualitative analysis was performed in order to assess the presence (or absence) and region of occurrence of the immunomarkers. Regarding the quantitative investigation, this analysis was performed to evaluate the immunolabeling intensity of each immunomarker, in four predetermined fields inside the defect, according to a previously described scoring scale from 1 to 4 (1=absent, 2=weak, 3=moderate and 4=intense) (PEDROSA *et al.*, 2009; MATSUMOTO *et al.*, 2012). The analysis was performed by two observers (PRGA and KRF) in a blinded way using a light microscopy (Leica Microsystems AG, Wetzlar, Germany).

5.2.7 Mechanical test

The biomechanical properties of the left tibia were determined by a three-point bending test performed in an Instron® Universal Testing Machine (USA, 4444 model, 1 kN load cell). The tibiae were placed on a 3.8-cm metal device, which provided a 1.8-cm-distant double support on the bone diaphysis. The load cell was perpendicularly positioned at the exact site of the bone defect. A 5 N pre-load was applied in order to avoid specimen sliding. Finally, the bending force was applied at a constant deformation rate of 0.5 cm/min until fracture occurred. The maximum load (N) at the failure was obtained from the load-deformation curve.

5.2.8 Statistical analysis

The normality of all variable distribution was verified using Shapiro–Wilk's W test. For the variable that exhibited normal distribution, comparisons among the groups were made using one-way analysis of variance (ANOVA), complemented by Tukey post-test analysis. STATISTICA version 7.0 (data analysis software system - StatSoft Inc.) was used to carry out the statistics analysis. Values of $p<0.05$ were considered statistically significant.

5.3 Results

5.3.1 Morphology of the fibrous glassy scaffold

The structure of the fibrous scaffold was analyzed through SEM. Figure 10 shows that that the fibers of the scaffold were randomly positioned. The glass-shaped fibers constitute a very porous biomaterial with interconnected pores, presenting sufficient mechanical strength for handling.
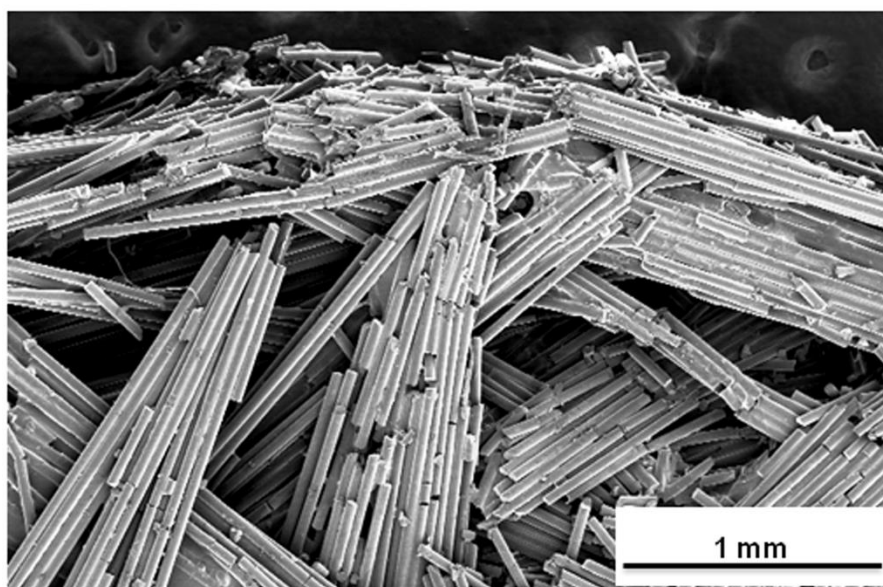
Figure 10. SEM image of the fibrous glassy scaffold. Magnification of 35x.

5.3.2 Morphology after incubation

SEM micrographs indicated signs of initial degradation of the fibers upon immersion in PBS after 1, 7 and 14 days (Figure 11). Ruptures, related to the degradation, were observed in the structures of the fibers over time.
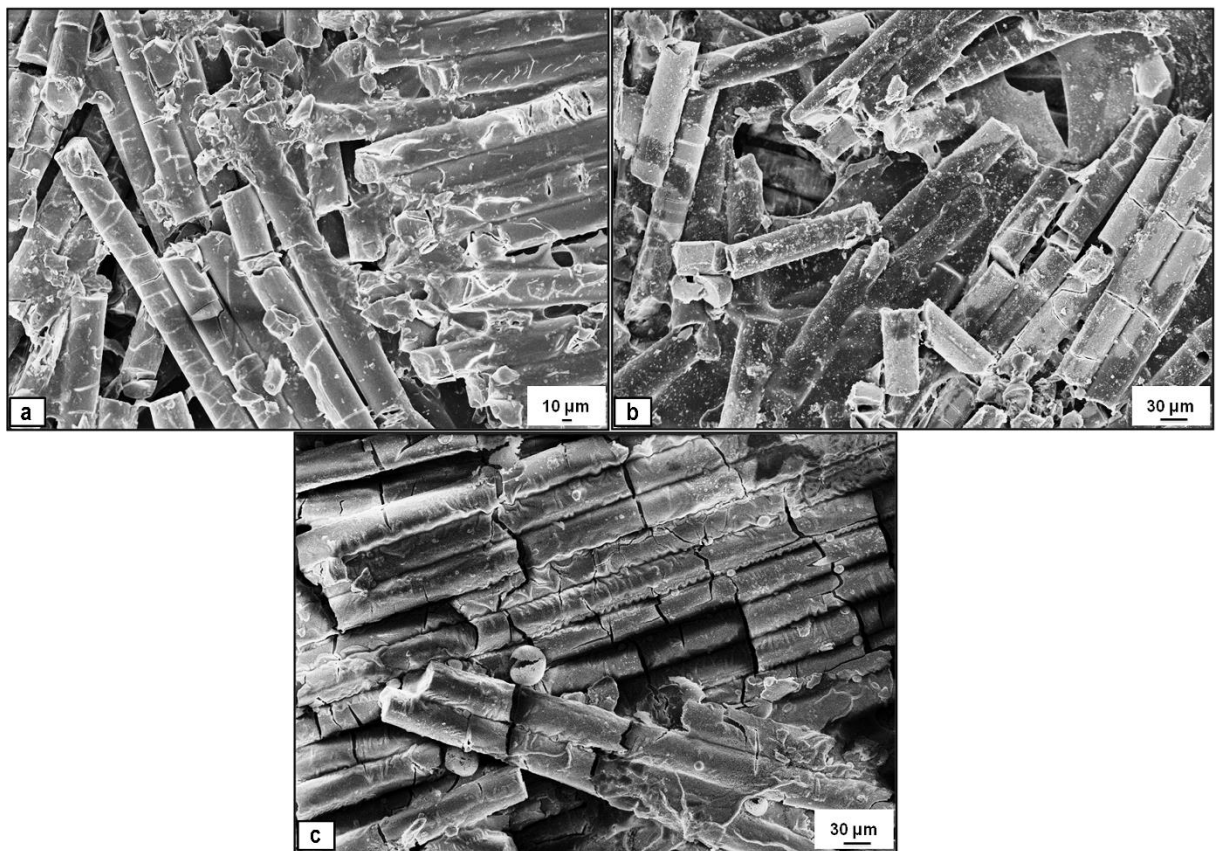
Figure 11. SEM micrographs of the fibrous glassy scaffold for up to 14 days post-incubation in PBS. (a) 1 day; (b) 7 days and (c) 14 days. Magnification of 500x.

5.3.3 General findings post-implantation

A number of 30 animals were used for the BG. From this number, 3 animals were lost because of respiratory depression induced by anesthesia. For the remaining animals, neither postoperative complications nor behavioral changes were observed. The rats returned rapidly

to their normal diet and showed no loss of weight in the experimentation (data not shown). Moreover, during the experiment, no infection in the surgical site was observed. After the later experimental period, 54 tibial implants were retrieved, of which 48 were included for analyzes (6 implants were lost due to tibia or implant fractures during histological procedures). Table 3 presents an overview of the number of implants that were placed, retrieved and used for analysis.

Table 3. Implants placed, retrieved and used for histological and immunohistochemistry analyzes

	Implants placed	Implants retrieved	Implants used for analyzes
15 days	20	18[a]	16[b]
30 days	20	20	18[b]
60 days	20	16[a]	14[b]

[a] Deviation versus implants placed due to animal dead
[b] Deviation versus implants retrieved due to tibial or implant fractures

5.3.4 Histopathological analysis of tibial implants

5.3.4.1 15 days

Representative histological sections of all experimental groups after implantation are depicted in Figure 12 (magnification of 10x). Fifteen days post-surgery, histology assessment revealed that the bone defect was almost completely filled with the biomaterial, which presented signs of initial degradation (Figure 12a).

Figure 13 shows the histological findings at a higher magnification. It was noticed, for CG and BG, granulation tissue with discrete inflammatory process at the site of the defect (Figures 13a and 13b). For both groups, it was also observed the presence of an early woven bone organization in the periphery of the defect. Histological analysis revealed signs of material degradation, although an intense presence of the biomaterial still could be observed

(Figure 13a). The degraded area of the implant allowed the ingrowth of soft tissue around the fibers of the scaffolds.
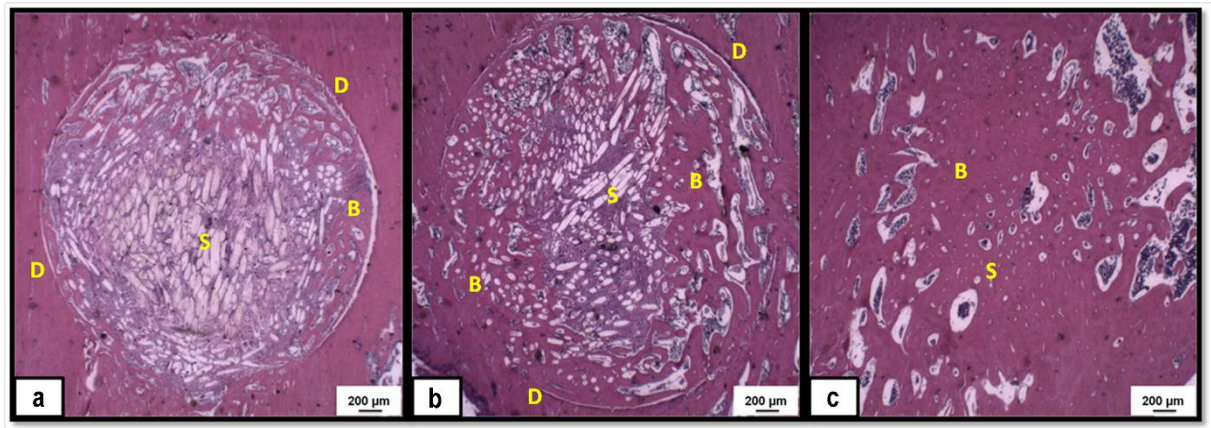
Figure 12. Tibial defects. Representative histological sections of BG in the 3 experimental periods: 15 days (a), 30 days (b), and 60 days (c). Fibers of the porous scaffold (S), Bone formation (B), and Defect line (D) are indicated in the sections. Bar represents 200 µm. Hematoxylin-Eosin staining. Magnification of 12.5x.

5.3.4.2   30 days

The material degradation has continued after 30 days of implantation and newly formed bone replaced the area previously occupied by the material (Figure 12b). At a higher magnification, no inflammatory process was observed either for CG or BG (Figures 13c and 13d). For CG, a minor amount of granulation tissue and newly formed bone were observed at the region of the defect (Figure 13c). Compared to the experimental period of 15 days, BG showed lower amounts of granulation tissue (mostly located in the central region of the scaffold). It was also noticed organized newly formed bone substituting the degraded material (Figure 13d). The borders of the defects were still delimited for both groups.
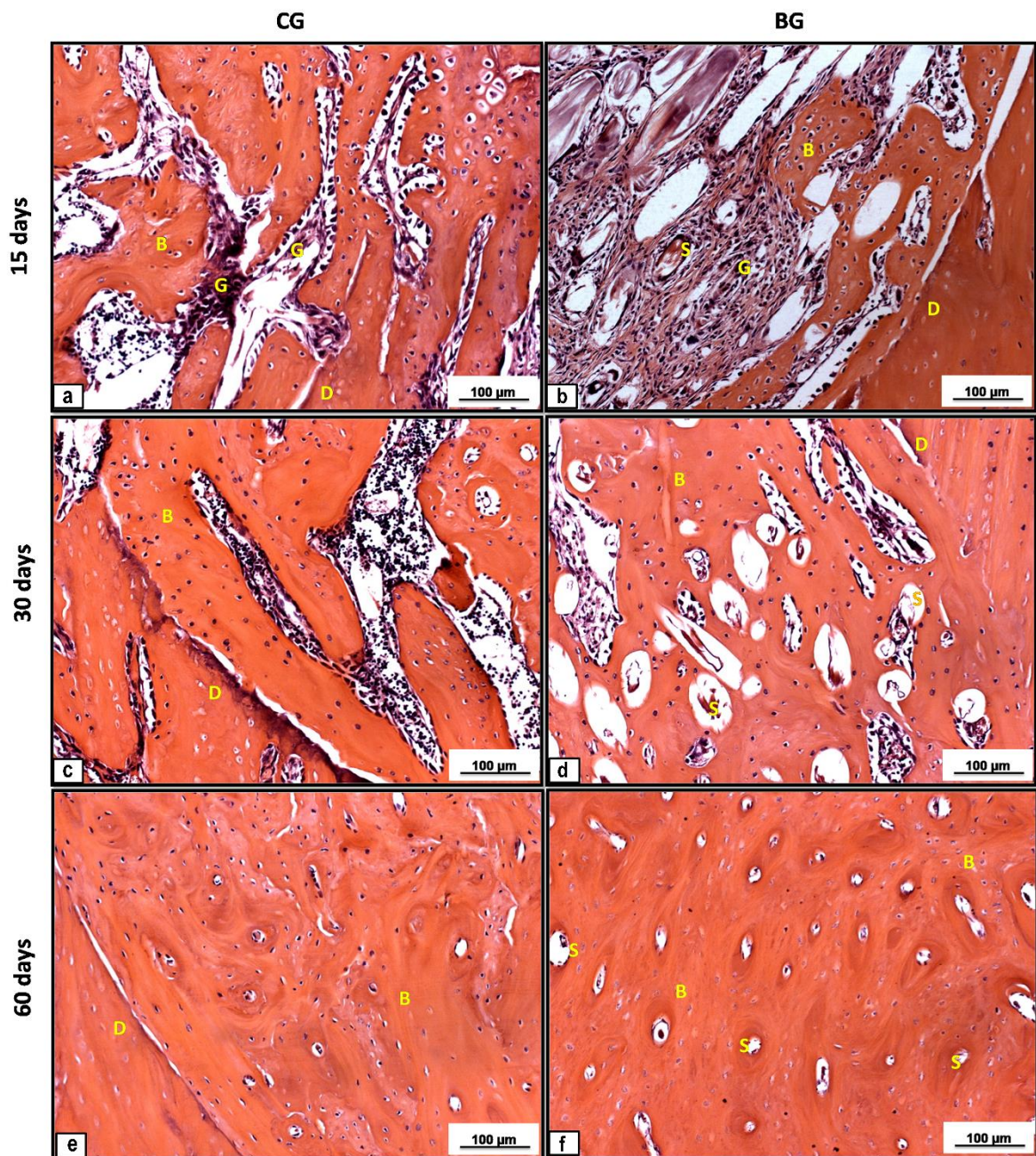
Figure 13. Representative histological sections of CG and BG in the 3 experimental periods; CG: 15 days (a), 30 days (c), and 60 days (e); BG: 15 days (b), 30 days (d), and 60 days (f). Granulation tissue (G), Fibers of the porous scaffold (S), Bone formation (B), and Defect line (D) are indicated in the sections. Bar represents 100 µm. Hematoxylin-Eosin staining. Magnification of 200x.

5.3.4.3 60 days

Figure 12c shows that 60 days after the implantation, the material was almost completely degraded and a mature formed bone occupied the defect (Figure 12c). At a higher magnification, no inflammatory process or granulation tissue were noticed for CG and BG (Figures 13e and 13f). In this period, both groups presented bone remodeling in the defect site. In BG, the borders of the defect were not noticed anymore in most cases, and some fibers still could be observed.

5.3.5 Histomorphometrical analysis

Histomorphometrical analysis revealed that, after 15 days of implantation, BG showed a significant decrease in the amount of newly formed bone compared to CG (21.3 ± 2.4 % and 46.8 ± 7.1 % respectively; $p<0.05$). After 30 and 60 days, however, CG and BG showed similar amount of newly formed bone at the site of the injury ($p>0.05$; Figure 14).
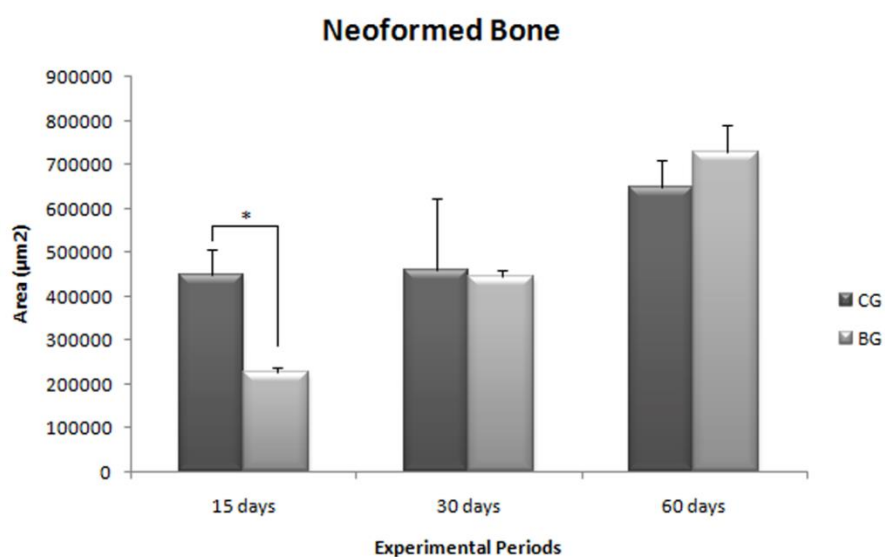
Figure 14. Means and standard error of the mean of the morphometry assessment. Significant differences of $p<0.05$ are represented by an asterisk.

5.3.6 Immunohistochemistry

5.3.6.1 *Qualitative analysis*

Regarding CG, after 15 and 30 days of implantation, the immunostaining for RUNX-2 was noticed mainly in the medullar tissue and in osteoblasts in the periphery of bone defect (Figures 15a e 15c). Sixty days post-surgery, the labeling for RUNX-2 was observed mainly in the remaining medullar tissue and in the newly formed bone (Figure 15e). Concerning BG, after 15 and 30 days post-surgery, the labeling for RUNX-2 was identified throughout the defect, being more evident in the central area among the fibers of the biomaterial (Figures 15b e 15d). Still in the treated group, on day 60, the immunoexpression of RUNX-2 was also in the medullar tissue and in some regions of the neoformed bone (Figure 15f).

RANK-L expression in CG was detected predominantly in the medullar tissue and in the border of the defect in all experimental groups (Figures 16a, 16c e 16e). In BG, after 15 and 30 days post-surgery, the labeling for RANK-L was observed in the entire defect, mainly in the granulation tissue around the fibers of the biomaterial (Figures 16b e 16d). At the last set point evaluated in BG, the immunoexpression of RANK-L was observed around the borders of the newly formed bone (Figure 16f).

Regarding the COL-1 expression, CG of all periods presented immunoreactivity throughout the neoformed bone (Figures 17a, 17c and 17e). In the case of BG, at 15 and 30 days post-implantation, the expression was detected mostly in the neoformed bone on the border of defect (Figure 17b and 17d). In the last experimental period, the immunolabeling of COL-1 could be noticed in the entire defect, since it was completely filled with newly formed bone (Figure 17f).
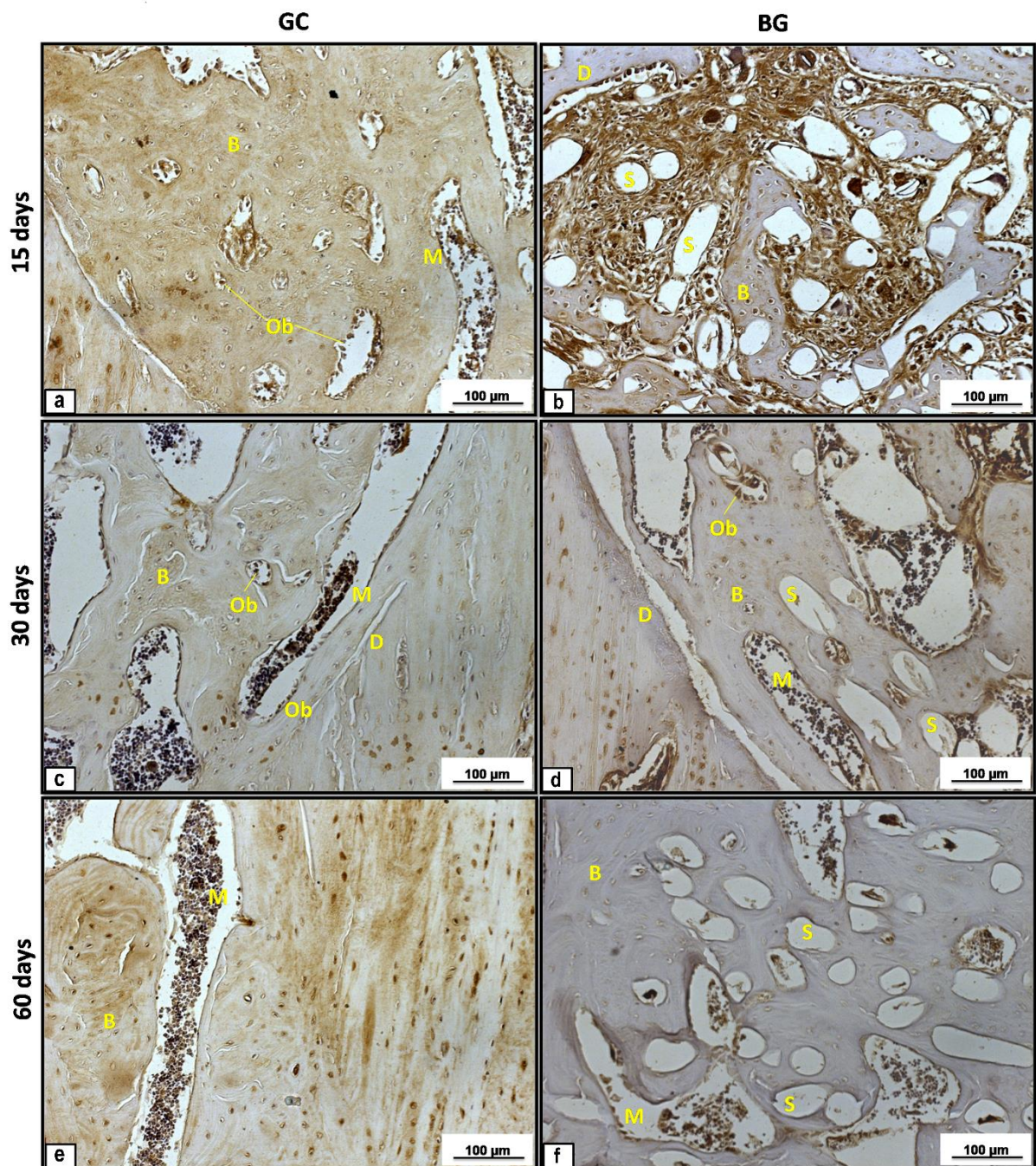
Figure 15. Immunohistochemistry of RUNX-2. CG: 15 days (a), 30 days (c), and 60 days (e); BG: 15 days (b), 30 days (d), and 60 days (f). Fibers of the porous scaffold (S), Bone formation (B), Medullar tissue (M), Osteoblasts (Ob), and Defect line (D) are indicated in the sections. Bar represents 100 μm. Magnification of 200x.
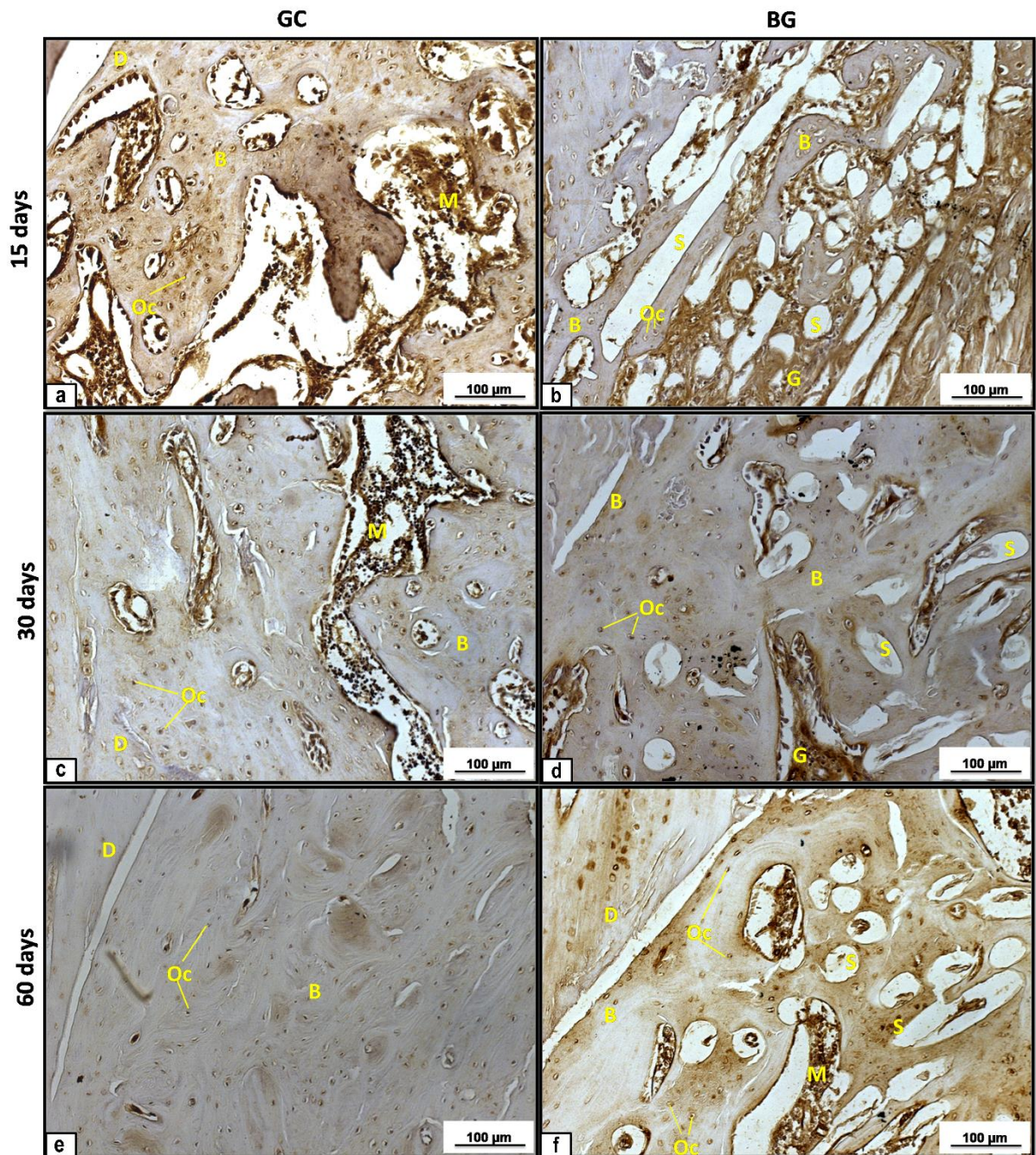
Figure 16. Immunohistochemistry of RANK-L. CG: 15 days (a), 30 days (c), and 60 days (e); BG: 15 days (b), 30 days (d), and 60 days (f). Granulation tissue (G), Fibers of the porous scaffold (S), Bone formation (B), Medullar tissue (M), Osteocytes (Oc), and Defect line (D) are indicated in the sections. Bar represents 100 µm. Magnification of 200x.
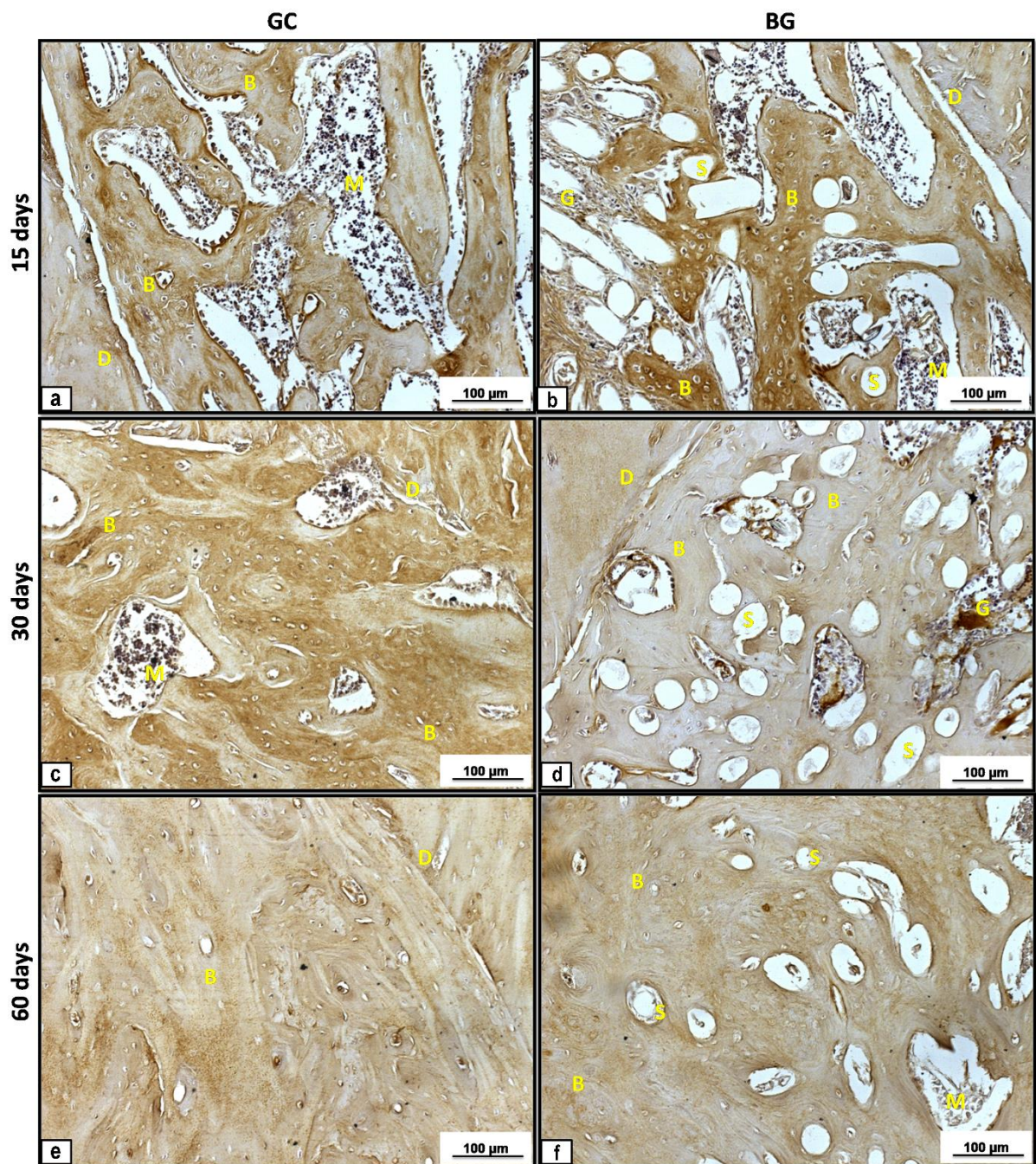
Figure 17. Immunohistochemistry of COL-1. CG: 15 days (a), 30 days (c), and 60 days (e); BG: 15 days (b), 30 days (d), and 60 days (f). Granulation tissue (G), Fibers of the porous scaffold (S), Bone formation (B), Medullar tissue (M), and Defect line (D) are indicated in the sections. Bar represents 100 μm. Magnification of 200x.

5.3.6.2 Quantitative analysis

The imunnolabeling for RUNX-2 at days 15 and 30 after surgery was significantly higher in BG compared to CG (Figura 18a). In the case of RANK-L, this immunomarker had a higher expression in BG compared to CG, 30 and 60 days after implantation (Figure 18b). Similar findings for COL-1 expression were noticed in CG and BG at different experimental periods analyzed (Figure 18c).

5.3.7 Mechanical test

The biomechanical analysis showed statistically difference in the maximal load comparing BG to CG at day 15 after surgery, with a significantly increase in the treated group (Table 4). No difference between CG and BG was observed for the other analyzed variables.

Table 4. Means and standard error of the mean for the biomechanical evaluation of the tibias

	15 days		30 days		60 days	
	CG	BG	CG	BG	CG	BG
Maximal load (kN)	0.048±0.003	0.069±0.005[*]	0.066±0.004	0.074±0.003	0.073±0.005	0.075±0.007
Resilience (J)	0.034±0.003	0.028±0.002	0.028±0.005	0.029±0.003	0.023±0.003	0.020±0.006
Tenacity (J)	0.043±0.003	0.043±0.006	0.048±0.007	0.038±0.003	0.021±0.006	0.021±0.006

GC=control group; BG=biomaterial group
[*] *p*<0.05 compared to CG after 15 days
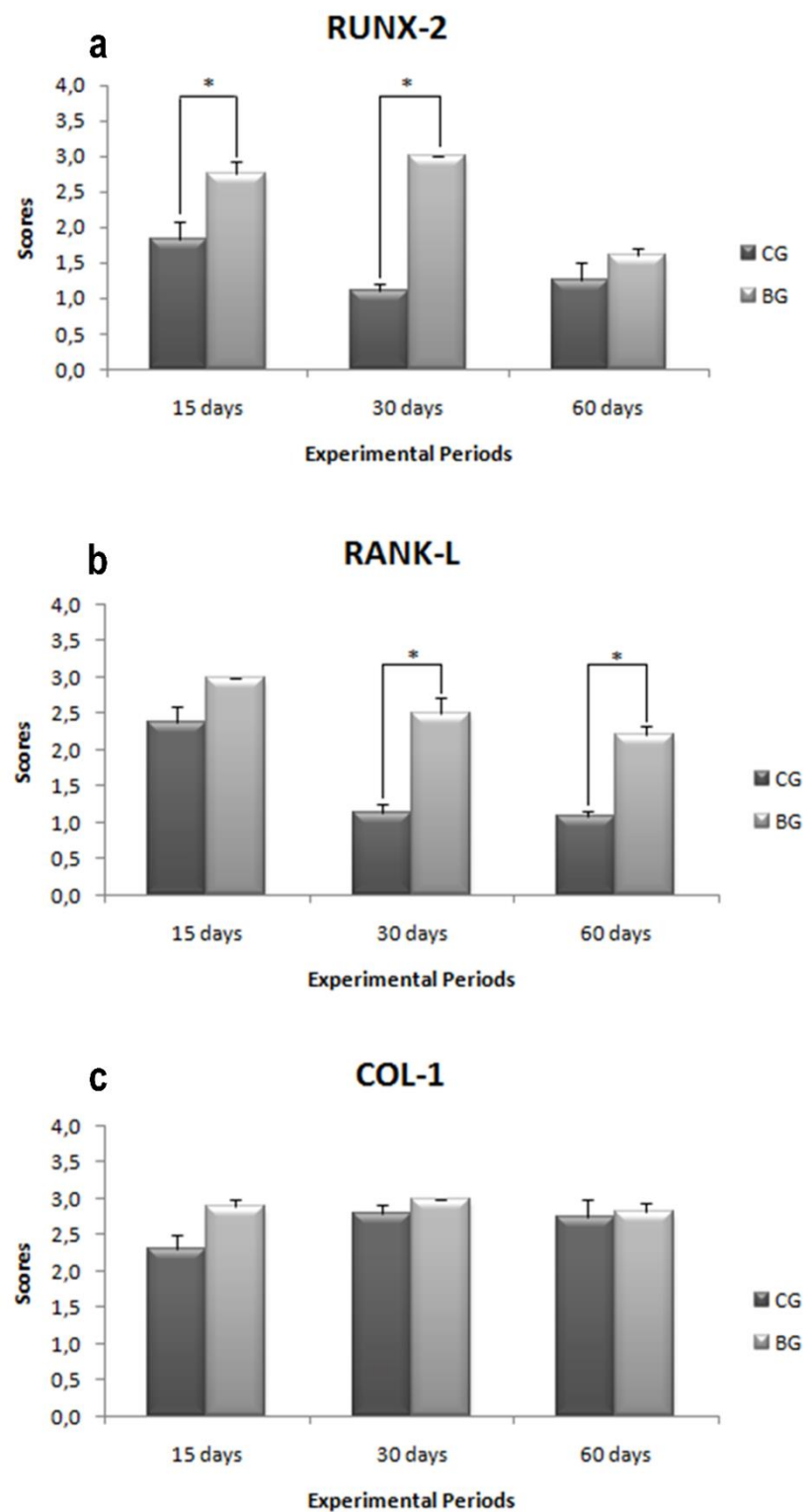
Figure 18. Means and standard error of the mean for the immunohistochemistry analysis. (a) RUNX-2, (b) RANK-L and, (c) COL-1. Significant differences of $p<0.05$ are represented by an asterisk.

5.4 Discussion

The aim of this study was to assess the morphology of the fibrous glassy scaffold and investigate the *in vivo* tissue response of this biomaterial. For this purpose, the scaffolds were evaluated via SEM and, also, implanted into tibial bone defects and analyzed after 15, 30 and 60 days. The hypothesis was that the fibrous bioactive material would present an appropriate structure and an adequate bioactivity to permit bone cell growth and bone formation. SEM micrographs showed that the fibrous glassy scaffold constitutes a very porous biomaterial with interconnected pores, degrading over time upon immersion in PBS. Histology revealed that the material degraded at the site of the injury with increasing time, allowing bone ingrowth. Histomorphometry analysis demonstrated that the newly formed bone area in CG was higher than BG, 15 days post-surgery. However, no difference was found in the other experimental periods. In addition, the BG showed an upregulation of RUNX-2 and RANK-L expression, and increased maximal load values 15 days post-surgery.

SEM evaluation of the scaffold's morphology after incubation indicated an initial degradation over time accompanied by ruptures in the structures of the fibers. These breaks might be beneficial since it increases degradation of the scaffold, allowing the substitution of the material by bone tissue (SCHEPERS e DUCHEYNE, 1997; ABIRAMAN, 2002).

Furthermore, the histological findings also revealed a degradation of the material with increasing implantation time, and its substitution by granulation tissue and newly formed bone. Such data are in line with previous studies conducted by our group, which investigated the effects of a glass-ceramic biomaterial, with similar chemical compositions (Biosilicate[®], P_2O_5–Na_2O–CaO–SiO_2), on bone formation in rat tibial defects. Likewise these studies showed a degradation of Biosilicate[®] over time, followed by replacement of the material with granulation tissue and woven bone (OLIVEIRA *et al.*, 2010; BOSSINI *et al.*, 2011).

Bone resorption of material and liberation of space are necessary for tissue ingrowth (RUHE *et al.*, 2006; QI, YE e WANG, 2008; GU *et al.*, 2011; VAN DE WATERING *et al.*, 2012). It seems that the degradation of the highly porous material, found in this study, indeed substantially allowed bone formation. Furthermore, the superior biological properties presented by BG may also be related to the ion dissolution from the fibrous scaffold. Immediately after the contact of the material with fluids, ions are leached and a silica rich layer is formed, acting as a template for calcium phosphate precipitation, and inducing new bone formation (XYNOS *et al.*, 2000; HENCH e POLAK, 2002; HENCH, XYNOS e POLAK, 2004; VALIMAKI e ARO, 2006; MOURA *et al.*, 2007). These results corroborate those of Renno (RENNO *et al.*, 2013), who tested a porous composite of calcium phosphate cement, poly(D,L-lactic-co-glycolic) acid and Biosilicate® using implantation into femoral condyle defects.

Concerning the immunohistochemistry, it is noteworthy that RUNX-2 expression was higher in BG when compared to CG on days 15 and 30 after implantation. RUNX-2 immunofactor is mainly expressed in osteoblasts and it is required for the differentiation of mesenchymal progenitors toward osteoblast cell lineage. It is well known that RUNX-2 is fundamental for upregulation of other osteoblastic markers, like osteocalcin, osteopontin and alkaline phosphatase (ZHANG, 2002; AFZAL, POLAK e BUTTERY, 2004), which also may have influenced bone formation and deposition. The *in vivo* findings observed in this study are in agreement with previous studies which have detected higher RUNX-2 immunoexpression in tibial and calvaria defect models filled with Biosilicate® (BOSSINI *et al.*, 2011; MATSUMOTO *et al.*, 2012).

Additionally, the resorption and remodeling of bone tissue by osteoclasts is also necessary for a successful bone healing process. In this context, RANK-L is known as a key

factor for differentiation and activation of osteoclasts (LEMAIRE *et al.*, 2004; KEARNS, KHOSLA e KOSTENUIK, 2008; ANANDARAJAH, 2009). The present study demonstrated a higher immunoexpression of RANK-L in BG, 30 and 60 days post-surgery. Probably, the higher expression of RANK-L indicates an increased presence of osteoclasts in an attempt of degrading the material. Investigations conducted by Pinto (PINTO *et al.*, 2013) verified a more evident immunoexpression of RANK-L around the particles of Biosilicate® glass-ceramic in tibial defects. Similar findings were observed by Kondo (KONDO *et al.*, 2005) who tested b- tricalcium phosphate (b-TCP) using implantation in femoral condyle of rats.

Similarly, COL-1 is the major organic component of bone matrix produced by osteoblasts, and the increase of this protein level is important and critical in mediating the signal cascade for the expression of mature osteoblasts and mineralization of the extracellular matrix (SAINO *et al.*, 2011). Interestingly, in the present study, no statistically significant difference was observed in the COL-1 immunolabeling between the experimental groups. These results do not corroborate those of Valerio (VALERIO *et al.*, 2004) who showed that osteoblasts in the presence of ionic products from a bioactive glass (60% of silica-BG60S) dissolution presented a higher cell proliferation and collagen secretion when compared to control group. It is unclear at this stage why the results of the present study occurred, since it was hypothesized that the ionic products of the biomaterial might stimulate collagen organization. In this context, further investigations are necessary to a better understanding of this mechanism.

The mechanical test revealed a higher value of maximal load in the treated group 15 days after the surgery, showing a positive effect in the initial period. Thus, these results show an improvement of the mechanical properties in the tibial callus for the initial group, whose defect was filled with the porous scaffold. This fact may have occurred due to the quality and

arrangement of the biomaterial microstructure in the defect, influencing the bone load-bearing capacity. Likewise, Granito (GRANITO *et al.*, 2009) evidenced improved mechanical of tibial callus in defects filled with particulate Biosilicate® in comparison with control animals 20 days post-surgery. Regarding other experimental periods, no difference was observed. This fact may be related to the biomaterial degradation, conferring equal amount of newly formed bone with similar tissue organization compared to CG.

The results of the present investigation confirmed our hypothesis that the fibrous glassy scaffold can stimulate bone repair due to its bioactive properties. Nevertheless, once there are differences between the metabolism of healthy bone and the metabolism of compromised conditions (e.g. osteoporosis), the bio-performance of the fibrous porous material might be different and need to be further investigated. Additionally, it would be interesting to evaluate the response of this porous biomaterial in critical-size bone defects (CSD), since in this model the spontaneous bone consolidation does not occur (BOSCH, MELSEN e VARGERVIK, 1998). Thereby, future research is necessary to evaluate this information, as this work was limited to the evaluation of the biomaterial performance under optimal conditions in non-CSDs.

In summary, the results indicated that the fibrous glassy scaffold has potential to be used for bone healing. The novel biomaterial enhanced the expression of osteogenic factors and also improved mechanical properties of the tibial callus at day 15 after surgery. Further long-term studies should be carried out to provide additional information concerning the late stages of material degradation and the bone regeneration induced by the fibrous material. Moreover, further research is required to evaluate the biological performance of this new biomaterial in compromised situations to support the use of this promising fibrous material for bone engineering applications.

5.5 Acknowledgments

6 Considerações finais e perspectivas futuras

Com base nos dois estudos expostos na presente tese, pode-se concluir:

- *Scaffolds* vítreo-fibrosos altamente porosos foram obtidos, apresentando biocompatibilidade e alta bioatividade;

- Tais *scaffolds* são capazes de estimular o reparo ósseo, devido suas propriedades bioativas. O novo biomaterial aumentou a expressão de fatores osteogênicos (RUNX-2 e RANK-L) e melhorou as propriedades mecânicas do calo tibial 15 dias após o procedimento cirúrgico;

- Estes resultados indicam o novo *scaffold* vítreo fibroso como um material promissor para o desenvolvimento de novas terapias relacionadas à biotecnologia biomédica e à engenharia do reparo ósseo.

Sobre as perspectivas futuras, estudos ainda são necessários para avaliar a *performance* biológica deste biomaterial em situações patológicas, como, por exemplo, osteoporose. Além disso, é necessário investigar as resposta biológicas do novo material vítreo fibroso em modelos de defeito ósseo crítico (*critical-size bone defects*, CSD), sendo que nesse modelo a consolidação óssea não ocorre espontaneamente. Todas essas informações darão um suporte para o uso deste promissor biomaterial na engenharia do tecido ósseo, levando ao desenvolvimento de novos produtos que melhorem a qualidade de vida dos indivíduos acometidos.

7 Referências bibliográficas

AARON, R. K., D. M. CIOMBOR e B. J. SIMON. Treatment of nonunions with electric and electromagnetic fields. **Clin Orthop Relat Res**, p.21-9. 2004.

ABIRAMAN, S., VARMA, H., K., KUMARI, T., V. , UMASHANKAR, P., R., JOHN, A. Preliminary in vitro and in vivo characterizations of a sol–gel derived bioactive glass–ceramic system. **Bull Mater Sci**, v.25, p.419-29. 2002.

AFZAL, F., J. POLAK e L. BUTTERY. Endothelial nitric oxide synthase in the control of osteoblastic mineralizing activity and bone integrity. **J Pathol**, v.202, p.503-10. 2004.

AKAZAWA, T., M. MURATA, T. SASAKI, J. TAZAKI, M. KOBAYASHI, T. KANNO, K. NAKAMURA e M. ARISUE. Biodegradation and bioabsorption innovation of the functionally graded bovine bone-originated apatite with blood permeability. **J Biomed Mater Res A**, v.76, p.44-51. 2006.

ANANDARAJAH, A. P. Role of RANKL in bone diseases. **Trends Endocrinol Metab**, v.20, p.88-94. 2009.

ANDERSON, J. M. e A. K. MCNALLY. Biocompatibility of implants: lymphocyte/macrophage interactions. **Semin Immunopathol**, v.33, p.221-33. 2011.

ARCHER, C. W., P. ROONEY e L. WOLPERT. Cell shape and cartilage differentiation of early chick limb bud cells in culture. **Cell Differ**, v.11, p.245-51. 1982.

AXELRAD, T. W., S. KAKAR e T. A. EINHORN. New technologies for the enhancement of skeletal repair. **Injury**, v.38 Suppl 1, p.S49-62. 2007.

BAINO, F. e C. VITALE-BROVARONE. Mechanical properties and reliability of glass–ceramic foam scaffolds for bone repair. **Materials Letters**, v.118, p.27-30. 2014.

BOCCACCINI, A. R. e V. MAQUET. Bioresorbable and bioactive polymer/Bioglass® composites with tailored pore structure for tissue engineering applications. **Compos Sci Technol**, v.63, p.2417-2429. 2003.

BOSCH, C., B. MELSEN e K. VARGERVIK. Importance of the critical-size bone defect in testing bone-regenerating materials. **J Craniofac Surg**, v.9, p.310-6. 1998.

BOSSINI, P. S., A. C. RENNO, D. A. RIBEIRO, R. FANGEL, O. PEITL, E. D. ZANOTTO e N. A. PARIZOTTO. Biosilicate(R) and low-level laser therapy improve bone repair in osteoporotic rats. **J Tissue Eng Regen Med**, v.5, p.229-37. 2011.

BRETCANU, O., F. BAINO, E. VERNE e C. VITALE-BROVARONE. Novel resorbable glass-ceramic scaffolds for hard tissue engineering: from the parent phosphate glass to its bone-like macroporous derivatives. **J Biomater Appl**, v.28, p.1287-303. 2014.

BROWN, R. F., D. E. DAY, T. E. DAY, S. JUNG, M. N. RAHAMAN e Q. FU. Growth and differentiation of osteoblastic cells on 13-93 bioactive glass fibers and scaffolds. **Acta Biomater**, v.4, p.387-96. 2008.

CALORI, G. M., W. ALBISETTI, A. AGUS, S. IORI e L. TAGLIABUE. Risk factors contributing to fracture non-unions. **Injury**, v.38 Suppl 2, p.S11-8. 2007.

CHEN, Q. Z., I. D. THOMPSON e A. R. BOCCACCINI. 45S5 Bioglass-derived glass-ceramic scaffolds for bone tissue engineering. **Biomaterials**, v.27, p.2414-25. 2006.

CLAES, L. e B. WILLIE. The enhancement of bone regeneration by ultrasound. **Prog Biophys Mol Biol**, v.93, p.384-98. 2007.

COORDS, M., E. BREITBART, D. PAGLIA, N. KAPPY, A. GANDHI, J. COTTRELL, N. CEDENO, N. POUNDER, J. P. O'CONNOR e S. S. LIN. The effects of low-intensity pulsed ultrasound upon diabetic fracture healing. **J Orthop Res**, v.29, p.181-8. 2011.

CORTEZ, A. L., G. O. RABELO e R. MAZZONETTO. Reconstrução de Maxila Atrófica utilizando Osso Autogéneo e Malha de Titânio para Posterior Reabilitação com Implantes– Caso Clínico. **Rev Port de Estomatol Cir Maxilofac**, v.45, p.163-67. 2004.

DAY, R. M., V. MAQUET, A. R. BOCCACCINI, R. JEROME e A. FORBES. In vitro and in vivo analysis of macroporous biodegradable poly(D,L-lactide-co-glycolide) scaffolds containing bioactive glass. **J Biomed Mater Res A**, v.75, p.778-87. 2005.

DIAS, A. G., M. A. LOPES, J. D. SANTOS, A. AFONSO, K. TSURU, A. OSAKA, S. HAYAKAWA, S. TAKASHIMA e Y. KURABAYASHI. In vivo performance of biodegradable calcium phosphate glass ceramics using the rabbit model: histological and SEM observation. **J Biomater Appl**, v.20, p.253-66. 2006.

DOROZHKIN, S. e T. AJAAL. Toughening of porous bioceramic scaffolds by bioresorbable polymeric coatings. **Proc Inst Mech Eng H**, v.223, p.459-70. 2009.

DROSSE, I., E. VOLKMER, R. CAPANNA, P. DE BIASE, W. MUTSCHLER e M. SCHIEKER. Tissue engineering for bone defect healing: an update on a multi-component approach. **Injury**, v.39 Suppl 2, p.S9-20. 2008.

FERNANDES, K. P. S., S. K. BUSSADORI, M. M. MARQUES, N. S. Y. WADT, E. BACH e M. D. MARTINS. Healing and cytotoxic effects of Psidium guajava (Myrtaceae) leaf extracts. **Braz J Oral Sci**, v.9, p.449-454. 2010.

FERNANDES, K. R., D. A. RIBEIRO, N. C. RODRIGUES, C. TIM, A. A. SANTOS, N. A. PARIZOTTO, H. S. DE ARAUJO, P. DRIUSSO e A. C. RENNO. Effects of low-level laser therapy on the expression of osteogenic genes related in the initial stages of bone defects in rats. **J Biomed Opt**, v.18, p.038002. 2013.

FOLKMAN, J. e A. MOSCONA. Role of cell shape in growth control. **Nature**, v.273, p.345-9. 1978.

FRANCA, R., T. D. SAMANI, G. BAYADE, L. YAHIA e E. SACHER. Nanoscale surface characterization of biphasic calcium phosphate, with comparisons to calcium hydroxyapatite and beta-tricalcium phosphate bioceramics. **J Colloid Interface Sci**, v.420, p.182-8. 2014.

GABBAI-ARMELIN, P. R., D. A. CARDOSO, E. D. ZANOTTO, O. PEITL, S. C. G. LEEUWENBURGH, J. A. JANSEN, A. C. M. RENNO e J. J. J. P. VAN DEN BEUCKEN. Injectable composites based on biosilicate[registered sign] and alginate: handling and in vitro characterization. **RSC Advances**, v.4, p.45778-45785. 2014.

GAUTIER, E. e C. SOMMER. Guidelines for the clinical application of the LCP. **Injury**, v.34 Suppl 2, p.B63-76. 2003.

GHASEMI-MOBARAKEH, L., D. SEMNANI e M. MORSHED. A novel method for porosity measurement of various surface layers of nanofibers mat using image analysis for tissue engineering applications. **J Appl Polym Sci**, v.106, p.2536-2542. 2007.

GIANNOUDIS, P. V., H. DINOPOULOS e E. TSIRIDIS. Bone substitutes: an update. **Injury**, v.36 Suppl 3, p.S20-7. 2005.

GORUSTOVICH, A. A., J. A. ROETHER e A. R. BOCCACCINI. Effect of bioactive glasses on angiogenesis: a review of in vitro and in vivo evidences. **Tissue Eng Part B Rev**, v.16, p.199-207. 2010.

GRANITO, R. N., A. C. RENNO, C. RAVAGNANI, P. S. BOSSINI, D. MOCHIUTI, V. JORGETTI, P. DRIUSSO, O. PEITL, E. D. ZANOTTO, N. A. PARIZOTTO e J. OISHI. In vivo biological performance of a novel highly bioactive glass-ceramic (Biosilicate(R)): A biomechanical and histomorphometric study in rat tibial defects. **J Biomed Mater Res B Appl Biomater**, v.97, p.139-47. 2011.

GRANITO, R. N., D. A. RIBEIRO, A. C. RENNO, C. RAVAGNANI, P. S. BOSSINI, O. PEITL-FILHO, E. D. ZANOTTO, N. A. PARIZOTTO e J. OISHI. Effects of biosilicate and bioglass 45S5 on tibial bone consolidation on rats: a biomechanical and a histological study. **J Mater Sci Mater Med**, v.20, p.2521-6. 2009.

GU, Y., L. CHEN, H. L. YANG, Z. P. LUO e T. S. TANG. Evaluation of an injectable silk fibroin enhanced calcium phosphate cement loaded with human recombinant bone morphogenetic protein-2 in ovine lumbar interbody fusion. **J Biomed Mater Res A**, v.97, p.177-85. 2011.

GU, Y., W. HUANG, M. N. RAHAMAN e D. E. DAY. Bone regeneration in rat calvarial defects implanted with fibrous scaffolds composed of a mixture of silicate and borate bioactive glasses. **Acta Biomater**, v.9, p.9126-9136. 2013.

HADJIARGYROU, M., K. MCLEOD, J. P. RYABY e C. RUBIN. Enhancement of Fracture Healing by Low Intensity Ultrasound. **Clin Orthop Relat Res**, v.355, p.S216-S229. 1998.

HENCH, L. L. Glass and genes: the 2001 W.E.S. Turner Memorial Lecture. **Glass Tech**, v.44, p. 1-10. 2003.

_____. The story of Bioglass. **J Mater Sci Mater Med**, v.17, p.967-78. 2006.

_____. Introduction to Bioceramics. 2nd Ed. Imperial College Press 2013. ISBN: 978-1-908977-15-1. 620 p. 2013

HENCH, L. L. e J. M. POLAK. Third-generation biomedical materials. **Science**, v.295, p.1014-7. 2002.

HENCH, L. L. e I. THOMPSON. Twenty-first century challenges for biomaterials. **J R Soc Interface**, v.7 Suppl 4, p.S379-91. 2010.

HENCH, L. L., I. D. XYNOS, A. J. EDGAR, L. D. K. BUTERRY, J. M. POLAK, J.-P. ZHONG, X.-Y. LIU e J. CHANG. Gene Activating Glasses. **J Inorg Mater**, v.17, p.897-909. 2002.

HENCH, L. L., I. D. XYNOS e J. M. POLAK. Bioactive glasses for in situ tissue regeneration. **J Biomater Sci Polym Ed**, v.15, p.543-62. 2004.

HOPPE, A., N. S. GULDAL e A. R. BOCCACCINI. A review of the biological response to ionic dissolution products from bioactive glasses and glass-ceramics. **Biomaterials**, v.32, p.2757-74. 2011.

HUBBELL, J. A. Synthetic biodegradable polymers for tissue engineering and drug delivery. **Curr Opin Solid State Mater Sci**, v.3, p.4. 1998.

HUTMACHER, D. W., J. T. SCHANTZ, C. X. LAM, K. C. TAN e T. C. LIM. State of the art and future directions of scaffold-based bone engineering from a biomaterials perspective. **J Tissue Eng Regen Med**, v.1, p.245-60. 2007.

ISO, I. O. F. S. Biological Evaluation of Medical Devices Part 3: Tests for Genotoxicity, Carcinogenicity,and Reproductive Toxicity, 10993-3. Geneva, Switzerland 2003.

ISO, I. O. F. S. Biological Evaluation of Medical Devices Part 5: Tests for in vitro cytotoxicity, 10993-5. Geneva, Switzerland 2009.

JAMES, P. F. Glass ceramics: new compositions and uses. **J Non-Cryst Solids**, v.181, p.1-15. 1995.

JANSEN, J. A., W. J. DHERT, J. P. VAN DER WAERDEN e A. F. VON RECUM. Semi-quantitative and qualitative histologic analysis method for the evaluation of implant biocompatibility. **J Invest Surg**, v.7, p.123-34. 1994.

JING, D., J. CAI, G. SHEN, J. HUANG, F. LI, J. LI, L. LU, E. LUO e Q. XU. The preventive effects of pulsed electromagnetic fields on diabetic bone loss in streptozotocin-treated rats. **Osteoporos Int**, v.22, p.1885-95. 2011.

JONES, J. R. Review of bioactive glass: from Hench to hybrids. **Acta Biomater**, v.9, p.4457-86. 2013.

KARAGEORGIOU, V. e D. KAPLAN. Porosity of 3D biomaterial scaffolds and osteogenesis. **Biomaterials**, v.26, p.5474-91. 2005.

KEARNS, A. E., S. KHOSLA e P. J. KOSTENUIK. Receptor activator of nuclear factor kappaB ligand and osteoprotegerin regulation of bone remodeling in health and disease. **Endocr Rev**, v.29, p.155-92. 2008.

KIDO, H. W., P. OLIVEIRA, N. A. PARIZOTTO, M. C. CROVACE, E. D. ZANOTTO, O. PEITL-FILHO, K. P. FERNANDES, R. A. MESQUITA-FERRARI, D. A. RIBEIRO e A. C. RENNO. Histopathological, cytotoxicity and genotoxicity evaluation of Biosilicate(R) glass-ceramic scaffolds. **J Biomed Mater Res A**, v.101, p.667-73. 2013.

KOKUBO, T., H. KUSHITANI, S. SAKKA, T. KITSUGI e T. YAMAMURO. Solutions able to reproduce in vivo surface-structure changes in bioactive glass-ceramic A-W. **J Biomed Mater Res**, v.24, p.721-34. 1990.

KONDO, N., A. OGOSE, K. TOKUNAGA, T. ITO, K. ARAI, N. KUDO, H. INOUE, H. IRIE e N. ENDO. Bone formation and resorption of highly purified beta-tricalcium phosphate in the rat femoral condyle. **Biomaterials**, v.26, p.5600-8. 2005.

LACROIX, J., E. JALLOT e J. LAO. Gelatin-bioactive glass composites scaffolds with controlled macroporosity. **Chem Eng J**, v.256, p.9-13. 2014.

LEMAIRE, V., F. L. TOBIN, L. D. GRELLER, C. R. CHO e L. J. SUVA. Modeling the interactions between osteoblast and osteoclast activities in bone remodeling. **J Theor Biol**, v.229, p.293-309. 2004.

LIN, Y., R. F. BROWN, S. B. JUNG e D. E. DAY. Angiogenic effects of borate glass microfibers in a rodent model. **J Biomed Mater Res A**, v.102, p.4491-4499. 2014.

LINK, D. P., J. VAN DEN DOLDER, J. J. VAN DEN BEUCKEN, V. M. CUIJPERS, J. G. WOLKE, A. G. MIKOS e J. A. JANSEN. Evaluation of the biocompatibility of calcium phosphate cement/PLGA microparticle composites. **J Biomed Mater Res A**, v.87, p.760-9. 2008.

LIU, W. e J. CHANG. Setting properties and biocompatibility of dicalcium silicate with varying additions of tricalcium aluminate. **J Biomater Appl**, v.27, p.171-8. 2012.

LIU, X., W. HUANG, H. FU, A. YAO, D. WANG, H. PAN, W. W. LU, X. JIANG e X. ZHANG. Bioactive borosilicate glass scaffolds: in vitro degradation and bioactivity behaviors. **J Mater Sci Mater Med**, v.20, p.1237-43. 2009.

MASTROGIACOMO, M., S. SCAGLIONE, R. MARTINETTI, L. DOLCINI, F. BELTRAME, R. CANCEDDA e R. QUARTO. Role of scaffold internal structure on in vivo

bone formation in macroporous calcium phosphate bioceramics. **Biomaterials**, v.27, p.3230-7. 2006.

MATSUMOTO, M. A., G. CAVIQUIOLI, C. C. BIGUETTI, L. A. HOLGADO, P. P. SARAIVA, A. C. M. RENNO e R. Y. KAWAKAMI. A novel bioactive vitroceramic presents similar biological responses as autogenous bone grafts. **J Mater Sci Mater Med**, v.23, p.1447-1456. 2012.

MELICAN, M. C. Biocompatible tissue implant for repairing tissue tear such as soft tissue injury, comprises bioabsorbable polymeric foam component, and reinforcing component formed of biocompatible mesh-containing material. EP1987850-A1, EP012231. Ethicon Inc(Ethi-C) 2008.

MIRHADI, S. M. Synthesis and characterization of nanostructured forsterite scaffolds using two step sintering method. **J Alloy Comp**, v.610, p.399-401. 2014.

MISRA, S. K., T. ANSARI, D. MOHN, S. P. VALAPPIL, T. J. BRUNNER, W. J. STARK, I. ROY, J. C. KNOWLES, P. D. SIBBONS, E. V. JONES, A. R. BOCCACCINI e V. SALIH. Effect of nanoparticulate bioactive glass particles on bioactivity and cytocompatibility of poly(3-hydroxybutyrate) composites. **J R Soc Interface**, v.7, p.453-65. 2010.

MOIMAS, L., M. BIASOTTO, R. DI LENARDA, A. OLIVO e C. SCHMID. Rabbit pilot study on the resorbability of three-dimensional bioactive glass fibre scaffolds. **Acta Biomater**, v.2, p.191-9. 2006.

MOSMANN, T. Rapid colorimetric assay for cellular growth and survival: application to proliferation and cytotoxicity assays. **J Immunol Methods**, v.65, p.55-63. 1983.

MOURA, J., L. N. TEIXEIRA, C. RAVAGNANI, O. PEITL, E. D. ZANOTTO, M. M. BELOTI, H. PANZERI, A. L. ROSA e P. T. DE OLIVEIRA. In vitro osteogenesis on a highly bioactive glass-ceramic (Biosilicate). **J Biomed Mater Res A**, v.82, p.545-57. 2007.

MURATA, M., T. AKAZAWA, J. TAZAKI, K. ITO, T. SASAKI, M. YAMAMOTO, Y. TABATA e M. ARISUE. Blood permeability of a novel ceramic scaffold for bone morphogenetic protein-2. **J Biomed Mater Res B Appl Biomater**, v.81, p.469-75. 2007.

NAGHAVI, N., J. GHODDUSI, H. R. SADEGHNIA, E. ASADPOUR e S. ASGARY. Genotoxicity and cytotoxicity of mineral trioxide aggregate and calcium enriched mixture cements on L929 mouse fibroblast cells. **Dent Mater J**, v.33, p.64-69. 2014.

NARAYAN, R. Scanning electron microscopy combined with image analysis software can also be used to estimate porosity, pores size and distribution. Chapel Hill, NC, USA: Springer. 2009. 37 p.

NATH, S., S. KALMODIA e B. BASU. Densification, phase stability and in vitro biocompatibility property of hydroxyapatite-10 wt% silver composites. **J Mater Sci Mater Med**, v.21, p.1273-87. 2010.

NICOLA, R. A., V. JORGETTI, J. RIGAU, M. T. PACHECO, L. M. DOS REIS e R. A. ZANGARO. Effect of low-power GaAlAs laser (660 nm) on bone structure and cell activity: an experimental animal study. **Lasers Med Sci**, v.18, p.89-94. 2003.

OLIVEIRA, P., D. A. RIBEIRO, E. F. PIPI, P. DRIUSSO, N. A. PARIZOTTO e A. C. RENNO. Low level laser therapy does not modulate the outcomes of a highly bioactive glass-ceramic (Biosilicate) on bone consolidation in rats. **J Mater Sci Mater Med**, v.21, p.1379-84. 2010.

OREFICE, R., J. WEST, G. LATORRE, L. HENCH e A. BRENNAN. Effect of long-term in vitro testing on the properties of bioactive glass-polysulfone composites. **Biomacromolecules**, v.11, p.657-65. 2010.

PASCU, E. I., J. STOKES e G. B. MCGUINNESS. Electrospun composites of PHBV, silk fibroin and nano-hydroxyapatite for bone tissue engineering. **Mater Sci Eng C Mater Biol Appl**, v.33, p.4905-16. 2013.

PATROCINIO-SILVA, T. L., A. M. DE SOUZA, R. L. GOULART, C. F. PEGORARI, J. R. OLIVEIRA, K. FERNANDES, A. MAGRI, R. M. PEREIRA, D. R. ARAKI, M. R. NAGAOKA, N. A. PARIZOTTO e A. C. RENNO. The effects of low-level laser irradiation on bone tissue in diabetic rats. **Lasers Med Sci**, v.29, p.1357-64. 2014.

PEDROSA, W. F., JR., R. OKAMOTO, P. E. FARIA, M. F. ARNEZ, S. P. XAVIER e L. A. SALATA. Immunohistochemical, tomographic and histological study on onlay bone graft remodeling. Part II: calvarial bone. **Clin Oral Implants Res**, v.20, p.1254-64. 2009.

PEITL, O., E. DUTRA ZANOTTO e L. L. HENCH. Highly bioactive P2O5–Na2O–CaO–SiO2 glass-ceramics. **J Non-Cryst Solids**, v.292, p.115-126. 2001.

PELÁEZ, A., GARCÍA, C., P., PAREJA, A., MÁRQUEZ, M., E., TORO, A., CASTAÑEDA, R., ABAD, P. Genotoxicity effects of ceramic coatings applied on metallic substrates using Single Cell Gel electrophoresis assay In Vitro. **Key Eng Mater**, v.284-86, p.593-96. 2005.

PICKERING, S. A. W. e B. E. SCAMMELL. Electromagnetic Fields for Bone Healing. **Int J Low Extrem Wounds**, v.1, p.152-160. 2002.

PINTO, K. N., C. R. TIM, M. C. CROVACE, M. A. MATSUMOTO, N. A. PARIZOTTO, E. D. ZANOTTO, O. PEITL e A. C. RENNO. Effects of biosilicate((R)) scaffolds and low-level laser therapy on the process of bone healing. **Photomed Laser Surg**, v.31, p.252-60. 2013.

POOLOGASUNDARAMPILLAI, G., D. WANG, S. LI, J. NAKAMURA, R. BRADLEY, P. D. LEE, M. M. STEVENS, D. S. MCPHAIL, T. KASUGA e J. R. JONES. Cotton-wool-like bioactive glasses for bone regeneration. **Acta Biomater**, v.10, p.3733-3746. 2014.

PORTAL DA SAÚDE. Ministério da Saúde. Brasil 2011. Disponível em: <http://portalsaude.saude.gov.br/>. Acesso em: 15 de outubro 2014.

QI, X., J. YE e Y. WANG. Improved injectability and in vitro degradation of a calcium phosphate cement containing poly(lactide-co-glycolide) microspheres. **Acta Biomater**, v.4, p.1837-45. 2008.

RADETZKI, F., D. WOHLRAB, A. ZEH, K. S. DELANK, T. MENDEL, G. BERGER, F. SYROWATKA, O. MAYR e A. BERNSTEIN. Cellular compatibility of highly degradable bioactive ceramics for coating of metal implants. **Biomed Mater Eng**, v.21, p.307-21. 2011.

RAHAMAN, M. N., D. E. DAY, B. S. BAL, Q. FU, S. B. JUNG, L. F. BONEWALD e A. P. TOMSIA. Bioactive glass in tissue engineering. **Acta Biomater**, v.7, p.2355-73. 2011.

RENNO, A. C., F. M. DE MOURA, N. S. DOS SANTOS, R. P. TIRICO, P. S. BOSSINI e N. A. PARIZOTTO. Effects of 830-nm laser, used in two doses, on biomechanical properties of osteopenic rat femora. **Photomed Laser Surg**, v.24, p.202-6. 2006.

RENNO, A. C., P. A. MCDONNELL, N. A. PARIZOTTO e E. L. LAAKSO. The effects of laser irradiation on osteoblast and osteosarcoma cell proliferation and differentiation in vitro. **Photomed Laser Surg**, v.25, p.275-80. 2007.

RENNO, A. C., F. C. VAN DE WATERING, M. R. NEJADNIK, M. C. CROVACE, E. D. ZANOTTO, J. G. WOLKE, J. A. JANSEN e J. J. VAN DEN BEUCKEN. Incorporation of bioactive glass in calcium phosphate cement: An evaluation. **Acta Biomater**, v.9, p.5728-39. 2013.

REZWAN, K., Q. Z. CHEN, J. J. BLAKER e A. R. BOCCACCINI. Biodegradable and bioactive porous polymer/inorganic composite scaffolds for bone tissue engineering. **Biomaterials**, v.27, p.3413-31. 2006.

RUHE, P. Q., O. C. BOERMAN, F. G. RUSSEL, A. G. MIKOS, P. H. SPAUWEN e J. A. JANSEN. In vivo release of rhBMP-2 loaded porous calcium phosphate cement pretreated with albumin. **J Mater Sci Mater Med**, v.17, p.919-27. 2006.

RUTTEN, S., P. A. NOLTE, G. L. GUIT, D. E. BOUMAN e G. H. R. ALBERS. Use of Low-Intensity Pulsed Ultrasound for Posttraumatic Nonunions of the Tibia: A Review of Patients Treated in The Netherlands. **J Trauma Acute Care Surg**, v.62, p.902-908. 2007.

SAINO, E., S. GRANDI, E. QUARTARONE, V. MALIARDI, D. GALLI, N. BLOISE, L. FASSINA, M. G. DE ANGELIS, P. MUSTARELLI, M. IMBRIANI e L. VISAI. In vitro calcified matrix deposition by human osteoblasts onto a zinc-containing bioactive glass. **Eur Cell Mater**, v.21, p.59-72; discussion 72. 2011.

SCHEPERS, E. J. e P. DUCHEYNE. Bioactive glass particles of narrow size range for the treatment of oral bone defects: a 1-24 month experiment with several materials and particle sizes and size ranges. **J Oral Rehabil**, v.24, p.171-81. 1997.

SCHINDELER, A., M. M. MCDONALD, P. BOKKO e D. G. LITTLE. Bone remodeling during fracture repair: The cellular picture. **Semin Cell Dev Biol**, v.19, p.459-66. 2008.

SENA, K., R. M. LEVEN, K. MAZHAR, D. R. SUMNER e A. S. VIRDI. Early gene response to low-intensity pulsed ultrasound in rat osteoblastic cells. **Ultrasound Med Biol**, v.31, p.703-8. 2005.

SERRANO, M. C., M. PORTOLES, R. PAGANI, J. S. DE GUINOA, E. RUIZ-HERNANDEZ, D. ARCOS e M. VALLET-REGI. In vitro positive biocompatibility evaluation of glass-glass ceramic thermoseeds for hyperthermic treatment of bone tumors. **Tissue Eng Part A**, v.14, p.617-27. 2008.

SHYNG, Y. C., C. Y. CHI, H. DEVLIN e P. SLOAN. Healing of tooth extraction sockets in the streptozotocin diabetic rat model: Induction of cartilage by BMP-6. **Growth Factors**, v.28, p.447-51. 2010.

SOUZA, M. T. Desenvolvimento de manta flexível altamente bioativa. Dissertação de Mestrado-PPG em Ciência e Engenharia de Materiais. Centro de Ciências Exatas e Tecnologia, Universidade Federal de São Carlos, São Carlos, 2011.

SOUZA, M. T., ZANOTTO, E. D., PEITL-FILHO, O. Vitreous composition, bioactive glassy fibers and tissues. Patent Application No. BR 10 2013 020961 9. Universidade Federal de São Carlos, Brazil 2013.

SPECTOR, M. Biomaterials-based tissue engineering and regenerative medicine solutions to musculoskeletal problems. **Swiss Med Wkly**, v.136, p.293-301. 2006.

TABOAS, J. M., R. D. MADDOX, P. H. KREBSBACH e S. J. HOLLISTER. Indirect solid free form fabrication of local and global porous, biomimetic and composite 3D polymer-ceramic scaffolds. **Biomaterials**, v.24, p.181-94. 2003.

TICE, R. R., E. AGURELL, D. ANDERSON, B. BURLINSON, A. HARTMANN, H. KOBAYASHI, Y. MIYAMAE, E. ROJAS, J. C. RYU e Y. F. SASAKI. Single cell gel/comet assay: guidelines for in vitro and in vivo genetic toxicology testing. **Environ Mol Mutagen**, v.35, p.206-21. 2000.

TIM, C. R., K. N. PINTO, B. R. ROSSI, K. FERNANDES, M. A. MATSUMOTO, N. A. PARIZOTTO e A. C. RENNO. Low-level laser therapy enhances the expression of osteogenic factors during bone repair in rats. **Lasers Med Sci**, v.29, p.147-56. 2014.

TSIRIDIS, E., N. UPADHYAY e P. GIANNOUDIS. Molecular aspects of fracture healing: which are the important molecules? **Injury**, v.38 Suppl 1, p.S11-25. 2007.

VALERIO, P., M. M. PEREIRA, A. M. GOES e M. F. LEITE. The effect of ionic products from bioactive glass dissolution on osteoblast proliferation and collagen production. **Biomaterials**, v.25, p.2941-8. 2004.

VALIMAKI, V. V. e H. T. ARO. Molecular basis for action of bioactive glasses as bone graft substitute. **Scand J Surg**, v.95, p.95-102. 2006.

VALIMAKI, V. V., N. MORITZ, J. J. YRJANS, M. DALSTRA e H. T. ARO. Peripheral quantitative computed tomography in evaluation of bioactive glass incorporation with bone. **Biomaterials**, v.26, p.6693-703. 2005.

VALLET-REGI, M. Revisiting ceramics for medical applications. **Dalton Trans**, p.5211-20. 2006.

VAN DE WATERING, F. C., J. J. VAN DEN BEUCKEN, X. F. WALBOOMERS e J. A. JANSEN. Calcium phosphate/poly(D,L-lactic-co-glycolic acid) composite bone substitute materials: evaluation of temporal degradation and bone ingrowth in a rat critical-sized cranial defect. **Clin Oral Implants Res**, v.23, p.151-9. 2012.

VIRK, M. S., F. ALAEE, H. TANG, M. S. OMINSKY, H. Z. KE e J. R. LIEBERMAN. Systemic administration of sclerostin antibody enhances bone repair in a critical-sized femoral defect in a rat model. **J Bone Joint Surg Am**, v.95, p.694-701. 2013.

WANG, X., H., ZHU, Y., FENG, Q., L., CUI, F., Z. Responses of Osteo- and Fibroblast cells to phosphorylated chitin. **J of Bioact and Compat Polym**, v.18, p.135-46. 2003.

WIESE, A. e H. C. PAPE. Bone defects caused by high-energy injuries, bone loss, infected nonunions, and nonunions. **Orthop Clin North Am**, v.41, p.1-4, table of contents. 2010.

WU, C., Y. RAMASWAMY e H. ZREIQAT. Porous diopside (CaMgSi(2)O(6)) scaffold: A promising bioactive material for bone tissue engineering. **Acta Biomater**, v.6, p.2237-45. 2010.

WU, C., Y. ZHU, J. CHANG, Y. ZHANG e Y. XIAO. Bioactive inorganic-materials/alginate composite microspheres with controllable drug-delivery ability. **J Biomed Mater Res B Appl Biomater**, v.94, p.32-43. 2010.

XIE, Z. P., C. Q. ZHANG, C. Q. YI, J. J. QIU, J. Q. WANG e J. ZHOU. In vivo study effect of particulate Bioglass in the prevention of infection in open fracture fixation. **J Biomed Mater Res B Appl Biomater**, v.90, p.195-201. 2009.

XYNOS, I. D., A. J. EDGAR, L. D. BUTTERY, L. L. HENCH e J. M. POLAK. Ionic products of bioactive glass dissolution increase proliferation of human osteoblasts and induce insulin-like growth factor II mRNA expression and protein synthesis. **Biochem Biophys Res Commun**, v.276, p.461-5. 2000.

YANG, J.-Z., R. SULTANA, X.-Z. HU e P. ICHIM. Novel Layered Hydroxyapatite/Tri-Calcium Phosphate–Zirconia Scaffold Composite with High Bending Strength for Load-Bearing Bone Implant Application. **Int J Appl Ceram Tec**, v.11, p.22-30. 2014.

YAOITA, H., H. ORIMO, Y. SHIRAI e T. SHIMADA. Expression of bone morphogenetic proteins and rat distal-less homolog genes following rat femoral fracture. **J Bone Miner Metab**, v.18, p.63-70. 2000.

ZHANG, X. S., E. M.; YOUNG, D. A.; PUZAS, J. E.; ROSIER, R. N.; O'KEEFE, R. J. Cyclooxygenase-2 regulates mesenchymal cell differentiation into the osteoblast lineage and is critically involved in bone repair. **J Clin Invest**, v.109, p.1405-1415. 2002.

ANEXO A

Parecer da Comissão de Ética

115

UNIVERSIDADE FEDERAL DE SÃO CARLOS
PRÓ-REITORIA DE PESQUISA
Comissão de Ética no Uso de Animais
Via Washington Luís, km. 235 - Caixa Postal 676
Fones: (016) 3351.8025 / 3351.9679
Fax: (016) 3351.8025
CEP 13560-970 - São Carlos - SP - Brasil
ceua@ufscar.br - www.propq.ufscar.br

Parecer da Comissão de Ética no Uso de Animais
n° 043/2012

Protocolo n°. 039/2012

A Comissão de Ética no Uso de Animais da Universidade Federal de São Carlos - CEUA/UFSCar **APROVOU** o projeto de pesquisa intitulado "Estudos de Biocompatibilidade e Reparo Ósseo: Testes in vitro e in vivo a partir de uma Nova Manta Flexível Altamente Bioativa", submetido pelo pesquisador *Paulo Roberto Gabbai Armelin*.

São Carlos, 17 de julho de 2012.

Profa. Dra. Luciana Thie Seki Dias

Presidente da Comissão de Ética no Uso de Animais

ANEXO B

Publicação do Estudo I

RESEARCH ARTICLE

Characterization and biocompatibility of a fibrous glassy scaffold

P. R. Gabbai-Armelin[1,4], M. T. Souza[2], H. W. Kido[1,4], C. R. Tim[1,4], P. S. Bossini[3], K. R. Fernandes[3], A. M. P. Magri[3], N. A. Parizotto[4], K. P. S. Fernandes[5], R. A. Mesquista-Ferrari[5], D. A. Ribeiro[3], E. D. Zanotto[2], O. Peitl-Filho[2] and A. C. M. Renno[3]*

[1]*Post-Graduate Programme of Biotechnology, Federal University of São Carlos (UFSCar), SP, Brazil*
[2]*Vitreous Materials Laboratory (LaMaV), Department of Materials Engineering, Federal University of São Carlos (UFSCar), SP, Brazil*
[3]*Department of Biosciences, Federal University of São Paulo (UNIFESP), Santos, SP, Brazil*
[4]*Department of Physiotherapy, Federal University of São Carlos (UFSCar), SP, Brazil*
[5]*Department of Rehabilitation Sciences and Biophotonics Applied to Health Sciences, Nove de Julho University (UNINOVE), São Paulo, SP, Brazil*

Abstract

Bioactive glasses (BGs) are known for their ability to bond to living bone and cartilage. In general, they are readily available in powder and monolithic forms, which are not ideal for the optimal filling of bone defects with irregular shapes. In this context, the development of BG-based scaffolds containing flexible fibres is a relevant approach to improve the performance of BGs. This study is aimed at characterizing a new, highly porous, fibrous glassy scaffold and evaluating its *in vitro* and *in vivo* biocompatibility. The developed scaffolds were characterized in terms of porosity, mineralization and morphological features. Additionally, fibroblast and osteoblast cells were seeded in contact with extracts of the scaffolds to assess cell proliferation and genotoxicity after 24, 72 and 144 h. Finally, scaffolds were placed subcutaneously in rats for 15, 30 and 60 days. The scaffolds presented interconnected porous structures, and the precursor bioglass could mineralize a hydroxyapatite (HCA) layer in simulated body fluid (SBF) after only 12 h. The biomaterial elicited increased fibroblast and osteoblast cell proliferation, and no DNA damage was observed. The *in vivo* experiment showed degradation of the biomaterial over time, with soft tissue ingrowth into the degraded area and the presence of multinucleated giant cells around the implant. At day 60, the scaffolds were almost completely degraded and an organized granulation tissue filled the area. The results highlight the potential of this fibrous, glassy material for bone regeneration, due to its bioactive properties, non-cytotoxicity and biocompatibility. Future investigations should focus on translating these findings to orthotopic applications. Copyright © 2015 John Wiley & Sons, Ltd.

1. Introduction

Bone fractures occur daily worldwide, with 6.2 million cases/year being reported in the USA alone (Claes and Willie, 2007). Among these, 5–10% showed delayed healing, with some persisting for > 9 months or even resulting in non-union fractures. Multiple factors can impair fracture consolidation, including significant bone loss caused by diseases, trauma or tumour resection (Gautier and Sommer, 2003). To ensure the proper repair of the skeleton and decrease the chances of complications from abnormal bone repair, the development of strategies based on the mechanisms of the fracture-healing process is required (Gautier and Sommer, 2003).

Biomaterials that can induce bone biomineralization have been in high demand for clinical regenerative medicine and tissue engineering (Hench, 2006). They combine a number of materials of natural or synthetic origins that

---

Correspondence to: Ana C. M. Renno, Department of Biosciences, Federal University of São Paulo (UNIFESP), Avenida Ana Costa 95, Santos, SP 11050-240, Brazil. E-mail: a.renno@unifesp.br

ANEXO C

Aceite do Estudo II

Date: Mar 11, 2015

To: "Paulo Gabbai-Armelin" paulogabbai@gmail.com

From: "Journal of Materials Science: Materials in Medicine (JMSM)" Kamatchi.Ulagappan@springer.com

Subject: JMSM-D-14-00050R1 - Editor Decision

Dear Paulo Gabbai-Armelin,

We are pleased to inform you that your manuscript, "Effect of a new bioactive fibrous glassy scaffold on bone repair", has been accepted for publication in

Journal of Materials Science: Materials in Medicine.

You will receive an e-mail from Springer in due course with regards to the following items:

1.Offprints

2.Colour figures

3.Transfer of Copyright

Please remember to quote the manuscript number, JMSM-D-14-00050R1, whenever inquiring about your manuscript.

Best regards,
Kamatchi Ulagappan
Springer Journals Editorial Office
Journal of Materials Science: Materials in Medicine